The development of HDAC(6) selective Inhibitors for the treatment of pediatric leukemia

Inaugural-Dissertation

zur Erlangung des Doktorgrades (Dr. rer. nat.)
der Mathematisch-Naturwissenschaftlichen Fakultät
der Heinrich-Heine-Universität Düsseldorf

vorgelegt von

Melf Sönnichsen
aus Niebüll

Düsseldorf, Januar 2023

Aus dem Institut für Kinder-Onkologie,- Hämatologie und Klinische Immunologie der Heinrich-Heine-Universität Düsseldorf

Angefertigt mit der Genehmigung der Mathematisch-Naturwissenschaftlichen Fakultät der Heinrich-Heine-Universität Düsseldorf

Referent: Prof. Dr. Thomas Kurz

Korreferent: Prof. Dr. Arndt Borkhardt

Tag der mündlichen Prüfung: 10.07.2023

Table of contents:

Affirmation

Hereby, I declare on oath that I composed this dissertation independently by myself. I used only the references and resources indicated in this thesis. With the exception of such quotations, the work presented in this thesis is my own. I have accredited all the sources of help. This Ph.D. thesis was never submitted or presented in a similar form to any other institution or examination board. I have not undertaken a doctoral examination without success so far.

_____

Melf Sönnichsen

Summary:

Acute lymphoblastic leukemia (ALL) is the most common cancer in childhood. Although cure rates are exceeding up to 85-90%, the incidence (4 - 6/100.000/year) is high, and leukemia remains a major cause of death in children aged 2 - 6 years. Moreover, therapy-related toxicity could be traumatizing for the patient with potential long-term health consequences due to the intensive use of chemotherapeutics. Furthermore, there are still subtypes of leukemia that are up until today incurable, like TCF3-HLF+ ALL. To prevent long-term health consequences and treat the therapy refractory subtypes, new therapeutic approaches are urgently needed. Next to genetic alterations, epigenetic dysregulation is involved in the development of diseases such as leukemia. The epigenetic machinery can be dysregulated by mutations or overexpression of important enzymes like histone deacetylases. Therefore, HDAC inhibitors are a promising option for the development of novel therapeutics. Pan-HDAC inhibitors, like panobinostat, romidepsin, vorinostat, or belinostat are already applied in the clinic against hematological malignancies. However, pan-HDACi are often associated with side effects in the clinics, and therefore to mitigate them, it was focused on targeting isoform-specific HDAC inhibitors. HDAC6 is an attractive molecular target as it is widely expressed across the tested leukemia cell lines and involved in tumorigenesis. Therefore, several HDAC inhibitors were developed in this work, ranging from very selective HDAC6 inhibitors (**6l**, **10p**) to less specific, so-called preferential HDAC6 inhibitors (**4a-d**, **KSK64**, **8a,** and **8e**), and finally a pan-HDAC inhibitor (**10h**). All developed HDAC inhibitors were initially screened on our (in-house) *ex vivo* high throughput drug screening facility against a variety of leukemic cell lines. The selected hit candidates were later subjected to functional assays for evaluation of their selectivity and anti-leukemia properties. It was found that very selective HDAC6 inhibitors are not cytotoxic even at high concentrations. In contrast, less selective, so-called preferential inhibitors, were effective as monotherapy in the low nanomolar concentration range. Furthermore, RNA sequencing of leukemia cells (TCF3-HLF1+ or TCF3-PBX1+) treated with preferential HDAC6 inhibitors (**KSK64** and Ricolinostat) revealed the upregulation of pro-apoptotic genes. Although, the tested pan-HDAC inhibitor (**10h**) with the highest cytotoxic profile failed as a monotherapy in the leukemia xenograft mouse model.

However, several beneficial combination partners of HDAC6 selective inhibitors were deciphered in this study, such as the anthracyclines epirubicin and daunorubicin. The

selective HDAC6 inhibitor significantly enhanced the cytotoxicity of the anthracyclines making it an interesting partner for combinational therapy, to reduce the concentration of anthracyclines, which are known for their harsh-side effects and the development of resistance. Furthermore, it was shown that HDAC6 selective inhibitors enhanced apoptosis induction when used in combination with the clinically used proteasome inhibitor bortezomib. Lastly, in a genetic knockout (KO) approach followed by *ex vivo* high throughput drug screening, HDAC6 ablation resulted in differential hypersensitivity of the leukemia cells toward clofarabine, aurora A inhibitor, and gemcitabine, in contrast to the wild-type control cells, making these inhibitors interesting for future combination experiments. Taken together, these approaches represent a rational effort towards the development of novel targeted strategies for the treatment of relapsed/refractory ALL with a lower toxicity burden.

Zusammenfassung:

Die akute lymphoblastische Leukämie (ALL) ist die häufigste Krebserkrankung im Kindesalter. Obwohl die Heilungsraten 85-90 % übersteigen, ist die Inzidenz (4 - 6/100.000/Jahr) hoch, und Leukämie ist nach wie vor eine der Haupttodesursachen bei Kindern im Alter von 2 - 6 Jahren. Darüber hinaus kann die therapiebedingte Toxizität für den Patienten traumatisierend sein und aufgrund des intensiven Einsatzes von Chemotherapeutika potenzielle langfristige gesundheitliche Folgen haben. Außerdem gibt es immer noch Subtypen von Leukämie, die bis heute unheilbar sind, wie die TCF3-HLF+ ALL. Um langfristige gesundheitliche Folgen zu verhindern und die therapierefraktären Subtypen zu behandeln, werden dringend neue Therapieansätze benötigt. Neben genetischen Veränderungen ist auch eine epigenetische Dysregulation an der Entstehung von Krankheiten wie Leukämie beteiligt. Die epigenetische Maschinerie kann durch Mutationen oder die Überexpression wichtiger Enzyme wie Histondeacetylasen dysreguliert werden. Daher sind HDAC-Inhibitoren eine vielversprechende Option für die Entwicklung neuer Therapeutika. Pan-HDAC-Inhibitoren wie Panobinostat, Romidepsin, Vorinostat oder Belinostat werden bereits in der Klinik gegen hämatologische Malignome eingesetzt. Pan-HDACi sind jedoch in der Klinik häufig mit Nebenwirkungen verbunden, weshalb man sich auf isoformspezifische HDAC-Inhibitoren konzentrierte, um diese zu mildern. HDAC6 ist ein attraktives molekulares Zielmolekül, da es in den getesteten

Leukämiezelllinien weit verbreitet und an der Tumorentstehung beteiligt ist. Daher wurden in dieser Arbeit mehrere HDAC-Inhibitoren entwickelt, die von sehr selektiven HDAC6-Inhibitoren (**6l**, **10p**) über weniger spezifische, so genannte präferentielle HDAC6-Inhibitoren (**4a-d**, **KSK64**, **8a** und **8e**) bis hin zu einem pan-HDAC-Inhibitor (**10h**) reichen. Alle entwickelten HDAC-Inhibitoren wurden zunächst in unserer Ex-vivo-Hochdurchsatz-Wirkstoffscreening-Anlage gegen eine Vielzahl von Leukämiezelllinien getestet. Die ausgewählten Hit-Kandidaten wurden später funktionellen Assays unterzogen, um ihre Selektivität und ihre Anti-Leukämie-Eigenschaften zu bewerten. Es zeigte sich, dass sehr selektive HDAC6-Inhibitoren selbst bei hohen Konzentrationen nicht zytotoxisch sind. Im Gegensatz dazu waren weniger selektive, so genannte präferentielle Inhibitoren, als Monotherapie im niedrigen nanomolaren Konzentrationsbereich wirksam. Darüber hinaus ergab die RNA-Sequenzierung von Leukämiezellen (TCF3-HLF1+ oder TCF3-PBX1+), die mit präferentiellen HDAC6-Inhibitoren (**KSK64** und Ricolinostat) behandelt wurden, eine Hochregulierung von pro-apoptotischen Genen. Der getestete pan-HDAC-Inhibitor (**10h**) mit dem höchsten zytotoxischen Profil versagte jedoch als Monotherapie im Leukämie-Xenograft-Mausmodell.

In dieser Studie wurden jedoch mehrere vorteilhafte Kombinationspartner von selektiven HDAC6-Inhibitoren entschlüsselt, wie die Anthrazykline Epirubicin und Daunorubicin. Der selektive HDAC6-Inhibitor verstärkte die Zytotoxizität des Anthrazyklins signifikant, was ihn zu einem interessanten Partner für die Kombinationstherapie macht, mit dem Ziel, die Konzentration der Anthrazykline zu reduzieren, die für ihre harten Nebenwirkungen und die Entwicklung von Resistenzen bekannt sind. Darüber hinaus wurde gezeigt, dass selektive HDAC6-Inhibitoren die Apoptoseinduktion verstärken, wenn sie in Kombination mit dem klinisch eingesetzten Proteasom-Inhibitor Bortezomib eingesetzt werden. Schließlich führte die Ablation von HDAC6 in einem genetischen Knockout-Ansatz (KO), gefolgt von einem Ex-vivo-Hochdurchsatz-Wirkstoffscreening, zu einer unterschiedlichen Überempfindlichkeit der Leukämiezellen gegenüber Clofarabine, dem Aurora-A-Inhibitor und Gemcitabin, im Gegensatz zu den Wildtyp-Kontrollzellen, was diese Inhibitoren für zukünftige Kombinationsexperimente interessant macht. Zusammengenommen stellen diese Ansätze einen rationalen Versuch dar, neue zielgerichtete Strategien für die Behandlung der rezidivierten/refraktären ALL mit geringerer Toxizität zu entwickeln.

1. Introduction

1.1 Hematopoiesis

Humans and all mammals in general need to produce blood constantly throughout their lives, a process called hematopoiesis. All cells of the blood system are generated by hematopoietic stem cells (HSC), which are located in the bone marrow and give rise to all types of blood cells[1]. HSCs have the crucial ability for asymmetric cell divisions, which means that HSCs can self-renew themselves, ensuring that the pool of stem cells will not be depleted. Other daughter cells will differentiate into lymphoid and myeloid progenitor cells but lose the capacity for self-renewal[2]. The common myeloid progenitors can differentiate into megakaryocytes, erythrocytes, mast cells, or myeloblasts and the common lymphoid progenitor cells can differentiate into the small
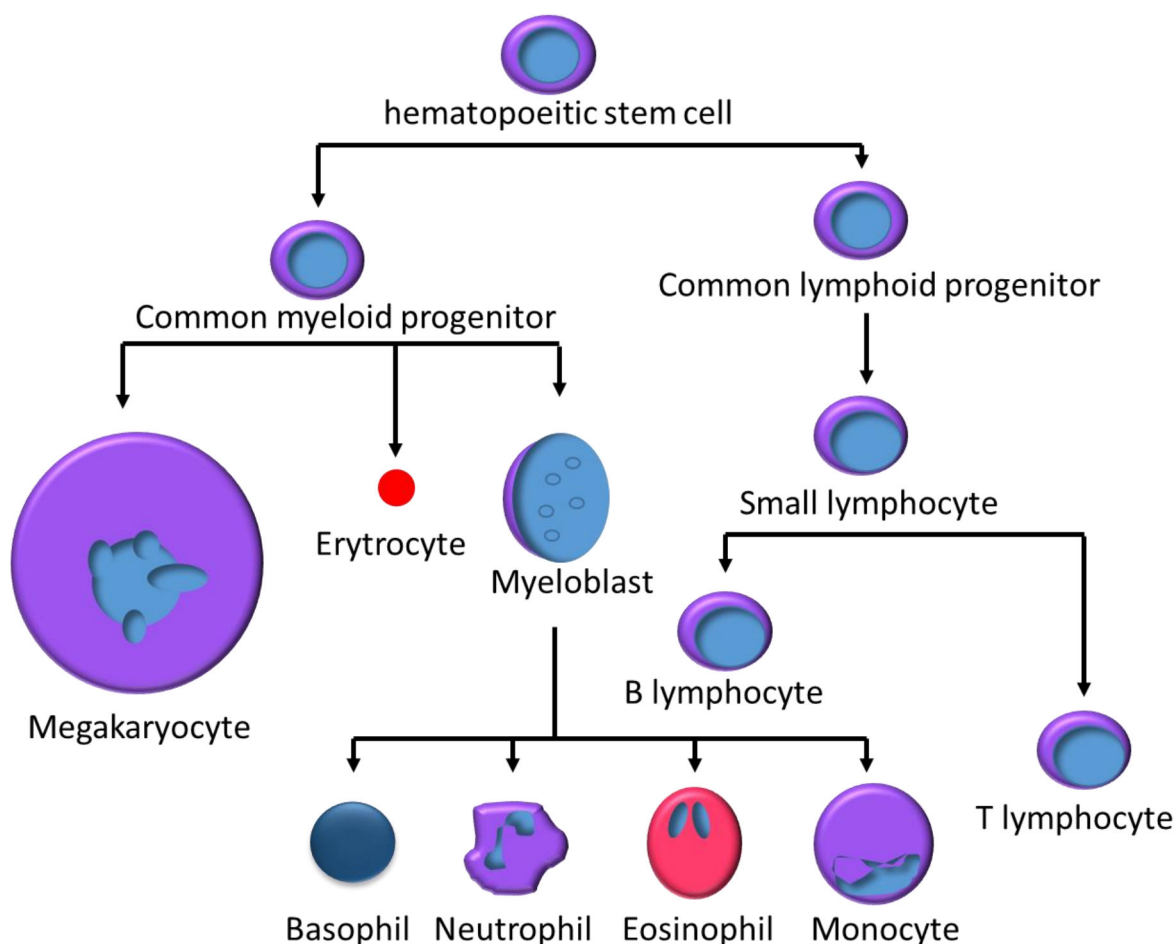
Figure 1: Development and differentiation of blood cells.[176]

lymphocytes, B and T cells. The production and development of red and white blood cells are strictly regulated by growth factors (GFs) (fig. 1). Key GFs are e.g. stem cell factor (SCF), glycoprotein growth factors like interleukins that play a major role in the regulation of the proliferation and maturation of cells[33,4]. The effect of GFs on cells is complex and depends upon their combination and amount present, and also on the stage of differentiation of a cell[3,5]. Even more, the time dynamics of exposure to GF's are also important e.g. the long-term expression of the transcription factor PU. 1 results in a commitment to the myeloid lineage, whereas short-term expression results in the generation of immature eosinophils[3]. Hematopoiesis is thus a highly complex interplay of GFs that will activate signal transduction pathways, which results in the expression of specific transcription factors, which all together determine the cellular fate like lineage commitment or further differentiation. Moreover, signals from TFs are not unidirectional, as differentiated cells can also acquire characteristics of progenitor cells again[6]. Therefore, it is not surprising that the alterations of such a highly and tightly regulated system can result in a variety of malignancies such as acute myeloid or lymphoblastic leukemia[7].

1.2 Pediatric Leukemia

Pediatric leukemia is the most prevalent childhood cancer accounting for 1 out of 3 cancers in children under the age of 14[8]. There are two major forms of leukemia in children. The most prevalent one is acute lymphoblastic leukemia (ALL) followed by acute myeloid leukemia (AML). Even though major progress was achieved in the treatment of pediatric leukemia in the form of combinational chemotherapy and the survival rates can be as high as 90%, however, the treatment is still traumatizing, toxic, and harbors the risk for long-term health consequences[9,10]. Furthermore, there are still subsets of ALL that are resistant to current therapies.

Even though the treatment of pediatric leukemia is a success story, the cause of the disease is surprisingly unknown. Many external environmental exposures are linked to ALL, but the associations are weak and unclear[11]. The most convincing model proposed is a 2-step model for the most prevalent form of B-cell precursor acute lymphoblastic leukemia (BCP-ALL) [12]. The first step is a genetic alteration, acquired either in utero or as a germline variant. It was already shown that a significant amount of healthy newborns carry such a genetic alteration and thus there needs to be more

than just the genetic predisposition[13]. The second step, according to the model, would be the exposure to infectious agents that confronts the already altered immune system[14,15]. Interestingly, in developed societies, with high levels of personal hygiene standards, the incidence of ALL has increased[16,17]. Furthermore, it was shown that birth order, mode of delivery, daycare attendance, breastfeeding, and the composition of the microbiome are linked to the risk of a child developing leukemia[17–22]. Hence, disrupted immunological training could lead to a disturbed immune response when confronted with infectious agents[12].

Leukemia develops in the bone marrow, where new blood cells are generated. In a leukemic patient, the blood cells do not develop properly and stay undifferentiated. Depending on the type of leukemia, different subsets of cells are affected. In the case of ALL, which makes up the vast majority of all pediatric leukemia (75-80% of all diagnosed cases) lymphocytes are affected and will constantly produce lymphoblasts that stay undifferentiated and cannot function properly to fight infections[23]. Even more, they also take up the space for other blood cells to be produced. There are several sub-types of ALL but the most prevalent one is BCP-ALL, followed by T-cell acute lymphoblastic leukemia (T-ALL). The peak incidence of pediatric ALL is between 2-5 years[11,23,24]. Another type is acute myeloid leukemia (AML), in which cells of the myeloid lineage are malignant and will produce immature myeloblasts that do not function properly and cannot fight infections. Also, in this case, the myeloblasts over-produce and are responsible for crowding other cells in the bone marrow. Other rare forms of pediatric leukemia are acute promyelocytic, chronic myelogenous leukemia (CML), and juvenile myelomonocytic leukemia[25]. These forms are rare in children and will not be further discussed.

The symptoms of pediatric ALL and AML are similar as they are mostly related to complications regarding bone marrow functions. Furthermore, as ALL and AML are both acute forms of leukemia symptoms will arise quickly (days or weeks) and include mainly fatigue, repetitive infections, bone, and joint pain, bruising, abdominal pain, swollen lymph nodes, and enlarged spleen or liver[26].

The diagnosis of leukemia is to determine if the disease is present and if so, to what extent and which kind of subset of leukemia has developed. Bone marrow aspirations and biopsies are performed to analyze the fluids of the aspiration and cells from the biopsy for the presence of leukemic cells. Immunophenotyping is used to further determine the underlying form of leukemia. Therefore, leukemic cells will be analyzed

by flow cytometry after cells were stained with fluorophore-conjugated antibodies targeting a specific cluster of differentiation (CD), mostly expressed on the surface of blood cells. CD markers for myeloid classification are e.g. CD13, CD33, CD117, and CD65. B-cell markers include CD10, CD19, CD20, CD22, CD23, CD25 and CD79a for T-cell classification there are CD2, CD3, CD4, CD5, CD6 and CD7. Depending on the expression of such markers the disease can be further classified into different subtypes of ALL or AML[27].

1.3 Treatment of pediatric leukemia

The treatment of pediatric leukemia is dependent on several factors such as the specific type of leukemia, prognostic characteristics, response to therapy, and extent of the disease at the time of diagnosis. In Germany, patients are treated according to the treatment regimens defined by the ALL-BFM (Berlin.Frankfurt_Münster) and COALL (cooperative study group for childhood acute lymphoblastic leukemia)[28]. Generally, the treatment options can be divided into 4 categories. The first and most important one is chemotherapy. The treatment with chemotherapy is dependent on the specific sub-type of leukemia. For ALL it is usually given in four phases: Induction therapy with subsequent induction consolidation, extra compartment therapy, reduction therapy, and maintenance (up to 2 years after diagnosis)[29,30]. In the induction phase the goal is to achieve remission and mainly three therapeutics are used, which are L-asparaginase, vincristine, and steroid drugs such as dexamethasone[31]. For children with high-risk leukemia, anthracycline is added such as daunorubicin. Furthermore, also the drugs methotrexate and 6-mercaptopurine are given early. Next to this, there is also intrathecal chemotherapy (methotrexate), which is important to kill leukemic cells that have spread to the brain and or spinal cord, whereas in high-risk children hydrocortisone and cytarabine can be added to the treatment regime. The induction phase is the most intense phase for the patients and >95% of children with ALL enter remission after 1 month of induction treatment. After the induction phase, the consolidation phase starts and usually lasts for a month. The golden standard is combinational chemotherapy to prevent the remaining cancer cells to become therapy resistant. The standard therapy regime consists of of methotrexate, 6-mercaptopurine (6-MP), vincristine, L-asparaginase, and prednisone but regimes can differ between cancer centers[31]. If the leukemia is still in remission after consolidation the maintenance therapy will begin, which is also based on combinational therapy. Next to

4

chemotherapy, patients can be treated with stem cell transplantations (SCT) under specific circumstances. SCT can be used for high-risk groups of patients, when it is expected that the disease will relapse after the induction chemotherapy or when children have a fast relapse after the first remission[32]. Children that have a late relapse are more complicated to decide for SCT as they often can be treated well with the standard dose of chemotherapy. Other cases that are suited for SCT are leukemias which carry the Philadelphia chromosome or are poor responding T-ALL[33]. SCT is associated with a major risk for the patient and is only suitable if a fitting donor is available, like a sibling or donors that must match the receiving child's human leukocyte antigen (HLA). A third kind of possible therapy is radiotherapy which is mainly used for children that have a high-risk form or when leukemic cells are found in the CSF[29]. However, radiotherapy of the CNS is known to harbor a high risk for severe side effects, like secondary tumors[34].

Another kind of therapy is targeted therapy. The molecular mechanism of targeted therapy is fundamentally different from classical chemotherapy, which broadly targets all rapidly dividing cells. The basic principle behind targeted therapies is to target molecules, in most cases enzymes, that harbor a mutation or alteration specific for the cancer cells but absent in normal cells or tissues[35]. This way the therapy is expected to be more effective but more importantly has less severe side effects as, in contrast to classical chemotherapy, not all fast-dividing cells are targeted. For instance, Imatinib (Gleevec) is one of the major success stories of targeted therapies. Imatinib is a small molecule targeting the oncofusion protein BCR-ABL1, resulting from the translocation of chromosomes t(9;22)(q34;q11) also known as the Philadelphia chromosome[36]. BCR-ABL1 is a strong driver of tumorigenesis and imatinib, like other tyrosine kinase inhibitors, targets its active site and blocks it and thereby decreasing its kinase activity, resulting in reduced growth rates or inducing apoptosis. However, cancers can become resistant to targeted therapies in multiple ways[37]. Either, the target protein, in the case of imatinib BCR-ABL1 protein mutates in a way that the drug can no longer bind the active site or the cancer cells develop resistance by activating another signaling pathway, and as a result, they are no longer dependent on the initial driver pathway[38]. Another limitation of targeted therapies today is that only "druggable" proteins can be targeted. For instance, the RAS gene family members (KRAS, NRAS, and HRAS) are the most frequently mutated gene family in cancers and were considered to be "undruggable" due to the lack of structures that can be targeted such as active sites or

ATP binding sides. Furthermore, RAS signaling, as an example, is complex, with multiple feedback loops, blocking one pathway can result in the activation of other pathways as a compensatory mechanism[39,40]. Therefore, the development of new treatment strategies is urgently needed. One viable approach can be by expanding the portfolio of potential anti-leukemia treatments, for instance, inhibitors of epigenetic regulators such as histone deacetylases, which will be introduced in the following sections.

1.4 Epigenetics

The term epigenetics describes all heritable changes in gene expression that are not related to changes in the DNA itself. It was discovered in the 1940s by the British embryologist C. H. Waddington[41]. He used the term "epigenesis" to describe the development of totipotent stem cells to more differentiated cells during embryonic development. In 1990, R. Holliday defined the contemporary understanding of epigenetics as "the study of mechanisms of temporal and spatial control of gene activity during the development of complex organisms"[42].

In the cell, DNA is tightly packed into chromatin structures that consist of the DNA itself and proteins like e.g. histones[43]. The chromatin state regulates gene expression. Chromatin can occur in different condensation states, whereby euchromatin describes the open or relaxed state of chromatin. In this state, genes are accessible for DNA-binding enzymes like e.g. RNA-polymerase. The opposite, closed or condensed state is called heterochromatin and is associated with inactive genes as they are not accessible for DNA-binding proteins[44]. This mechanism makes it possible that two cells with the same genome can have different phenotypes (e.g. a neuron vs keratinocyte) and completely different functions. It is the combination of the genome and the epigenome that defines their phenotype and thereby its function. Therefore, epigenetic regulation is crucial during the development of organisms but also for the adaptation to environmental changes. There are two major mechanisms known, that are based on covalent modifications, to regulate the epigenome, which are DNA methylation and histone modifications[44].

DNA methylation describes a process by which methyl groups are added to the cytosine base of DNA and are associated with gene repression. It plays an essential role during development and is involved in processes like genomic imprinting[45], X-chromosome inactivation[46], and aging[47]. DNA methylation plays a relevant role during

cancer development, whereby the hypermethylation of CpG sites in promotor regions of tumor suppressor genes (TSGs) and hypomethylation of CpG sites of the promotor regions of oncogenes are associated with carcinogenesis. In mammalian cells, DNA-methyltransferase (DNMT) is responsible for the DNA methylation at the C5 position
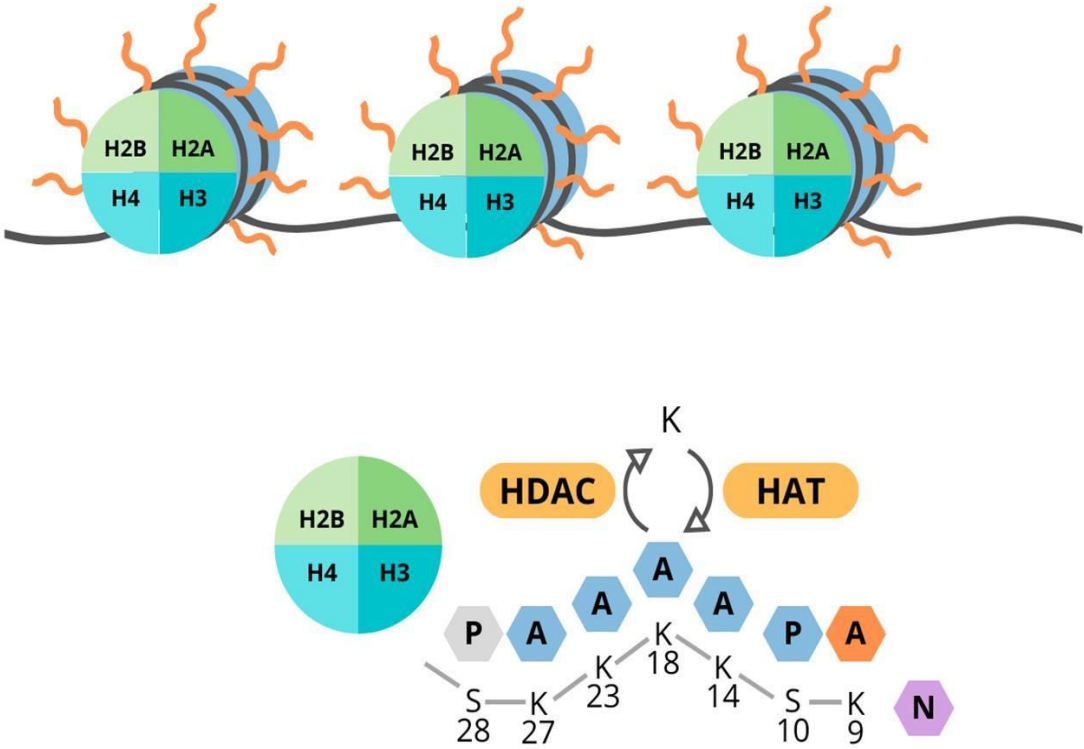
Figure 2: Schematic structure of histones in nucleosomes. **a)** The core histones are present in two copies and the DNA (black) is wrapped around an octamer of histones. **b)** The tails of histones can be modified by HATs and HDACs by acetylation and deacetylation.[177]

of CpG dinucleotides after cell replication[48]. DNA methylation is involved in carcinogenesis e.g. by the silencing of TSGs. There are drugs that are able to inhibit the function of DNMTs and thus allowing the expression of TSGs. For instance, 5-Aza-2'-deoxycytidine (Decitabine) is a nucleoside analog that needs to be incorporated into the genome and then can trap DNMTs by forming a covalent complex on the DNA[49]. After that, the DNMTs can be degraded. The other mechanism is the post-translational modification of histones. Histones are highly conserved proteins that can wrap DNA around them and this way form nucleosomes. Histones are crucial for the cell as a diploid human cell contains about 1.8 meters of DNA that can be reduced to 90

micrometers of chromatin by wounding the DNA around histones and the formation of nucleosomes[50]. A nucleosome consists of four core histone proteins: H2A, H2B, H3, and H4, which exist as dimers and interact with the DNA. The N-terminal region of these core histones has a tail-like structure that can be post-translationally modified and thereby affecting their function of gene regulation (fig. 2). The most important known histone modifications are acetylation, methylation, ubiquitination, and phosphorylation. The main function of the histone modification is to alter the condensational state of chromatin, whereby condensed and inaccessible heterochromatin is associated with inactive genes and open, accessible euchromatin is associated with active genes (fig. 3).

1.5 Histone deacetylases

As already mentioned, gene expression is regulated by epigenetic modifications, like DNA methylation and histone modifications. Epigenetic modifications are deposited
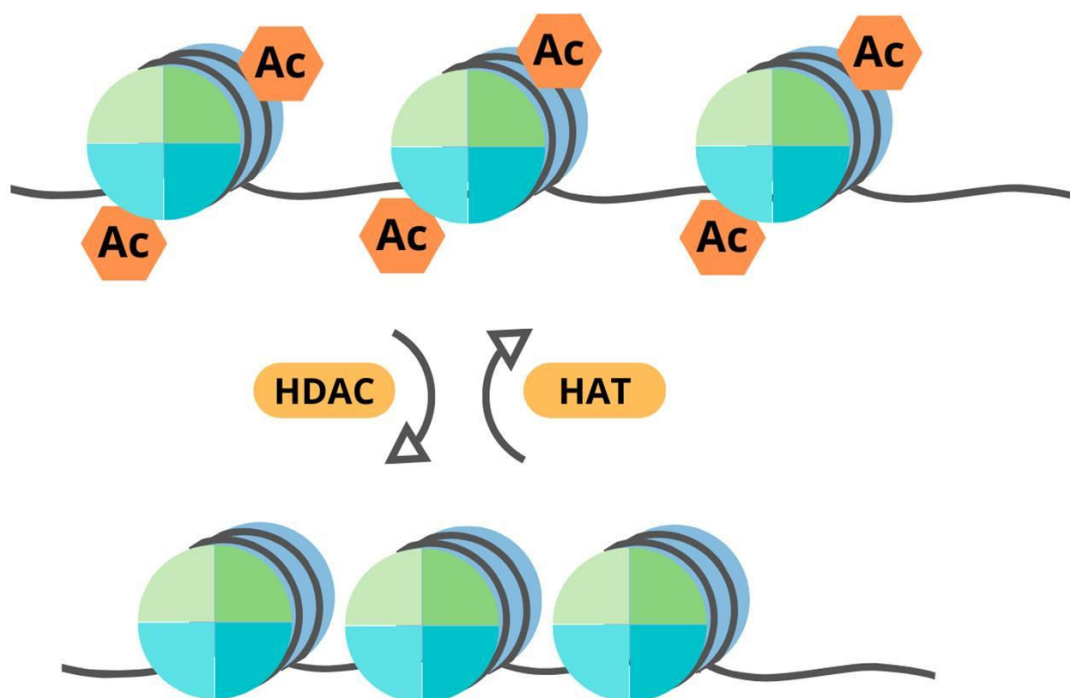
Figure 3: Mechanism of action of HATs and HDACs. The inhibition of HDACs, histones are acetylated and the tightly wrapped DNA relaxes. With the relaxed DNA transcription can take place and genes that potentially induce cell-growth arrest, differentiation or apoptosis can be expressed.[177]

onto the DNA or histones by specific enzymes, the "writers". These enzymes add chemical groups, like acetyl, methyl, and phosphate groups to the tails of histones or DNA itself, in the case of DNA methylation. These marks get recognizes by effector proteins, the "readers" and most of the marks are reversible and can be removed by the "erasers". It is known that epigenetic dysregulation is involved in the formation of diseases such as cancer[51]. The epigenetic machinery can be dysregulated by mutations or overexpression of important enzymes like histone deacetylases (HDACs). HDACs are enzymes that have the function to remove acetyl groups from an ε-N-acetyl of histone tails. Histone tails are under normal circumstances positively charged due to the lysine and arginine amino acids and bind the negatively charged DNA backbone. Thereby the DNA is tightly wrapped around the histones and is not accessible to epigenetic "readers". Histone acetyltransferases (HATs) can add acetyl groups to the lysine residues of histone tails or other proteins and thereby neutralizing the positively charged histone tails. This way the ability of histones to bind DNA will be reduced and the chromatin will become more relaxed and thus accessible for e.g. transcription factors. The function of HDACs is to remove such acetyl groups and thereby increase the positive charge of histone tails, which is again associated with tightly packed, inaccessible chromatin, which cannot be transcribed. However, HDACs are not only involved in the modification of histones but also can control the function or activity of other proteins, like transcription factors or chaperone proteins, by post-translational modifications. HDAC6 is one prominent example and will be discussed later.

Human HDACs can be divided into four groups based on their homology to the original yeast HDACs. The "classical" HDACs are Class I, IIa, IIb, and IV and have a zinc-dependent active site. Class III HDACs are known as sirtuins and are not zinc-dependent but NAD^{+}-dependent and will not be further discussed in this work. The class I HDAC family members are HDAC1, 2, 3, and 8 and are localized in the nucleus of every human cell. HDAC1-3 fulfilling their functions in larger multi-protein complexes and is recruited to chromatin by their interaction with repressive transcription factors or other silencing co-factors[52]. HDAC1 and 2 are together involved in several co-repressor complexes such as NuRD, Sin3A, or CoREST[53]. HDAC3 is only recruited to the SMRT/NCoR co-repressor complex[54]. HDAC8 is distinct from the other class I HDACs as it fulfills its function alone, without a multi-protein complex[55]. HDAC class IIa family members are HDAC 4, 5, 7, and 9. These isoforms show poor catalytic activity and are considered to be pseudoenzymes that have a function as adapters of

repressor complexes[56]. They are expressed in a tissue-specific manner in contrast to the class I HDAC family members, which are virtually expressed in every human cell. The class IIb HDAC family members are HDAC6 and 10 and are characterized by a tandem deacetylase domain. HDAC6 has the unique feature to be a predominantly cytoplasmic enzyme and HDAC10 can be found in the cytoplasm as well as in the nucleus[57,58]. HDAC11 is the only member of the class IV HDACs as it shows no homology to any of the original yeast HDACs and is involved in the deacetylation of fatty acids[59]
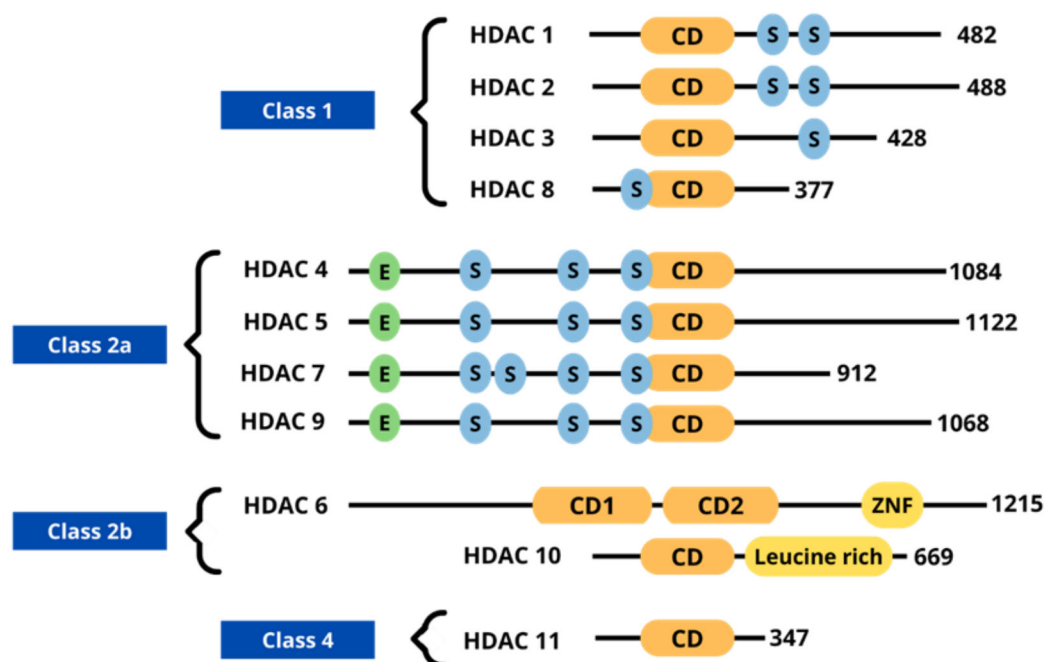
Figure 4: Schematic representation of the zinc-dependent HDAC superfamily. The HDAC family consists of members of class I, IIa, IIb and IV HDACs. Orange domain represents the conserved HDAC catalytic domain. S represents serine residues that can be phosphorylated. The green E represents the MEDF-2 binding sites and the numbers represent number of amino acids in human.

.

1.6 The biological role of Histone deacetylase 6 (HDAC6)

HDAC6 is a unique HDAC as it is mainly localized in the cytoplasm and performs a variety of functions in the cells (fig. 5). Its molecular substrates are thus also mainly cytoplasmic proteins like α-tubulin, cortactin, peroxiredoxins, and HSP90[60,61]. It is the largest protein of the HDAC family with 1215 amino acids. It contains two catalytic domains, separated by a dynein-binding domain and a C-terminal ubiquitin-binding zinc finger domain (BUZ), relevant for the regulation of ubiquitination-mediated degradation. It further has a nuclear export sequence and a SE14 motif, which are both

important for its cytoplasmic retention. HDAC6 has many different substrates but the most important and most studied substrates are α-tubulin and cortactin, which are involved in microtubule-dependent cell mobility and actin-mediated cell motility, respectively[62]. Another important and well-known target substrate is HSP90, which is an important chaperone protein and is thus involved in the maturation and maintenance of proteins[63]. Next to this, HDAC6 is involved in many other important cellular mechanisms, which will be discussed in more detail in the following section. The most profound role of HDAC6 is its function in cytoskeletal dynamics. α-tubulin was the first discovered substrate of HDAC6[64]. HDAC6 is able to deacetylate α-tubulin and thereby induce microtubule depolymerization, thus contributing to the dynamics of microtubules. Next to this, cortactin, a protein involved in the polymerization of actin filaments, is a substrate of HDAC6. When cortactin is deacetylated it can bind to F-actin and enhance its polymerization and thereby contributing to cytoskeletal dynamics. Tubulin and cortactin are both important components of the cytoskeleton and by altering their acetylation status HDAC6 has a role in cell motility and cell division. Another important feature of HDAC6 is its ubiquitin-binding domain, showing that not only protein lysine acetylation but also ubiquitination is recognized by HDAC6. HDAC6 is thus involved in two different cellular signaling systems[65,66]. Important interaction proteins of HDAC6 with regards to the ubiquitin signaling system are p97/VCP (valosin-containing protein) and UFD3/PLAP (phospholipase A2-activating protein), both are involved in the ubiquitin and proteasome system (UPS). P97/VCP is a chaperone-like ATPase that can disassemble protein complexes with their segregase activity and thereby release, among others, ubiquitinated proteins[67]. UFD3/PLAP is linked to the maintenance of ubiquitin level[68]. Furthermore, HDAC6 has a major impact on the fate of ubiquitinated proteins as high-affinity binding of HDAC6 to ubiquitinated proteins blocks their accessibility for other ubiquitin-binding factors and thereby prevents proteasomal degradation via the UPS[67,69]. Furthermore, HDAC6 also mediates the transport of misfolded proteins along the microtubule to protein aggregates called aggresomes. TRIM50, an E3 ligase, and p62 in cooperation with HDAC6 release the misfolded, ubiquitinated proteins from their complex into the aggresomes. HDAC6 is further responsible, through its cortactin-dependent actin remodeling, for the autophagosome-lysosome fusion, which is needed for the lysosomal degradation of the ubiquitinated protein aggregates by autophagy[69–71]. HDAC6 is thus an important regulator of proteasome-independent protein degradation

by aggresome formation and finally its autophagic degradation. In general, aggresomes have a protective function when cells are overwhelmed with misfolded protein that cannot be cleared by the UPS pathway. Furthermore, HDAC6 is also involved in protease-dependent protein degradation via its substrate HSP90α. HSP90α is a chaperone protein and is involved in the stabilization of proteins when deacetylated by HDAC6. Acetylated HSP90α cannot function as a chaperone protein, which results in the degradation of its client proteins by the UPS pathway[72]. Under normal circumstances, HDAC6 is in complex with HSP90α, heat shock factor 1 (HSF1), and VCP/p97. But when misfolded proteins accumulate in the cell, the complex dissociates and HSF1 can induce the transcription of its target genes, mainly HSP proteins with a chaperone function, and also allow HDAC6 binding to the misfolded proteins[69,73]. Moreover, HDAC6 is involved in the process of apoptosis through its substrate Ku70. Ku70 was found to be involved in the process of nonhomologous end-joining DNA repair[74]. Next to this, Ku70 has also a function in the cytoplasm. Deacetylated Ku70 binds to the pro-apoptotic Bcl-2 family member Bax and thereby repressing the BAX-induced cell death. When acetylated, Ku70 releases Bax and thereby inducing apoptosis[75]. HDAC6 is also the deacetylase of redox regulatory proteins, such as peroxiredoxin (PRX) I and PRX II. These proteins have an anti-oxidant function by reducing H_2O_2. When acetylated, PRX I and II have an increased reducing function and thereby may decrease cancer cell resistance to chemotherapy[76].

1.7 The role of HDAC6 in cancer

HDAC6 has many, different important functions under physiological circumstances, as described above. Therefore, it is not surprising that its overexpression is linked to many different types of cancers by altering the acetylation status of its target proteins. There is evidence that its overexpression is correlated with increased tumor-aggressiveness and hence a lower survival rate in oral squamous cell carcinoma, AML, ovarian cancer, and hepatocellular carcinomas[77–79]. One likely reason for this observation might be its role in anchorage-independent proliferation, which allows cells to circumvent anoikis, a form of programmed cell death that prevents cells from detaching from the extracellular matrix and the basement membrane[80]. It was observed that the knockdown of HDAC6 in ovarian and breast cancer cell lines reduced anchorage-independent growth by 3-20%[81]. Also in vivo, it was observed that immunocompromised severe combined immunodeficient-Beige mice that were treated

with shRNA against HDAC6 showed fewer tumors compared to the control shRNA-injected mice[80]. In another study, mouse embryonic fibroblasts (MEFs) from either wild-type or HDAC6 KO embryos were transformed into tumor cells and later analyzed for their anchor-independent growth in soft agar. It was shown that the HDAC6 KO MEFs formed 10 times fewer colonies compared to the wild-type MEFs, indicating the important role of HDAC6 in the formation of tumors[57]. Interestingly, in inflammatory breast cancer (IBC), the function of HDAC6 is not only governed by its expression levels (e.g. overexpression) but also related to its activity. As was shown with ricolinostat, a selective HDAC6i, which was able to inhibit the proliferation of IBC-cells significantly higher compared to non-IBC cells, even though HDAC6 was not overexpressed in the IBC cells[82]. Moreover, HDAC6 has also a role in cell cycle progression by deacetylation of α-tubulin and thereby inducing its interaction with CYLD and BCL3, and thus increasing the cell cycle progression[83]. When HDAC6 is knockdown, the interaction of CLYD and BCL3 is reduced, which finally leads to less BCL3 in the nucleus. This leads to the less transcriptional activity of nuclear factor kappa B and thus less cyclin-D1 expression, an important factor for cell cycle progression. This way the cell cycle progression is delayed in the G_1/S transition[83]. Furthermore, the expression or activity of HDAC6 modulates immunity in cancer through several mechanisms. First, HDAC6 is involved in the upregulation of tumor-associated antigens, MHC class 1 proteins, co-stimulatory molecules, and cytokine production[84]. For example, in melanoma cell lines, after treatment with HDAC6 inhibitors, the expression of specific melanoma antigens increases (*gp100*, *MRT1*, *TYRP1* and *TYRP2*)[84]. Next to this, HDAC6 is involved in the regulation of STAT3 pathway and more specifically the STAT3-PD-L1 pathway[85]. STAT3 is an important regulator of cancer immunity through the induction and maintenance of tumor immune tolerance[86]. HDAC6 expression leads to the phosphorylation of STAT3, which can then bind to its target genes and enhance their expression. In the nucleus, pSTAT3 together with HDAC6 bind to the promotor of PD-L1 and initiate its transcription. The expression of PD-L1 enables cancer cells to evade the immune system. Therefore, PD-L1 expression is correlated with more aggressive tumor behavior and a higher risk of death[85]. HDAC6 is also specifically involved in leukemia. Even though HDAC6 is primarily localized in the cytoplasm, in leukemic cells a significant amount of nuclear HDAC6 was observed, which might be linked to higher acetylation levels of the NLS region, compared to other cell types[87]. Furthermore, the inhibition of HDAC6 leads to

lower levels of nuclear HDAC6 and less HDAC6-p53 interaction. That finally leads to less p53 target gene expression and thereby inducing apoptosis and cell cycle arrest[88]. Another interesting function of HDAC6 in the context of leukemia, more specifically CML, is its ability to deacetylate HSP90α, which is involved in the stabilization of BCR-ABL[89]. HSP90α, as described earlier, is a chaperone protein that loses its function in the acetylated form, which will ultimately lead to the degradation of its client proteins via the proteasome. It was already shown that pan-HDACi and si-RNA targeting HDAC6 were able to increase the acetylation of HSP90α, thereby increasing the ubiquitination of BCR-ABL and decreasing its expression in K562 cells[90,91]. Furthermore, it was observed that leukemic stem cells, isolated from patients with CML showed more frequent overexpression of several HDAC isoforms but particularly HDAC6, compared to the expression profile of K562 cells. As leukemic stem cells, that are not targeted by tyrosine-kinase inhibition and have the capacity for self-renewal, are important for the relapse of CML patients this observation might be an interesting observation for the development of strategies to counteract the occurrence of relapse[92].
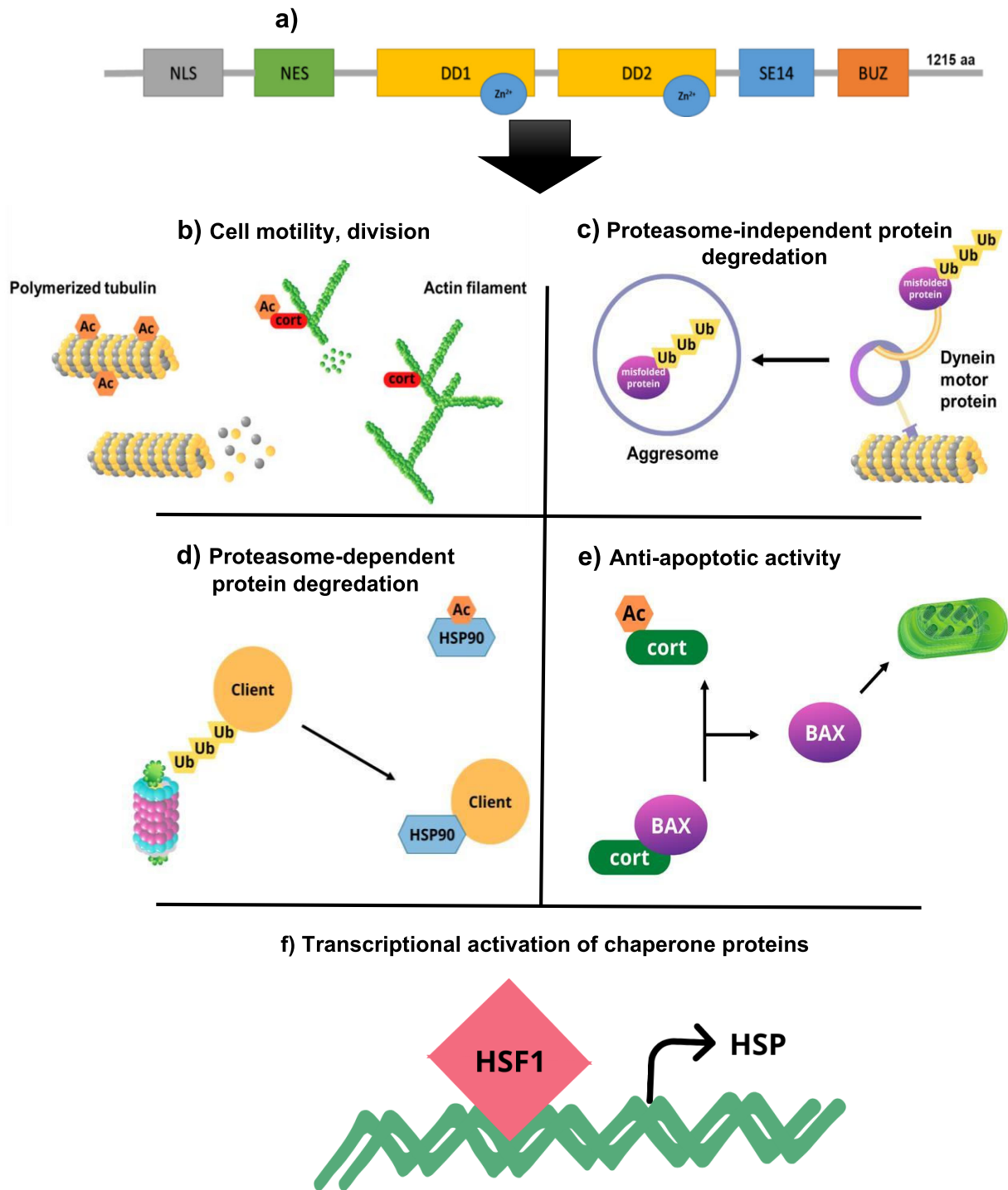
Figure 5: HDAC6 has a variety of important cellular functions. a) Structure of the HDAC6 protein. HDAC6 consists of 1215 amino acids and has a Nuclear localization signal (NLS), nuclear export signal (NES), two catalytic domains (DD1, DD2), a cytoplasmic retention signal (SE14) and an ubiquitin binding domain (BUZ). b) HDAC6 is involved in cell motility and cell division through α-tubulin and cortactin. c) HDAC6 is involved in the formation and degradation of the aggresomes through several mechanisms. d) HDAC6 is responsible for the deacetylation of HSP90 and has this way impact on the fate of misfolded proteins. e) HDAC6 is involved in anti-apoptotic activity by the deacetylation of Ku70, which captures Bax to inhibits its function in the deacetylated state. f) HDAC6 releases from the complex with HSF-1, VCP/p97 and HSP90α. This allows HSF-1 to initiate the transcription of other HSP chaperones.

1.8 Histone deacetylase inhibitors as anti-cancer therapeutics

The first FDA-approved HDAC inhibitor (HDACi) was Vorinostat in 2006 and it is a derivate of Trichostatin A (TSA), an organic, natural product and the first discovered HDACi[52]. It is selectively inhibiting the class I and II HDAC family members[93]. Its chemical structure follows the classical pharmacophore model, similar to other HDACi romidepsin, belinostat, and panobinostat, which were later approved in 2009, 2014, and 2015 respectively, for the treatment of hematologic malignancies by the US. Food and Drug Administration (FDA). The benzamide-based Tucidinostat was approved for the treatment of peripheral T-cell lymphoma (PTCL) by the Chinese Food and Drug Administration (CFDA)[94]. The classic pharmacophore model is based on three main features. These are a zinc-binding group (ZBG), a hydrophobic linker, and a cap group[95]. The ZBG interacts with the zinc ion in the active site and is connected with the hydrophobic linker domain to the cap group. The cap group interacts with the rim region of the catalytic site[52]. Depending on the functional group of the ZBG, HDACi can be categorized into hydroxamic acids, benzamides, carboxylic acids, thiols, cyclic tetrapeptides, or depsipeptides[96]. The approved HDACi are pan-HDACi, meaning they are targeting multiple HDAC isoforms. As a consequence of being unspecific, the observed side effects of such pan HDACis are wide-ranged. First, they are associated with a lot of easily manageable side effects that are not strong enough to discontinue therapy, which is e.g. nausea, headache, fatigue, or fever[97]. Secondly, HDACis are also associated with life-threatening side effects, which can be divided into class-specific (in this case HDACi specific) and drug-specific[97]. Class-specific side effects are myelosuppression, cardiac toxicity, and gastrointestinal effects[97]. These side effects need to be observed in some cases and forced to quit the therapy to prevent life-threatening situations evokes by the therapy itself. The five approved HDACi have drug specific adverse effects as well (tab. 1).

Furthermore, HDACis are usually not given as monotherapy but in combination with other drugs[98]. Given the severe side effects of pan-HDACi, it would be of great therapeutic value to have HDACi that target only specific isoforms and thereby only inhibit specific functions, which in turn will reduce the number of side effects and make the HDACi more tolerable for the patient. HDAC6 is a potential target of great interest, as it is involved in many important cellular processes that are cancer-relevant (fig. 5), which could be exploited for cancer therapy. And indeed, it was already shown that specific HDAC6 inhibitors have shown anti-cancer properties in different cancer

types such as multiple myeloma, chronic lymphocytic leukemia, and AML[99,100,72]. Until today, no HDAC6 selective inhibitor was approved by the FDA. But two compounds, ACY-241 (Citarinostat) and ACY-1215 (Ricolinostat), which are both hydroxamic acids and classified as HDAC6 specific inhibitors, are currently in clinical trials for a variety of hematological as well as solid tumors[101,102]. However, the development of isozyme-specific HDACi is challenging due to the high structural similarity of the HDAC active sites and several HDACs are part of protein complexes, involved in multiple biological functions[52]. The selectivity of HDACi can be implemented by structural differences in other parts of HDAC enzymes, like the surface area close to the active side, and the entry area to the active site tunnel or can be based on differences in the catalytically important amino acid residues. Another approach is to target the specific subpockets of the different HDAC isozymes. Therefore, the pharmacophore model was extended for more selective targeting. HDAC 1-3 (class I) have an additional subpocket that can be exploited to target HDAC class I isozymes. HDAC class IIa isozymes have a lower pocket, absent in other isozymes that can be targeted by inhibitors. HDAC6 possesses a wider and more shallow entrance to the binding site and can be selectively targeted by bulkier and branched cap structures[52].

Table 1: Overview of approved HDACi with their drug-specific adverse effects.[97]

HDACi	FDA approval	EMA approval	CFDA/NMPA (Chinese FDA)	Specific adverse effects
Belinostat	2014	not approved	not approved	Infections, tumor lysis syndrome
Panobinostat	2015	2015	not approved	Hemorrhage, cardiac ischemia,
Romidepsin	2009	not approved	not approved	Infections, tumor lysis syndrome
Vorinostat	2006	not approved	not approved	Pulmonary embolism, deep vein thrombosis, hyperglycemia
Tucidinostat	not approved	not approved	2014	Raised creatine phosphokinase levels, pericardial effusion

1.9 Mechanism of resistance against HDACi

There are different reasons for the development of resistance against cancer therapeutics. The most profound and general reason is the ability of cancer cells to adapt to and respond to growth-inhibitory and damaging factors. This results from a constant selection of malignant cells that can survive or even proliferate under unfavorable circumstances. This way cancer can circumvent the effects of not only chemotherapeutics but also HDACi. Known mechanisms that are involved in the process of acquired resistances, concerning HDACi, are numerous. First, the drug efflux of cancer cells can be altered by overexpression of drug efflux pumps[103]. This is a general mechanism leading to a multidrug-resistant phenotype of cancer cells. Another likely reason for the development of resistance is based on either molecular changes in the target protein or overexpression of the target protein and thereby desensitizing the drug target for its drug[104]. Epigenetic or chromatin changes can also be the reason for acquired resistance to HDACi. For instance, DNA hypermethylation is an important mechanism of resistance concerning HDACi as it interferes with their ability to activate silenced tumor suppressor genes[105]. Furthermore, cancer cells that were treated with first-line therapeutics such as chemotherapeutics might be already selected for those cells able to cope with high levels of DNA damage or oxidative stress, which finally also contributes to their ability to deal with the oxidative stress evoked by HDACi[106]. One way to counteract the development of resistance is the use of drug combinations.

1.10 Drug combinations

As already mentioned, HDACis are not used as monotherapy but are always in combination with other drugs. Targeting a disease at different molecular targets offers some crucial advantages in comparison to monotherapeutic approaches. First, it can result in better overall efficacy paired with a reduced risk for side effects. Another important advantage is a reduced risk of the development of resistance, which is a major concern in the field of cancer medication. Therefore, a lot of research was invested into the analysis of drug combinations, and this way new methodologies and concepts have been formulated. One example is the combination of HDACi in combination with other epigenetic modifiers such as the hypomethylating agent's

decitabine and azacitidine. These drugs are anti-cancer drugs and FDA-approved for the treatment of AML and chronic myelomonocytic leukemia[107] It is hypothesized that the combination of pan-HDACi and hypomethylating agents disrupts transcriptional repressor complexes leads to favorable gene expression[108,109]. Another example is ricolinostat, the selective HDAC6 inhibitor that showed promising results in preclinical studies in multiple myeloma (MM) cells in combination with the proteasome inhibitor bortezomib. It was found that the combination of the HDAC6 inhibitor, ricolinostat, and the proteasome inhibitor, bortezomib, lead to a synergistic anti-cancer effect in MM cells[110]. Cancer cells are dependent on the UPS as they are proliferative and thus have an elevated protein synthesis thereby becoming vulnerable to proteasome inhibitors. As already explained, HDAC6 is a key factor for the formation of the aggresome and autophagic clearance of misfolded protein. The aggresome pathway is the "emergency" pathway, active when the UPS is overwhelmed or inhibited. By inhibiting both pathways, misfolded proteins accumulate, increasing cellular stress and inducing apoptosis. Moreover, the use of dual or multi-targeting drugs has gained increased consideration in drug discovery and is called polypharmacology[111]. Despite the success of combinational therapy, polypharmacology can offer some potential advantages such as less unforeseeable drug-drug interaction, or dynamic pharmacokinetic and pharmacological issues that during combinational therapy could lead to unexpected side effects or less treatment efficacy[112]. Another advantage would be the simultaneous presence of both inhibitors at the intended region of interest[111]. One example of such dual inhibitors is RTS-V, the first-in-class dual HDAC-proteasome inhibitor[113]. It was demonstrated that RTS-V has potent anti-cancer properties against leukemia and multiple myeloma cell lines as well as primary patient-derived leukemia cells. The anticancer properties were achieved by the simultaneous inhibition of the UPS and aggresome formation at the same time, which will lead to cellular stress through the accumulation of misfolded protein and finally the induction of apoptosis[113]. Another example is the dual HDAC-HSP90 inhibitor, MPT0G49[114]. MPT0G49 was able to suppress the expression of oncogenic pathways in acute leukemia and induced apoptosis and cell cycle arrest[114]. Taken together, different drug combinations have been tested in the past along with pan or isoform-specific HDAC inhibitors.

1.11 Proteolysis targeting Chimera (PROTAC)

Next to small molecule inhibitors, there are other strategies to target HDAC6. Recently proteolysis targeting chimeras (PROTAC) are getting a lot of attention[115,116]. PROTACs are heterobifunctional small molecules that have two active domains that are covalently linked by a linker structure. One of the active domains targets the protein of interest (POI) and the other active domains targets an E3 ubiquitin ligase. This way the E3 ligase will come close to the POI and induce ubiquitination, which will lead to the proteasomal degradation of the tagged POI (fig. 6). This is a promising technology as it can circumvent some of the drawbacks of small molecular inhibitors. Most importantly, PROTACs can target any side of the POI, in contrast to small molecules that need to target some functional important sites of the POI, like the active side, to be effective. Using PROTACs it becomes possible to target "undruggable" targets that e.g. have only scaffolding or structural functions and lack enzymatic activity[116]. Another advantage is that PROTACs can overcome drug resistance as they can be designed based on neutral binders that bind anywhere on the target protein, which gives new opportunities to target mutation variants [115,116]. Furthermore, another advantage is the complete removal of the target protein by target binding rather than function disruption as is usually the case for small molecule inhibitors. Many therapy-induced resistance mechanisms can be circumvented this way, such as 1) drug binding impairment by point mutations, 2) mutations resulting in target constitutive activation, 3) mutations inducing binding domain conformation changes, 4) target protein overexpression and 7) splicing mutations.
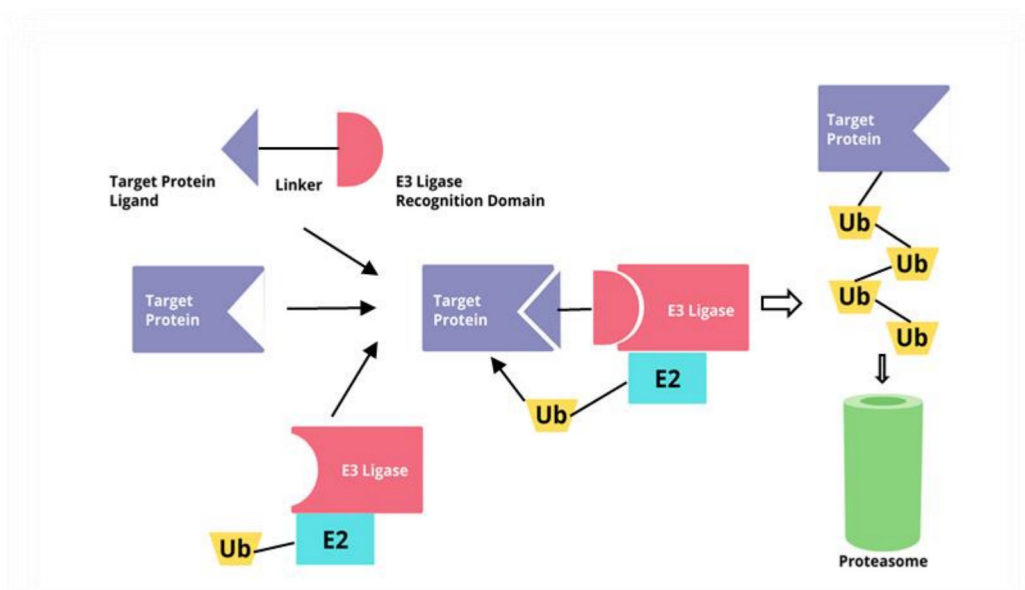
Figure 6: Mechanism of PROTAC-based degradation of the POI. The bifunctional molecule can bind the POI and E3 ligase complex and thereby bringing both targets nearby. The E3 ligase can then ubiquitinate the POI and mark it for proteasomal degradation.[116]

1.12 Aim of the thesis

HDAC inhibitors (HDACi), like panobinostat, vorinostat or belinostat are already applied in the clinic for hematological malignancies. However, these inhibitors are unselective and target a wide range of HDACs that are involved in many different important cellular mechanisms, and thus evoke a variety of severe forms of side effects. Thus, developing HDACi that targets specific isozymes and therefore reduces the side effects but still be clinically effective is a promising strategy. HDAC6 is a unique HDAC in the sense that is mainly localized in the cytoplasm and has non-histone proteins as substrate. Furthermore, it has also a targetable distinct structure, and a wider and shallow entrance to the binding site, compared to other HDAC isozymes. These features make HDAC6 a suitable target as a potential therapeutic target in hematologic malignancies, like pediatric ALL or AML. Other investigators showed that HDAC6i might be a potential target as it regulates cancer-associated signaling pathways[98,117]. Besides understanding the role of HDAC6 in leukemogenesis, this study aims to develop novel HDACi together with our collaboration partners, the working group of Prof. Dr. T. Kurz (Institut für Pharmazeutische und Medizinische Chemie Heinrich-Heine-Universität Düsseldorf) and the working group of Prof. Dr. F. K. Hansen (Pharmaceutical and Cell Biological Chemistry, Pharmaceutical Institute, University of Bonn).

Aim 1 is the identification of the effectiveness and selectivity of the compounds, synthesized by our chemical collaboration partners. First, selective HDAC6 inhibitors were characterized, going further to less selective, so-called, preferential HDAC6 inhibitors and finally characterizing pan-HDAC inhibitors. Furthermore, I investigate potential synergistic partners for these HDAC6 selective inhibitors. Therefore, our in-house drug screen platform was utilized to screen a large cohort of leukemic cell lines against the new experimental inhibitors and compare them to commercially available HDAC6i, and further use biochemical approaches to validate the cellular specificity of the lead structures. Next to this, I utilize the drug screen platform to investigate potential synergistic partners by printing two compounds in a semi-automated manner on a drug screen plate and analyzing their interactions.

Aim 2 is to analyze the molecular mechanism of HDAC6 inhibition. Therefore, a promising drug candidate will be further elaborated by analyzing the changes in the transcriptome of treated leukemic cells to identify its mechanism of action. In addition to this, I analyze the effect of HDAC6i by utilizing HDAC6 KO cell lines to identify the role of HDAC6 in the mechanism of actions of these new lead inhibitors. Moreover, an HDAC6 KO cell line model was utilized to identify potential synergistic drugs by screening the HDAC6 KO cell line against a large cohort of drugs by high-throughput drug screening.

With this approach, I hope to identify new compounds with potential therapeutic relevance for future clinical applications.

AIM 1: *In vitro* Characterization of novel HDACi/HDAC6i

- Highly selective tetrazole-capped HDAC6i: Compound **6l**
- Selective HDAC6i: Nexturastat A analogues **4a**, **4b**, **4c** and **4d**
- Preferential HDAC6i: Alkoxyurea-based Vorinostat analog **KSK64**
- HDAC class I/IIb inhibitors: Alkoxyamide **8a** and **8e**
- Fluorinated peptoid-based pan-HDACi: Compound **10h**
    - Evaluation of the *in-vivo* activity of compound **10h**
- In vitro characterization of the HDAC6 **PROTAC 4**

Aim 2: Analyzing the molecular mechanism of HDAC6 inhibition in leukemic cells

- RNAseq to reveal molecular changes after HDAC6i treatment
- Utilizing HDAC6 KD cell line models to reveal the biological importance of HDAC inhibition
- Utilizing HDAC6 KO leukemic cell line models to find potential synergistic partners

2. Materials and Methods

2.1 Consumables, Devices, and Cells

Table 2: List of used devices

Machine	Manufacturer
Centrifuge Haraeus Fresco 21	Thermo Fisher Scientific (Schwerte, Germany)
Centrifuge Multifuge 4KR	Thermo Fisher Scientific (Schwerte, Germany)
Centrifuge Pico Microcentrifuge	Themo Fisher Scientific (Schwerte, Germany)
CFX384 Touch Real-Time PCR Detection System	Bio-Rad (Düsseldorf, Germany)
CO_2 Incubator	Binder (Tuttlingen, Germany)
CytoFlex Flow Cytometer	Beckman Coulter (Krefeld, Germany)
D300e Digital Dispenser	Tecan (Crailsheim, Germany)
Freezer (-20°C)	Liebherr (Kirchdorf an der Iller, Germany)
Freezer (-80°C)	Thermo Fisher Scientific (Schwerte, Germany)
Fridge (4°C)	Liebherr (Kirchdorf an der Iller, Germany)
Incubator (37°C)	Thermo Fisher Scientific (Schwerte, Germany)
IVIS Spectrum	PerkinElmer (Rodgau, Germany)
Jess Proteinsimple	Bio-Techne (Wiesbaden, Germany)
LAS-300 Imaging System	Fujifilm (Düsseldorf, Germany)
Maxwell RSC instruments	Promega (Mannheim, Germany)
Mini Centrifuge	Bio-Rad (Düsseldorf, Germany)
Multidrop Combi Reagent Dispenser	Themo Fisher Scientific (Schwerte, Germany)
NanoDrop Spectrophotometer ND-1000	Peqlab (Erlangen, Germany)
Precision Balance	KERN & SOHN (Balingen, Germany)
Spark 10M Multimode microplate reader	Tecan (Crailsheim, Germany)
Thermo Block	Eppendorf (Hamburg, Germany)
Vi-Cell XR	Beckman Coulter (Krefeld, Germany)
Vortex Genie	neoLab (Heidelberg, Germany)
Water Bath	GFL (Burgwedel, Germany)

Table 3: List of used chemicals

Consumable	Distributor
Ammonium persulfate (APS)	Merck (Darmstadt, Germany)

Bromphenol blue	Carl Roth (Karlsruhe, Germany)
BSA powder	Carl Roth (Karlsruhe, Germany)
DTT	Sigma-Aldrich (Taufkirchen, Germany)
Glycerol	Sigma-Aldrich (Taufkirchen, Germany)
Glycine	Sigma-Aldrich (Taufkirchen, Germany)
NaCl	Thermo Fisher Scientific (Schwerte, Germany)
PEG300	Merck (Darmstadt, Germany)
Saline	G-Bioscoence (St. Louis, USA)
SDS	Carl Roth (Karlsruhe, Germany)
TEMED	VWR (Darmstadt, Germany)
Tris	Sigma-Aldrich (Taufkirchen, Germany)
Triton X-100	Thermo Fisher Scientific (Schwerte, Germany)
Tween 20	Sigma-Aldrich (Taufkirchen, Germany)

Table 4: List of consumables for cell culture

Consumable	Distributor
6 well-culture plate	Greiner Bio-One(Frickenhausen, Germany)
Annexin V Buffer	BD Bioscience (Heidelberg, Germany)
Caspase-Glo® 3/7 Assay System	Promega (Mannheim, Germany)
Cell culture flask T225	Greiner Bio-One(Frickenhausen, Germany)
Cell culture flask T25	Greiner Bio-One(Frickenhausen, Germany)
Cell culture flask T75	Greiner Bio-One(Frickenhausen, Germany)
Cell strainer	pluriSelect (Leipzig, Germany)
Cryoconservation tubes	Corning (Wiesbaden, Germany)
Dimethyl sulfoxid (DMSO)	Sigma-Aldrich (Taufkirchen, Germany)
Disposables pipettes	Corning (Wiesbaden, Germany)
DMEM Medium	Thermo Fisher Scientific (Schwerte, Germany)
Doxycyclin	Thermo Fisher Scientific (Schwerte, Germany)
Dulbecco's phosphate-buffered saline (PBS)	Sigma-Aldrich (Taufkirchen, Germany)
Erythrocyte lysis buffer	house-made
Falcon	Greiner Bio-One(Frickenhausen, Germany)

HDAC-Glo™ Class IIa Assay	Promega (Mannheim, Germany)
HDAC-Glo™ I/II Assay	Promega (Mannheim, Germany)
Heat inactivated Detal Bovine Serum	Sigma-Aldrich (Taufkirchen, Germany)
Parafilm	Bemis (Oshkosh, USA)
Penicillin (10.1000 U/ml) - Streptomycin (10mg/ml) (P/S)	Sigma-Aldrich (Taufkirchen, Germany)
Puromycin	Thermo Fisher Scientific (Schwerte, Germany)
RPMI 1640 Medium	Thermo Fisher Scientific (Schwerte, Germany)
Sodium pyruvate	Thermo Fisher Scientific (Schwerte, Germany)
TrypLE Express Phenol Red	Thermo Fisher Scientific (Schwerte, Germany)

Table 5: List of consumables for rt-qPCR

Consumable	Distributor
96-Well rt-qPCR Plate white, clear bottom	Bio-Rad (Düsseldorf, Germany)
dNTPs 25 µmol	Promega (Mannheim, Germany)
Maxwell® RSC simplyRNA Cells Kit	Promega (Mannheim, Germany)
Nuclease free water	Thermo Fisher Scientific (Schwerte, Germany)
Power SYBR Green Mastermix	Thermo Fisher Scientific (Schwerte, Germany)
Reverse Transcriptase Kit	Qiagen (Hilden, Germany)
RNAse away	Thermo Fisher Scientific (Schwerte, Germany)
RNasin plus, Rnase inhibitor 40 u/µL	Promega (Mannheim, Germany)
PCR Strip-Tubes 0.1 mL	Eppendorf (Hamburg, Germany)
0.5 mL PCR Tubes	Promega (Mannheim, Germany)

Table 6: List of consumables for drug screening

Consumable	Distributor
CellTiter-Glo Luminscent Cell Viability Assay	Promega (Mannheim, Germany)
D4+ cassette	Tecan (Crailsheim, germany)
Multidrop tubing	Thermo Fisher Scientific (Schwerte, Germany)
Multidrop tubing small	Thermo Fisher Scientific (Schwerte, Germany)
T8+ cassette	Tecan (Crailsheim, germany)
White 1536 well plates, sterile, TC treated	Corning (Wiesbaden, Germany)

White 384 well plates, sterile, TC treated	Corning (Wiesbaden, Germany)

Table 7: List of software used for experiments

Software	Distributor
CFX Manager	Bio-Rad Laboratories (Feldkirchen, Germany)
Combenefit (version2.021)	Cancer Research UK Cambridge Institute
CytExpert	Beckman Coulter (Krefeld, Germany)
D300e control (version 3.3.1)	Tecan (Crailsheim)
D300e merge	Tecan (Crailsheim)
GraphPad Prism 5 (version 5.03)	GraphPad Software (San Diego, USA)
Microsoft Office	Microsoft (Redmond, USA)
Spark control	Tecan (Crailsheim, Germany)

Table 8: List of cell lines used for experiments

Cell line	Entity	Medium
697	B-ALL	RPMI 1640 + 10% FCS + 1% P/S
BA/F3-E255K	murine pro-B cell	RPMI 1640 + 10% FCS + 10 ng/ml mouse IL-3 + 1% P/S
BA/F3-M351T	murine pro-B cell	RPMI 1640 + 10% FCS + 10 ng/ml mouse IL-3 + 1% P/S
BA/F3-T315I	murine pro-B cell	RPMI 1640 + 10% FCS + 10 ng/ml mouse IL-3 + 1% P/S
CMK	AML	RPMI 1640 + 20% FCS + 1% P/S
HAL-01	B-ALL	RPMI 1640 + 10% FCS + 1% P/S
HEK293T	normal human embryonic kidney cells	DMEM + 10% FCS + 1% P/S
HEL	erythroblast	RPMI 1640 + 10% FCS + 1% P/S
HL60	AML	RPMI 1640 + 10% FCS + 1% P/S
HL60-IMr	AML	RPMI 1640 + 10% FCS + 1% P/S
HSB-2	T-ALL	RPMI 1640 + 20% FCS + 1% P/S

Jurkat	T-ALL	RPMI 1640 + 20% FCS + 1% P/S
K562	CML	RPMI 1640 + 10% FCS + 1% P/S
K562-IMr	CML	RPMI 1640 + 10% FCS + 1% P/S
Kasumi-1	AML	RPMI 1640 + 20% FCS + 1% P/S
KCL22	CML	RPMI 1640 + 10% FCS + 1% P/S
KCL22-IMr	CML	RPMI 1640 + 10% FCS + 1% P/S
MOLM13	AML	RPMI 1640 + 20% FCS + 1% P/S
MOLT-4	T-ALL	RPMI 1640 + 20% FCS + 1% P/S
MUTZ5	B-ALL	RPMI 1640 + 10% FCS + 1% P/S
MV4-11	AML	RPMI 1640 + 20% FCS + 1% P/S
Nalm6	B-ALL	RPMI 1640 + 10% FCS + 1% P/S
REH	B-ALL	RPMI 1640 + 10% FCS + 1% P/S
SEM	B-ALL	RPMI 1640 + 10% FCS + 1% P/S
SUP-B15	B-ALL	McCoy's + 20 % FCS +1% P/S
SUP-B15-IMr	B-ALL	McCoy's + 20 % FCS +1% P/S
TALL-1	T-ALL	RPMI 1640 + 20% FCS + 1% P/S
THP1	AML	RPMI 1640 + 20% FCS + 1% P/S
THP1-BTZr	AML	RPMI 1640 + 20% FCS + 1% P/S

Table 9: List of compounds used for 1536 well plate drug screening

#	Inhibitor	Target	FDA approved
1	DMSO		
2	5-Azacytidine	Antimetabolites	Yes
3	5-Fluorouracil	Antimetabolites	Yes
4	6-Mercaptopurine (Monohydrate)	Antimetabolites	Yes
5	6-Thioguanine	Antimetabolites	Yes
6	Clofarabine	Antimetabolites	Yes
7	Cytarabine (Hydrochlorid)	Antimetabolites	Yes
8	Cyclocytidine HCL	Antimetabolites	No
9	Fludarabine (phosphate)	Antimetabolites	Yes
10	Nelarabine	Antimetabolites	Yes
11	Gemcitabine	Antimetabolites	Yes
12	Methotrexate	Antimetabolites	Yes
13	Pentostatin	Antimetabolites	Yes
14	Cladribine	Antimetabolites	Yes
15	Dacarbazine	Antimetabolites/ DNA alkylator/crosslinker;	Yes
16	Vinblastine (sulfate)	Antimitotics	Yes
17	Vincristine (sulfate)	Antimitotics	Yes
18	Busulfan	Alkylating agents	Yes
19	Carmustine	Alkylating agents	Yes
20	Cyclophosphamide (Clafen) (Monohydrate)	Alkylating agents	Yes
21	Lomustine	Alkylating agents	Yes
22	Cisplatin	Alkylating agents	Yes
23	Oxaliplatin	Alkylating agents	Yes
24	Procarbazine (Hydrochloride)	Alkylating agents	Yes
25	Thio-TEPA	DNA alkylator/crosslinker;	Yes
26	Temozolomide	Alkylating agents	Yes
27	Chlorambucil	Alkylating agents	Yes
28	Bendamustine (hydrochloride)	Alkylating agents	Yes
29	Mechlorethamine hydrochloride	DNA alkylator/crosslinker;	Yes
30	Epirubicin (hydrochloride)	Topoisomerase inhibitors	Yes
31	Etoposide	Topoisomerase inhibitors	Yes
32	Idarubicin (hydrochloride)	Topoisomerase inhibitors	Yes
33	Mitoxantrone (dihydrochloride)	Topoisomerase inhibitors	Yes
34	Teniposide	Topoisomerase inhibitors	Yes
35	Daunorubicin (Hydrochloride)	Topoisomerase inhibitors	Yes

36	Doxorubicin (hydrochloride)	Topoisomerase inhibitors	Yes
37	Amsacrine (Hydochlorid)	Topoisomerase inhibitors	Yes
38	Dexamethasone	GC/GCR complex	Yes
39	Prednisone	GC/GCR complex	Yes
40	Prednisolone (Acetate)	GC/GCR complex	Yes
41	Belinostat	HDACi	Yes
42	DMSO		
43	CI-994 (Tacedinaline)	HDACi	No
44	Panobinostat	HDACi	Yes
45	Romidepsin	HDACi	Yes
46	Quisinostat	HDACi	No
47	Tubastatin A (Hydrochloride)	HDAC6i	No
48	Givinostat (ITF2357)	HDACi	No
49	Vorinostat	HDACi	Yes
50	Entinostat	HDACi	No
51	Ricolinostat	HDAC6i	No
52	Pracinostat	HDACi	Yes
53	Abexinostat	HDACi	No
54	MPK544	HDACi	No
55	EPZ-6438 (Tazemetostat)	EZH2i/HMTasei	No
56	GSK126	EZH2i/HMTasei	No
57	GSK343	EZH2i/HMTasei	No
58	GSK 525762A	BET bromodomain;	No
59	Paclitaxel	Antimetabolites	
60	JQ1	BET bromodomain	No
61	Bortezomib	Proteasome inhibitor	Yes
62	MLN-9708 (Citrate)	Proteasome inhibitor	No
63	Carfilzomib	Proteasome inhibitor	No
64	Ganetespib	HSP90i	No
65	PUH71	HSP90i	No
66	AUY922 (LUMINESPIB)	HSP90i	No
67	NVP-HSP990	HSP90i	No
68	EC144	HSP90i	No
69	PF-04929113	HSP90i	No
70	BIIB021	HSP90i	No
71	VWK627	HSP90i	No
72	VWK603	HSP90i	No
73	Alisertib	Aurora Kinase A	No
74	Aurora A Inhibitor I	Aurora Kinase A inhibitor	No
75	MLN8054	Aurora Kinase A inhibitor	No
76	MK-5108 (VX-689)	Aurora Kinase A inhibitor	No
77	Danusertib	Aurora Kinase A	No
78	Barasertib	Aurora kinase B	No
79	Volasertib	Polo-like Kinase (PLK);	Yes

80	BI2536	PLK	No
81	LEE011 (Ribociclib)	CDK;	Yes
82	LY2835219 (Abemaciclib)	CDK;	Yes
83	Dinaciclib	CDK;	No
84	SY-1365-THZ1	cdk7i	No
85	Cabozantinib (S-malate)	VEGFR	Yes
86	Erlotinib	EGFR	Yes
87	Gefitinib (Hydrochlorid)	EGFR	Yes
88	Sunitinib (malate)	PDGFR; VEGFR	Yes
89	Axitinib	VEGFR	Yes
90	Midostaurin	PKC, vegfr2, pdgfr, FLT3	Yes
91	Foretinib	VEGFR2; c-MET	No
92	Dovitinib	FLT3; PDGFR; VEGFR; c-Kit;	No
93	Crenolanib	FLT3; PDGFR	No
94	Pexidartinib	FLT3, KIT, CSF1R	Yes
95	Lestaurtinib	FLT3	No
96	Quizartinib	FLT3;	No
97	KW-2449	FLT3	No
98	Pacritinib	FLT3; JAK;	No
99	Gilteritinib	FLT3/AXL	Yes
100	Buparlisib	PI3K	No
101	Idelalisib	PI3K;	Yes
102	Pictilisib GDC-0941	Pi3K	No
103	GSK2636771	PI3K/AKT	No
104	Alpelisib	PI3K/AKT	Yes
105	Dactolisib (BEZ235)	PI3K, mTOR	No
106	GSK2110183 (Afuresertib)	AKT;	No
107	Ro 08-2750		
108	ARQ-092 (Miransertib)	AKT	No
109	Ipatasertib (GDC-0068)	AKT;	Yes
110	Deforolimus	mTOR;	Yes
111	Everolimus	mTOR;	Yes
112	Rapamycin	mTOR;	Yes
113	Temsirolimus	mTOR;	Yes
114	PF-04691502	mTOR; PI3K;	No
115	INK 128 (MLN0128)	mTORC1/2	No
116	BMS-911543	JAK;	No
117	AT9283	JAK;	No
118	Baricitinib (phosphate)	JAK;	Yes
119	CYT387 (Momelotinib)	JAK;	Yes
120	Ruxolitinib	JAK;	Yes
121	Tofacitinib (citrate)	JAK;	Yes
122	Fedratinib (TG101348)	JAK; FLT3	Yes
123	Gandotinib	JAK mutant (JAK2V617F)	No

124	Tipifarnib	Farnesyl Transferase; Ras inhibitor	Yes
125	Lonafarnib	Rasi	No
126	Salirasib	Rasi	Yes
127	Dabrafenib (Mesylate)	Raf inhibitor	Yes
128	Sorafenib (Tosylate)	Raf inhibitor	Yes
129	Regorafenib (Monohydrate)	Raf inhibitor	Yes
130	Vemurafenib	Raf inhibitor	Yes
131	LGX818 (Encorafenib)	Rafi	Yes
132	Cobimetinib	MEK;	Yes
133	MEK162 (Binimetinib)	MEK;	Yes
134	Selumetinib	MEK;	No
135	Trametinib	MEK;	Yes
136	PD0325901	MEK	No
137	PD184352	MEK	No
138	Pimasertib	MEK	No
139	SHP099 (Dihydrochloride)	Ras-ERK	No
140	SCH772984	ERK1/2	No
141	GDC-0994	ERK	No
142	Losmapimod	p38 MAPK;	No
143	Zanubrutinib	BTKi	Yes
144	Tirabrutinib	BTKi	No
145	Spebrutinib	BTKi	No
146	Ibrutinib	(Ibruvica) 'Btk;	Yes
147	Imatinib (Mesylate)	Bcr-Abl inhibitor	Yes
148	Radotinib	Bcr-Abl inhibitor	No
149	Nilotinib (Hydrochlorid)	Bcr-Abl;	Yes
150	Ponatinib	Bcr-Abl; FGFR; FLT3; VEGFR;	Yes
151	Bosutinib	Bcr-Abl; Src;	Yes
152	Dasatinib (Hydrochlorid)	Bcr-Abl; Src;	Yes
153	Rebastinib (DCC-2036)	Bcr-Abl	No
154	Saracatinib	Src; Abl	No
155	Bafetinib	Bcr-Abl; Src;	Yes
156	Staurosporine	Multiple non-selective inhibitors of protein kinases	No
157	BSI-201 (Iniparib)	PARP;	No
158	Olaparib	PARP;	Yes
159	Rucaparib (phosphate)	PARP;	Yes
160	Veliparib (dihydrochloride)	PARP;	Yes
161	ABT-199 (Venetoclax)	Bcl-2 Family;	Yes
162	Obatoclax (Mesylate)	Bcl-2 Family;	No
163	Y-27632 (Dihydrochloride)	ROCK	No
164	QNZ (EVP4593)	NF-κBi	No

165	Omaveloxolone	NF-κBi	No
166	Enasidenib	isocitrate dehydrogenase type 2 (IDH2)	Yes
167	Ivosidenib	IDH1	Yes
168	Birinapant	XIAPi and cIAP1i	No
169	Tariquidar	P-glycoprotein;	No
170	Enzastaurin	PKC;	Yes
171	KYA1797K	wnt/catenin	No
172	Selinexor	CRM1 inhibitor	Yes
173	AZD6738	ATM/ATRi	No
174	Omacetaxine Mepesuccinate (Homoharringtonine)	Ribosome Inhibitor	Yes
175	Actinomycin D	Antibacterial	Yes
176	DMSO		
177	Bexarotene	Retinoid Inhibitor	Yes
178	PND-1186	FAK inhibitor	No
179	Nintedanib (BIBF1120)	LCK inhibitor	Yes
180	BAY 80-6946 (Copanlisib)	PI3K	Yes
181	Palbociclib	cdki	Yes

Table 10: List of consumables for protein analysis

Consumable	Distributor
Blottingmembrane Amersham Hybound P, PVDF, 0.45 µm	GE Healthcare (Solingen, Germany)
Blottingmembrane Amersham Protran, Nitrocellulose, 0.45 µm	GE Healthcare (Solingen, Germany)
BSA	Sigma-Aldrich (Taufkirchen, Germany)
Gel Blotting paper Whatman	GE Healthcare (Solingen, Germany)
PhosphosSTOP	Roche (Mannheim, Germany)
Protease Inhibitor	Roche (Mannheim, Germany)
Protein ladder (PageRuler Prestained)	Thermo Fisher Scientific (Schwerte, Germany)
RIPA lysis buffer	Thermo Fisher Scientific (Schwerte, Germany)

Table 11: List of Buffer used for western blotting

Buffer/Solution	Composition	
Stack buffer	·	0.5 M Tris/HCL pH 6.8
	·	0.4 % (w/v) SDS
	·	In dH2O
Separation buffer	·	1.5 M Tris/HCL pH 8.8
	·	0.4 % (w/v) SDS

	· in dH2O
SDS gel running buffer	· 0.05 M Tris · 0.2 M Glycin · In dH2O
Transfer buffer (WB)	· 25 mM Tris · 150 mM Glycin · 10 % MeOH · 0.05 % SDS · In dH2O
Laemmli buffer 5X	· 20% SDS · 1M Tris/HCL pH 6.8 · 0.25 % Bromophenol blue · 0.5 M DTT · 50 % Glycerol · In dH2O
TBS-T	· 13.7 mM NaCl · 2.7 mM KCL · 80.9 mM Na2HPO4 · 1.5 mM KH2PO4 · pH 7.4 · In dH2O · 0.5 % Tween 20
Blocking buffer	· TBS-T · 5 % BSA

Table 12: List of primary antibodies used for western blotting

Name	Species	Dilution	Order NR	Company
Ac-Alphatubulin	Rabbit	1:1000	5335S	Cell Signaling Technology (Frankfurt, Germany)
Acetyl Histone H3	Rabbit	1:1000	9677S	Cell Signaling Technology (Frankfurt, Germany)
Alpha Tubulin	Rabbit	1:1000	2144S	Cell Signaling Technology (Frankfurt, Germany)
Beta-actin	Mouse	1:10000	A5316	Sigma-Aldrich (Taufkirchen, Germany)
GAPDH	Rabbit	1:1000	2118S	Cell Signaling Technology (Frankfurt, Germany)
HDAC1	Mouse	1:1000	5356S	Cell Signaling Technology

				(Frankfurt, Germany)
HDAC6	Rabbit	1:1000	7558S	Cell Signaling Technology (Frankfurt, Germany)
Histone H3	Rabbit	1:1000	2650	Cell Signaling Technology (Frankfurt, Germany)
HSP90	Rabbit	1:1000	4877S	Cell Signaling Technology (Frankfurt, Germany)

Table 13: List of HRP-conjugated secondary antibodies used for western blotting

Name	Species	Dilution	Order NR	Company
Anti-rabbit	Goat	1:2000	7074S	Cell Signaling Technology (Frankfurt, Germany)
Anti-mouse	Horse	1:2000	7076S	Cell Signaling Technology (Frankfurt, Germany)

Table 14: List of consumables for flow cytometry

Name	Conjugate	Species	Dilution	Order NR
CD45 – APC	APC	Human	1:100	555485
CD45 – APC-AF700	AF700	Mouse	1:100	560693
Annexin V – APC	APC	Human	1:40	550474
Annexin V – FITC	FITC	Human	1:40	556419
Propidium Iodide	-	-	-	556463

2.2 Methods:

2.2.1 Cell culture

All cell lines were cultured at 37 °C at 5% CO_2 and passaged at least twice a week dependent on the growth rate in dilutions of 1:5 – 1:20 with their respective medium. The cultured cells were approved by short-tandem report profiling and controlled for mycoplasma contamination by PCR. Suspension cells were cultured in either T-25, T-75, or T-225 culture flasks that were kept vertically. Cells were cryopreserved by pelleting them at 400 g for 5 min and resuspending in 1 ml of freezing medium (90% FCS + 10% DMSO). Afterward, cells were immediately transferred to a cryo box filled with isopropanol and stored for at least 24 h at -80 °C to ensure proper freezing conditions, and the frozen cells were transferred into liquid nitrogen tanks where they were kept in the gas phase. For the thawing of cryopreserved cells, the frozen cells were warmed in the water bath (37 °C) and 10 ml fresh medium was added to the thawed cells. Next, cells were pelleted for 5 min at 400 g and afterward resuspended in a fresh medium. After 24 h, cells were pelleted again and resuspended in a fresh medium to ensure the complete removal of DMSO residues. Generally, it was taken care of during the cryopreservation or thawing process that cells were kept as short as possible in 10% of DMSO to circumvent harmful conditions. Patient-derived cells were, dependent on the individual needs, cultured on mesenchymal stem cells (MSCs) to ensure proper culture conditions.

2.2.2 CellTiter-Glo® Luminescent Cell Viability Assay (Drug Screen)

CellTiter-Glo® Luminescent Cell viability assay was performed following the manufacturer's guidelines (Promega) to determine the IC_{50} concentrations of all tested compounds in different cell lines. The IC50 concentration is defined as a half-maximal inhibitory concentration at which the tested drug inhibits 50% of the initial activity (viability). DMSO-treated cells served as a negative control for the normalization of the drug effect.

2.2.2.1 Printing drugs:

Before printing the test compounds on the drug screen plates all compounds were dissolved in DMSO with a concentration of 10 mM. The drug screen plates were printed by using a digital dispenser and at least six concentrations from 0.005 µM to 10 or 25 µM with a logarithmic distribution, if not stated otherwise. The inhibitors were printed

in triplicates on the drug screen plates (384 wells, Corning). All wells were normalized to the highest used concentration of DMSO on the plate by adding DMSO into each well. The two outer layers of wells were not used to circumvent plate effects, like faster evaporation of the outer layers of the drug screen plate during the 72 h of incubation at 37 °C. After printing, the plates were wrapped in parafilm and stored at -80 °C for at least 24 h before use to ensure that every plate had one freeze and thaw cycle.

2.2.2.2 Cell seeding:

The frozen plates were taken out 30 min before cells were seeded on them to ensure proper thawing of the frozen inhibitors. The cells were counted with VI-Cell XR cell counter and seeded only when they had > 90% viability directly before the seeding procedure. For the leukemic cell lines, 40.000 cells/ml were used as cell concentration as this was the concentration that was in the linear range for all tested cell lines. Patient cells or primary cells were printed with 500.000 cells /ml as they tend to die if printed at lower cell numbers. The cells were seeded in 30 µl of the appropriate medium using the semi-automated Multidrop Combi Reagent dispenser. After the cell seeding, the drug screen plates were incubated for 72 h under normal cell culture conditions.

2.2.2.3 Readout:

After 72 h of incubation under normal cell culture conditions, the plates were taken out of the incubator and 30 µl of the Celltiter-Glo® reagent was added to each well using the semi-automated Multidrop Combi Reagent dispenser and shortly shaken to ensure proper lysis of the cells. Afterward, the plates were stored for 10 min in the dark before the measurement. The rate-limiting step of the Celltiter-Glo® reaction is the availability of ATP. Under the presence of ATP, $Mg^{2+,}$ and oxygen, the luciferase catalysis the mono-oxygenation of luciferin to oxyluciferin, which gives a luminescent signal, which is proportional to the amount of ATP, which in turn is proportional to the number of viable cells. The luminescent signal was measured using the Spark microplate reader.

2.2.2.4 Combinatorial drug screening (synergy screen):

The compounds were printed on white 384-well plates (Thermo Fisher Scientific, Waltham, USA) with increasing concentrations in a dose-response 10x10 matrices by using a digital dispenser (D300e, Tecan, Männedorf, Switzerland). The inhibitors were printed in a logarithmic distribution with the indicated concentrations. Cell viability was

monitored after 72 h using CellTiter-Glo luminescent assay (as described above), using a microplate reader (Spark, Tecan). The Bliss synergy scores were determined by using the Combenefit synergy analysis software.

2.2.3 Cellular HDAC activity analysis

The compounds were printed on white 384-well plates (Thermo Fisher Scientific, Waltham, USA) with increasing concentrations (5nM - 10µM) by using a digital dispenser (D300e, Tecan, Männedorf, Switzerland). Cells were added to the plate and incubated for 30 min. The HDAC-Glo class I/II and HDAC-Glo class IIa Assay and Screening System (Promega) were used, following the manufacturer´s instructions. The HDAC activity for the compounds was determined by plotting raw data (normalized to controls) using a sigmoid dose curve and nonlinear regression (GraphPad Prism Inc., San Diego, CA).

2.2.4 RNA isolation, cDNA synthesis, and quantitative real-time PCR

The extraction of RNA was performed using the Maxwell RSC Instrument according to the manufacturer's guidelines. Briefly, 500.00 cells were used for the RNA extraction and the procedure is based on the binding of nucleic acids on magnetic beads followed by washing steps to remove DNA or protein contamination. After RNA isolation, it was eluted in RNase and DNase-free ddH$_2$O and stored at -80 °C. Afterward, the RNA concertation was measured using a spectrophotometer (Nanodrop) according to the manufacturer's guidelines. The cDNA synthesis was performed using the reverse transcription kit from Qiagen following the manufacturer's guidelines. The Quantitative real-time PCR was performed using the CFX384 Touch™ Real-Time PCR Detection System and Power SYBR Green Mastermix.

Table 15: rt-qPCR mix for one well in 384-well plate

Volume	Reagent
5 µL	Power SYBR Green Mastermix
0.5 µL	Primer Mix
3.5 µL	H2O
1 µL	cDNA

Table 16: Protocol settings for rt-qPCR

Step	Temperature	Time

1	50°C	2 min
2	95°C	10 min
3	95°C	15 s
4	60°C	1 min
		Go to step 3, 39x

2.2.5 Protein analysis

2.2.5.1 Cell lysis, protein isolation, and quantification

Cells (0.5×10^6 cells/ml) were treated with the indicated concentration of the compound or vehicle (DMSO) for 24 h under standard culture conditions. Cell pellets were lysed with 300 µl RIPA buffer, supplemented with protease and phosphatase inhibitor mini tablets, according to manufacturer's guidelines, and incubated for 20 min on ice. Afterward, the lysates were centrifuged at 14,000 g for 30 min at 4°C to sediment cell debris and DNA. The supernatant, containing the protein was further quantified using the BSA assay according to the manufacturer's guidelines.

2.2.5.2 SDS-polyacrylamide gel electrophoresis (SDS-PAGE) and Western Blotting

The gels for the SDS-PAGE were prepared in-house according to the recipes in table 17. The gel consists of two different parts, the stacking gel, and the separation gel. First, the separation gel was added to the gel chamber and covered with isopropanol to circumvent the formation of air bubbles. After the separation gel was polymerized, the isopropanol was removed and on top of the separation gel, the stacking gel was poured. A 15-slot comb was used to cover the stacking gel and form the pockets to load the protein samples. After the stacking gel has polymerized, the prepared gels can be used directly or stored at 4°C. For storage at 4°C, the gels were covered in wet tissues to circumvent the drying out of the gels.

Before the protein samples were loaded into the gel pockets, they were mixed with 5X Laemmli-buffer (1:5) and incubated at 95°C for 5 min to denature the proteins. Afterward, protein samples were used directly for SDS-PAGE or were stored at -20°C. For the SDS-PAGE, 20 µg of protein samples were loaded into the gel pockets and separated by electric force based on their size. The electrophoresis was performed at 50 mA for approximately 1 h.

Table 17: a) Formulation for four stack gels **b)** Formulation for four separation gels

a)

Substance	Acrylamide	dH2O	Stack buffer	APS	TEMED
Amount	1.5 ml	6 ml	2.5 ml	0.2 ml	0.05 ml

b)

Substance	Acrylamide	dH2O	Stack buffer	APS	TEMED
Amount	1.5 ml	6 ml	2.5 ml	0.2 ml	0.05 ml

After the protein separation by SDS-PAGE, the proteins were transferred to nitrocellulose or polyvinylidene fluoride (PVDF) membranes by electric force in a blotting apparatus for 120 min at 100V. Afterward, the membranes were blocked in 5 % BSA in TBS-T for 45 min. Next, the membranes were incubated overnight with the primary antibodies at 4°C. After the incubation, the membranes were washed three times for 10 min with TBS-T. After washing, the membranes were incubated with horseradish peroxidase (HRP)-conjugated secondary antibodies for 2 h at room temperature. Blots were washed three times with TBS-T and developed with the ECL system, according to the manufacturer's guidelines. Blots were detected and analyzed with the Jess western blot system (ProteinSimple).

2.2.6 Lentiviral transduction

2.2.6.1 Virus production

HEK293T cells were plated in Ø 10 cm dishes in a way that the cells reached a confluence of ~ 50% after 24 h. After 24 h the medium was changed and the transfection mix was prepared. Therefore, 700 μl of the serum-free medium was used and 7 μg of pLKO, 7 μg of psPAX2, and 3.5 μg of pMD2.G was added and mixed

gently. Afterward, 20 μl of CalFectin™ was added and mixed gently, and incubated for 15 min at RT. Next, 100 μl of the transfection mix was added to each of the HEK293T dishes. After 16-18 h post-transfection the medium was changed. 40-48 h post-transfection the medium of HEK293T cells was collected and filtered through a 0.45 μm filter. The virus can be stored at -80 °C or directly used for virus precipitation. For the virus precipitation, a Lenti-X concentrator was used and added to the medium containing the virus in a 1:3 dilution and incubated for 4 - 24 h at 4°C. After the incubation time, the solution was centrifuged for 30 min at 4°C with 1500 g. Next, the supernatant was discarded and the virus pellet was resuspended in the appropriate complete medium (according to the used cells).

2.2.6.2 Viral transduction

For the viral transduction, 12-well plates were coated with 20 μg/ml retronectin one day before the transduction and incubated at 4°C. On the day of transduction, the virus in the medium was added to the retronectin-coated wells of the 12-well plate and incubated for 6 h under normal cell culture conditions. Afterward, the virus was removed and the wells were washed with 5% BSA in PBS. Next, 10^6 cells were added in 1 ml of the appropriate medium (depending on the cells) containing 8 μg/ml polybrene and shortly centrifuged so that cells are attached to the bottom of the wells, in close contact with the virus, and cells were incubated overnight. The next day, the cells were collected and washed thoroughly to remove the remains of the virus. After washing, the cells were grown in 12-well plates and after 48 h of normal culture conditions, the cells were treated with the respective selection antibiotics. If a GFP-marker was used for the selection the cells were subjected to FACS sorting at the Institute of Transplantation Diagnostics and Cell Therapeutics (ITZ), Düsseldorf. In the case of shRNA constructs that were under doxycycline promotor, cells were treated with doxycycline for at least 24 h with 2 μg/ml doxycycline before they were subjected to FACS sorting.

2.2.7 Apoptosis Assays

2.2.7.1 Annexin V assay

To observe the apoptosis induction, the cells were plated into six-well plates and treated with the respective inhibitors at the indicated concentrations and DMSO control (< 1%) for either 24 h or 48 h under normal culture conditions. After the respective incubation time, cells were harvested and stained with propidium iodide (PI) and FITC labeled Annexin V according to the manufacturer's guidelines and analyzed by flow cytometry.

2.2.7.2 Caspase 3/7 assay

To evaluate the apoptosis induction, cells were plated into six-well plates and treated for 48 h with the respective inhibitor or DMSO control (< 1%) under normal culture conditions. After the incubation, cells were counted and a total number of 10.000 cells of each condition were transferred in 100 µl medium into a well of a flat 96-well plate. Afterward, 100 µl of the Caspase-Glo 3/7 Assay solution was added to the cells and after an incubation time of 30 min, the luminescent signal was measured using the Tecan Spark 10M.

2.2.8 RNA sequencing

2.2.8.1 Quality Control of Extracted RNA

The quantity and quality of total RNA were analyzed with Agilent BioAnalyzer 2100 using the Nano RNA 6000 Kit. RNA integrity number (RIN) scores and sample profiles were visually inspected to evaluate sample quality. Samples with RIN scores from 8 to 10 were used for further processing.

2.2.8.2 Total RNA Library Preparation

Total RNA library preparation was performed using TruSeq Stranded Total RNA Library Prep Kit with Ribo Zero-Gold by Illumina with 300 ng total RNA per sample as input. The fragmentation step was adapted depending on the quality of the RNA sample.

2.2.8.3 Library Validation

Total RNA and miRNA libraries were quantified by loading 1 µL of cDNA on a DNA-specific chip (DNA 1000 or High Sensitivity DNA). The concentration was measured with Agilent Bioanalyzer 2100.

2.2.8.4 Loading of the Flow Cell

Denaturation of template DNA was performed by adding 0.1 N NaOH to a final DNA concentration of 20 pM (10 µL 2 nM template DNA + 10 µL 0.1 N NaOH). The solution was vortexed and spun down at 280 x g for 1 min. The mixture was incubated at RT for 5 min. Afterward, 20 µL of denatured DNA was transferred to 980 µL of pre-chilled Hybridization buffer (HT1). Next, template DNA was diluted to 6.5 pM with HT1. Samples, flow cell, and cBot reagents were loaded on cBot and the S.R.Amp-Lin/Block/Hyb.V8 program was started to load samples on the flow cell.

2.2.8.5 Deep Sequencing

High-throughput sequencing was performed on a HiSeq 2500 for 51 cycles and 101 plus seven cycles for total RNA library sequencing according to standard protocols.

2.2.8.6 Data analysis

The sequencing data were uploaded to the galaxy web platform and the public server at usegalaxy.org were used to analyze the data[118]. FastQC was used to determine the data quality. MultiQC was used to compile single files into summarizing reports. FASTQ Trimmer was used to cutting the adapters from position 1 to 12 at the 5' end and the last base of the 3' end. The alignment of the read fragments to the reference genome (hg38 https://www.ncbi.nlm.nih.gov/assembly/GCF_000001405.26/) was done by RNAstar[119] with the help of the corresponding splice junction annotation. The quality control of the binary alignment map (BAM) files was done by MultiQC. The quantification of gene copy counts was done with featureCounts. The normalization and statistical analysis were performed using edgeR[120] (normalized foldchange, counts per million values, p values, q values).

Gene Annotation information was retrieved by using ensemble[121] (ensemble Genes 103, human genes (GRCH38.p13)), and filtering with the stable gene ID. Retrieved

was the gene name, stable gene ID & Gene description. The annotation was done by sorting duplicate gene identifiers and hierarchical sorting (success rate >99.99%), not identified genes were discarded. For primary hands-on analysis, the FDR had to be below 0.1 and the fold change had to be above 1 or below minus 1.

For the protein network analysis, String[122] was used with 500 genes with the highest downregulation and FDR below 0.1, 469 proteins, 15 clusters, and kmean. For the upregulation network 500 genes with the highest upregulation and FDR below 0.1, 334 proteins, 15 clusters, kmean. The volcano plots were generated via ggplot2. A gene set enrichment analysis (GSEA) was performed with the help of the GSEA software of the Broad Institute in combination with Cytoscape with the following crucial parameters:

- Number of Permutations = 10000

- Collapse/Remap to gene symbols = Collapse

- Permutation type = gene_set

- Chip platform = Human_ENSEMBL_Gene_ID_MSIGDB.v.7.0.chip

- Enrichment statistics = weighted

- Metric for ranking genes = Signal2Noise

- Max size: exclude larger sets = 500

- Min size: exclude smaller sets = 15

- P-value Cutoff= 0.005

- FDR Q-value Cutoff = 0.05

Additionally, fGSEA and clusterprofiler were used to complement and validate the GSEA results with a different algorithm. The inclusion criteria for each gene entry was FDR < 0.1 and as a method fgseaMultilevel was incorporated. Clusterprofile clusters were manually curated. Gage was used for combined fGSEA plots.

2.2.9 Xenograft models for in-vivo compound testing

The mouse line NOD-SCID IL2Rgamma[null], NOD-SCID IL2Rg[null,] or NSG (Strain #: 005557, The Jackson Laboratory) was used for the experiments and kept in the

institutional conventional animal facility. All experiments performed were approved by the North Rhine-Westphalia State Office for Nature, Environment, and Consumer Protection (LANUV) and were conducted in compliance with German animal welfare laws.

0.25×10^6 HPB-ALL luciferase-expressing cells were injected intravenously into the tail vein of ten mice. Three days post-injection the mice were monitored for engraftment of the injected cells by bioluminescent measurements using the Caliper IVIS Lumina II Multispectral Imaging System. Therefore, 15 mg/ml of D-luciferin potassium salt dissolved in PBS was injected intraperitoneally with 10 µl/kg of mouse weight. 10 min post-injection of the D-luciferin three pictures were taken each with a different exposure time (60, 30, and 5 sec.) The images were analyzed using the Living image software. Eight of the ten mice were found positive for the injected HPB-ALL cells and further divided into a treatment- or control- (vehicle) group. The treatment group was injected intraperitoneally with 200 µl of 100 mg/kg 10 h solved in 50% DMSO and 50% PEG300. The vehicle group was injected with 200 µl of 50% DMSO and 50% PEG300. The injections started 4 days post-injection of the HPB-ALL luciferase-expressing cells and were conducted twice a week for two consecutive weeks. The mice were monitored weekly by luminescent measurements for five weeks post-injection of the HPB-ALL cells and sacrificed after five weeks. Before mice were sacrificed, retrobulbar bleeding was performed to analyze the proportions of mice vs. human cells. After sacrificing the mice, the spleen was removed and minced to also analyze the spleen for the proportion of mice vs. human cells.

2.2.10 Data analysis

The drug-screening data were analyzed using the GraphPad Prism software. The dose-response curves were created using non-linear regression, log (inhibitor) vs normalized response parameters. DMSO-treated cells served as a control and were set to 100% viability. All data are presented as mean SD unless stated otherwise. Synergy was calculated using the Combenefit software (2.02). Heatmaps and unsupervised hierarchical clustering were kindly generated by Julian Schliehe-Diecks using the R-package Complex Heatmaps.

3. Results

The results presented in this thesis are organized by first describing compounds with a superior selectivity for HDAC6 and going towards less specific and finally pan-HDAC inhibitors and finally describing a novel class of compounds protein targeting chimera (PROTAC) (fig. 7).
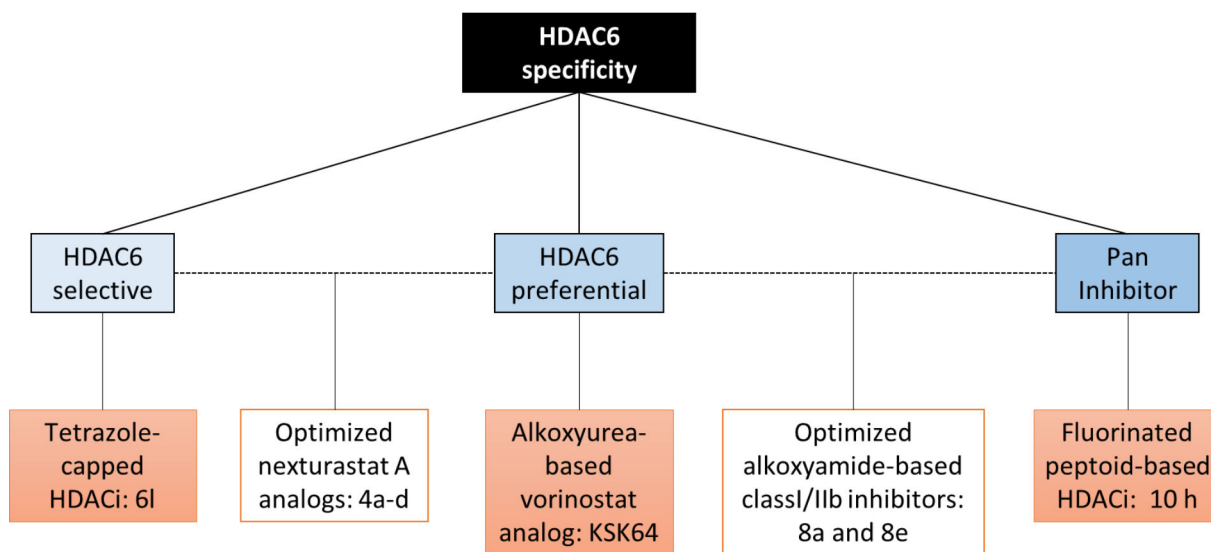
Figure 7: Overview of the research presented in this thesis. First, the inhibitors with high HDAC6 selectivity will be described, followed by HDAC6 preferential inhibitors. Afterward, the HDAC pan inhibitors will be presented.

In the second part of the result section the molecular changes evoked by HDAC6 inhibition and the relevance of HDAC6 as a molecular target based on drug screens performed using HDAC6 knockdown (KD) or knockout (KO) cell line models. Most of the experimental compounds described in this thesis were published and the corresponding publication will be referenced in the according section of the results. A list of the publications that arise from the work for the thesis is seen below:

1. Reßing, N. *et al.* **Multicomponent Synthesis, Binding Mode, and Structure-Activity Relationship of Selective Histone Deacetylase 6 (HDAC6) Inhibitors with Bifurcated Capping Groups**. *J. Med. Chem.* 63, 10339–10351 (2020). **(shared first authorship)**

2. Pflieger, M. *et al.* **Oxa Analogues of Nexturastat A Demonstrate Improved HDAC6 Selectivity and Superior Antileukaemia Activity**. *ChemMedChem* 16, 1798–1803 (2021). **(shared first authorship)**

3. Avelar, L. A. A. *et al.* **Synergistic induction of apoptosis in resistant head and neck carcinoma and leukemia by alkoxyamide-based histone deacetylase inhibitors**. *Eur. J. Med. Chem.* 211, 113095 (2021). **(shared first authorship)**

4. Sinatra, L. *et al.* **Hydroxamic Acids Immobilized on Resins (HAIRs): Synthesis of Dual-Targeting HDAC Inhibitors and HDAC Degraders (PROTACs)**. *Angew. Chemie - Int. Ed.* 59, 22494–22499 (2020).

5. Reßing, N. *et al.* **Development of Fluorinated Peptoid-Based Histone Deacetylase (HDAC) Inhibitors for Therapy-Resistant Acute Leukemia**. *J. Med. Chem.* (2022) doi:10.1021/acs.jmedchem.2c01418.

3.1 Characterization of HDAC6 expression in leukemic cell lines

To analyze the effects of HDAC6 inhibitors (HDAC6i) on different leukemic cell lines, the expression levels of HDAC6 were initially analyzed. The HDAC6 expression was

a)

b)
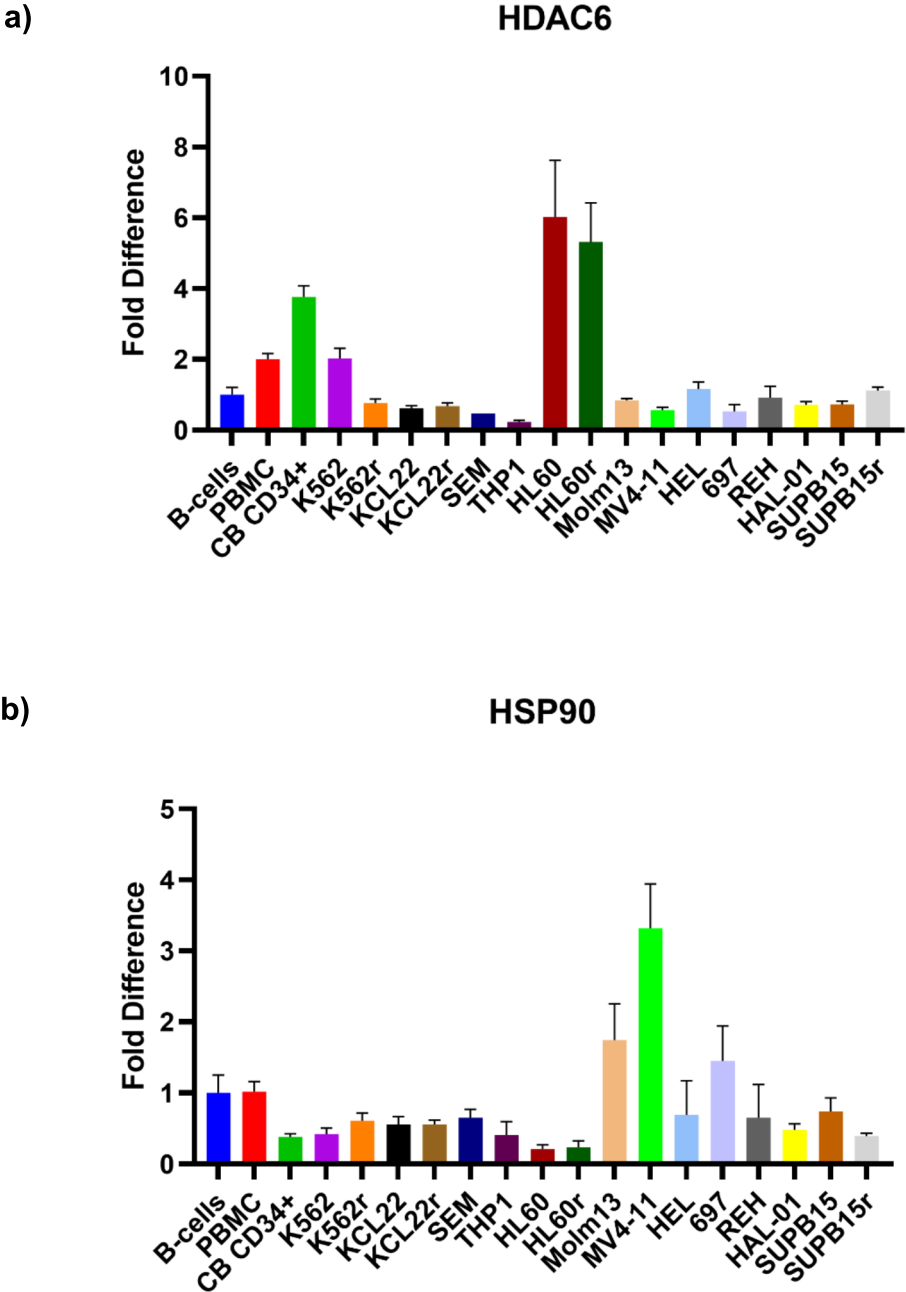
Figure 8: Characterization of leukemic cell lines for their HDAC6 and HSP90 RNA expression. 17 different leukemic cell lines were analyzed for their HDAC6 (a) and HSP90 (b) RNA expression and compared to healthy B-cells, PBMCs and CB 34+ cells.

investigated on the RNA level by RT-qPCR and the protein level by western blot analysis. First, the expression of HDAC6 on RNA level was analyzed (fig. 8). Therefore,

not only the HDAC6 expression was investigated but also the expression of HSP90 as it is known to interact with HDAC6 and potentially important for the function of HDAC6 inhibitors[113,123,124]. For the RT-qPCR analysis, 17 different cell lines were analyzed: K562 (CML), K562-Imatinib resistant (IMr) (CML), KCL22 (CML), KCL22-IMr, SEM (BCP-ALL), THP1 (AML), THP1 Bortezomib resistant (BTZr) (AML), HL60 (AML), HL60-BTZr (AML), MOLM13 (AML), MV4-11 (AML), HEL, 697 (BCP-ALL), REH (BCP-ALL), HAL-01 (BCP-ALL), SUP-B15 (BCP-ALL) and SUP-B15-IMr (BCP-ALL) and compared to healthy primary peripheral blood mononuclear cells (PBMCs). All tested cell lines showed HDAC6 expression on the RNA level and the HL60 cell line showed the highest expression compared to the other leukemic cell lines. Based on the analysis of the RT-qPCR, HL60 cells were chosen to be used for further functional assays of HDACi. Next, the expression of HDAC6 was investigated on the protein level by western blot in 11 different leukemic cell lines that were categorized into three different groups: 1) BCR-ABL1 +: K562, K562-IMr, KCL22, KCL22-IMr, SUP B15, SUP B15-IMr; 2) AML: HL60, HL60-BTZr, THP1, and BCP-ALL: SEM and Mutz5 (fig. 9). On the protein level, all tested cell lines showed detectable expression of HDAC6 and highest expression was observed in the K562 cell line.
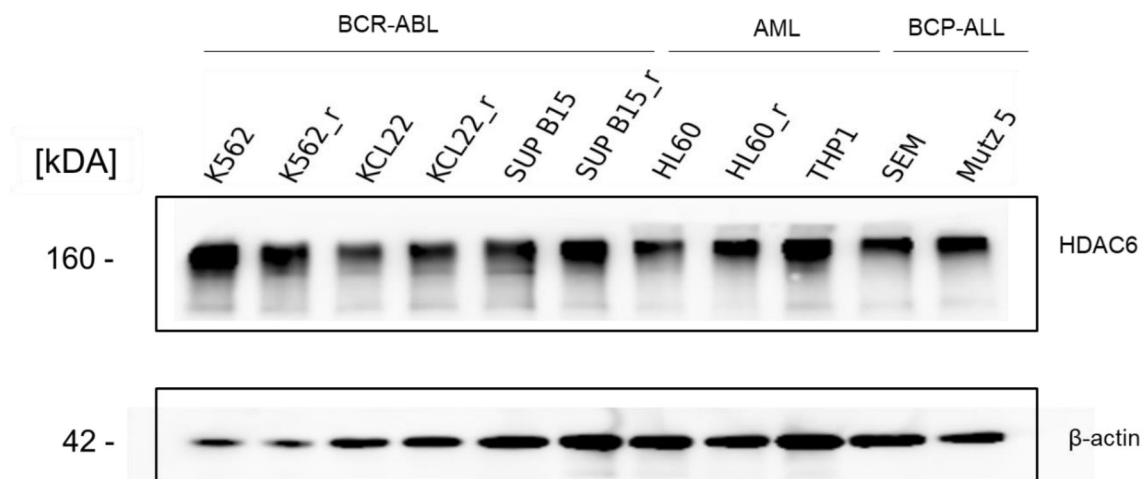
Figure 9: Characterization of leukemic cell lines for their HDAC6 expression on the protein level. 11 leukemic cell lines were investigated by western blot analysis for their expression of the HDAC6 protein. β-actin served as the loading control.

3.2 *In vitro* characterization of the highly selective HDAC6 inhibitor 6l

The following selective HDAC6 inhibitor (fig. 10) was developed by the working group of Prof. Dr. F. K. Hansen (Pharmaceutical and Cell Biological Chemistry, Pharmaceutical Institute, University of Bonn). The data in this section are taken from our publication: ***Multicomponent Synthesis, Binding Mode, and Structure-Activity Relationship of Selective Histone Deacetylase 6 (HDAC6) Inhibitors with Bifurcated Capping Groups. J. Med. Chem. 63, 10339–10351 (2020).***
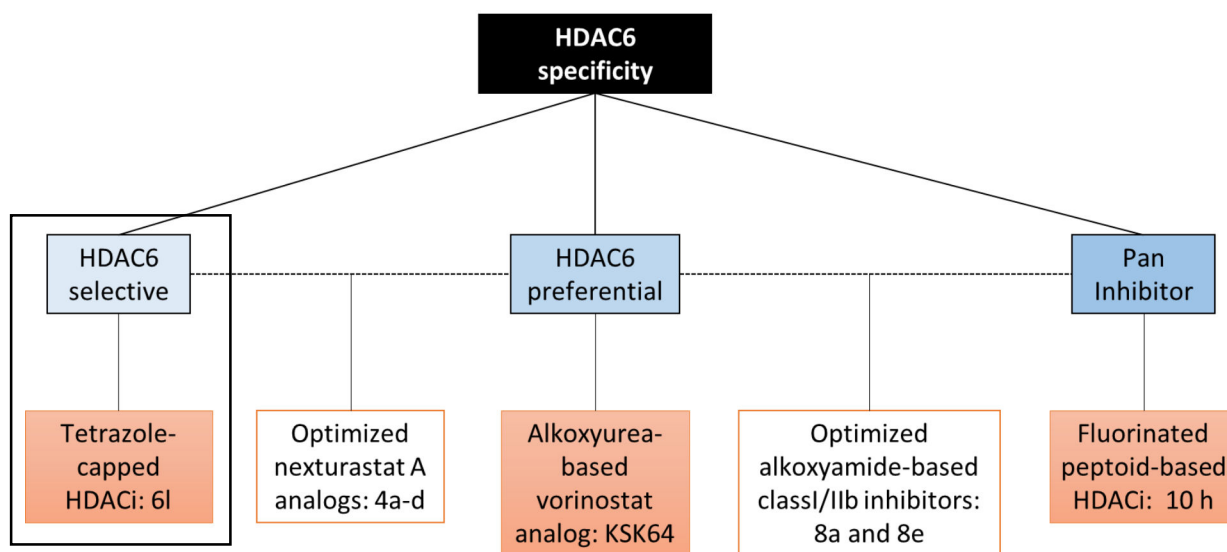
Figure 10: Overview of different HDAC inhibitors evaluated in this thesis. The black box highlights the inhibitor that will be described in this section.

The experimental inhibitor **6l** was analyzed by cell-free, biochemical enzyme inhibition assays to identify its selectivity towards the different HDAC isoforms (fig. 11). **6l** was tested against all class I isoforms (HDAC1: 5.18 µM, HDAC2: 2.26 µM, HDAC3: 8.48 µM), the class IIa isoform HDAC4 (55.40 µM) and the class IIb isoform HDAC6 (0.03 µM) (fig. 10A). Thus, **6l** can be classified as very potent HDAC6 inhibitor that also shows a high grade of selectivity (SI$^{1/6}$: 172). Strikingly, it shows better selectivity towards HDAC6 compared to the HDAC6i ricolinostat (SI$^{1/6}$: 11). Next to the isoform profiling, **6l** was also analyzed regarding its cellular selectivity for HDAC6. Therefore, the acute myeloid leukemia (AML) cell line HL60 was treated for 24 h with two different concentrations (2.5 µM and 5 µM) of **6l** together with the clinically relevant HDAC6 inhibitor ricolinostat as reference control at its IC$_{50}$ concentration. After treatment, the cells were lysed and immunoblotted to examine the ability of **6l** to induce acetylation of α-tubulin, as a marker for HDAC6 inhibition and the acetylation of Histone 3 (H3) as

a marker for HDAC class I inhibition. As seen in fig. 11B, **6l** was able to induce the acetylation of α-tubulin at both used concentrations but did not affect the level of acetylation of H3. The treatment with ricolinostat showed similar levels, compared to **6l**, of α-tubulin acetylation but in contrast to **6l** also induced the acetylation of H3. Together with the isoform profiling, these results confirm the HDAC6 selectivity of **6l** in a cell-free as well as in a cellular environment. Based on the promising selectivity of **6l** the antitumoral properties were further analyzed. Therefore, seven leukemia cell lines from different leukemic subtypes TALL-1, HSB-2, MOLT-4, Jurkat, HL60, SUPB15 and K562 were treated with a concentration gradient of compound **6l**, ranging from 1 – 50

a)

HDAC1 IC$_{50}$: 5.18±0.31 µM (SI$^{1/6}$: 172)
HDAC2 IC$_{50}$: 2.26±0.11 µM (SI$^{2/6}$: 75)
HDAC3 IC$_{50}$: 8.48±0.42 µM (SI$^{3/6}$: 282)
HDAC6 IC$_{50}$: 0.030±0.0002 µM

b)
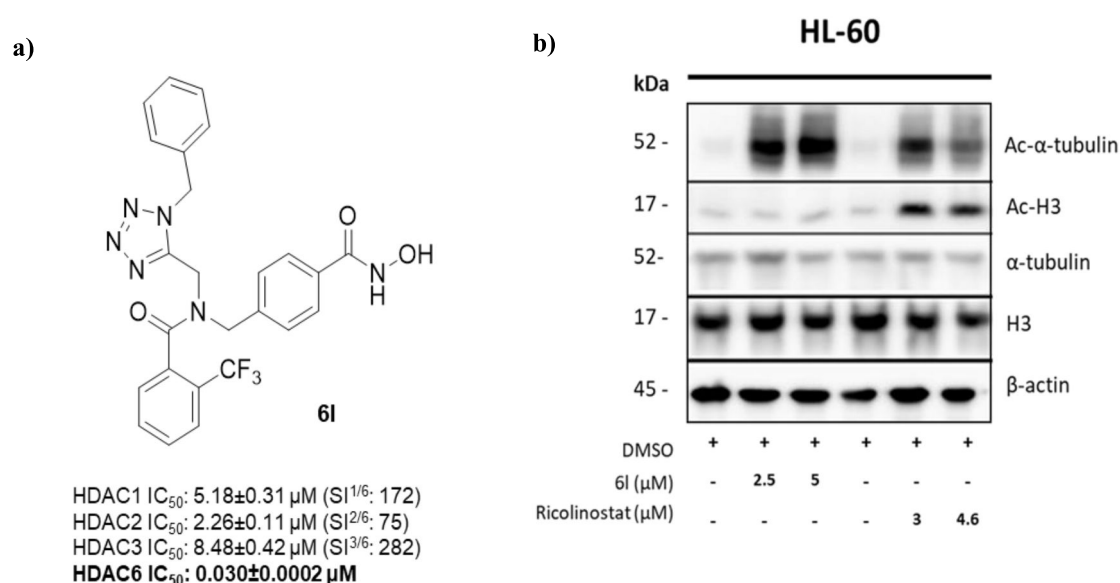
Figure 11. Functional specificity of **6l** against HDAC6. a) Inhibitory activities of compound **6l** against HDAC isoforms 1-4, 6 and 8. b) HL60 cells were treated for 24 hours with compound **6l** and ricolinostat at the indicated concentration. Afterwards, cell lysates were immunoblotted with anti-acetyl-α-tubulin, acetyl-histone H3, total α-tubulin, total histone H3. β-Actin was used as a loading control.

µM (fig. 12a) Compound **6l** had only minor effects on the cell viability with IC$_{50}$ values of >20µM. Based on the low cytotoxic properties of compound **6l** as a single agent, a combinatorial drug screening with compound **6l** and the proteasome inhibitor bortezomib (BTZ)[124] was performed. Briefly, increasing concentrations of **6l** against increasing concentrations of bortezomib in 10 x 10 dose-response matrices were screened using the semi-automated drug-screening platform in the HL60 and Jurkat cell lines. However, no synergistic interaction between compound **6l** and BTZ was found (fig. 12b). Next, the ability of compound **6l** or BTZ alone and in combination to

induce apoptosis was evaluated. HL60 cells were treated for 24 h with two different concentrations of **6I** or BTZ alone and in combination. The apoptosis induction was evaluated by an annexin V-propidium iodide (PI) apoptosis assay. As already shown before, **6I** showed no cytotoxic effects with both concentrations (2.5 µM and 5 µM), as the number of viable cells was not affected. However, in combination with BTZ, compound **6I** augmented the apoptosis induction of BTZ, as the number of late apoptotic/ dead cells significantly increased when compared to BTZ alone. This effect was enhanced with higher concentrations of both inhibitors (fig. 13). Encouraged by these results, a high-throughput drug combinational screen was performed using the T-ALL cell line HSB-2 on the semi-automated platform with **6I** at two different concentrations (2.5 µM and 5 µM) together with 36 chemotherapeutics and 3
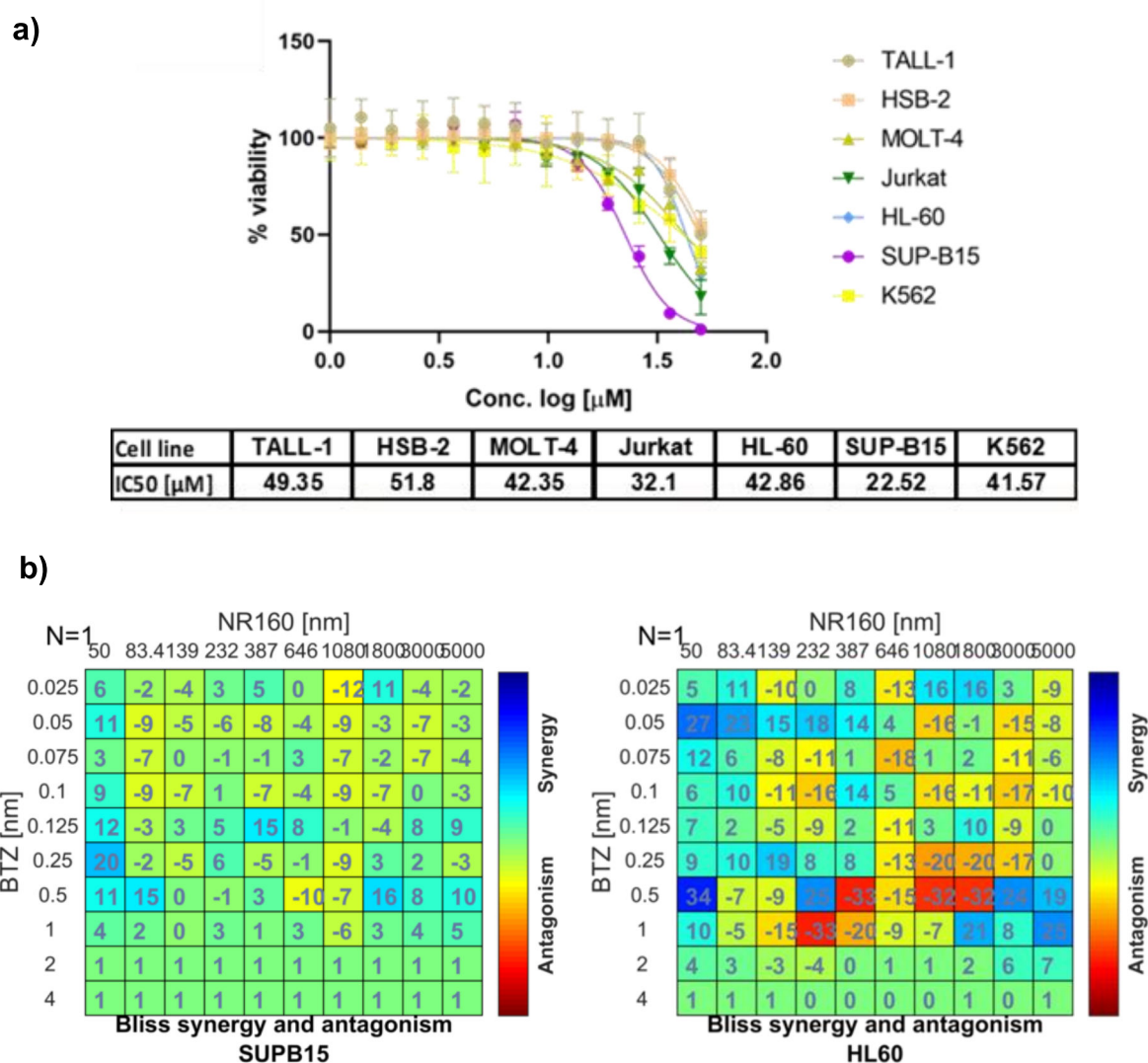
Figure 12. Cytotoxic analysis of compound **6I**. **a)** Cytotoxicity of compound **6I** against selected leukemic cell lines. **b)** Compound **6I** does not synergize with proteasome inhibitors. Bliss synergy plots of compound **6I** in combination with the proteasome inhibitor bortezomib in SUP-B15 (left) and HL60 (right) cells. Thee bliss synergy analysis and visualization were performed using the Combenefit software.

glucocorticoids that are regularly applied in the clinic to treat various cancers and leukemia. The chemotherapeutics and the glucocorticoids were printed with increasing concentrations ranging from 10 nM to 25 µM. Interestingly, a significant enhancement of the cytotoxic effect of the DNA intercalating anthracycline-based chemotherapeutics epirubicin (Epi) and daunorubicin (Dauno) combined with compound **6l** was found. Compound **6l** alone was not able to affect the viability of HSB-2 cells (fig. 14).
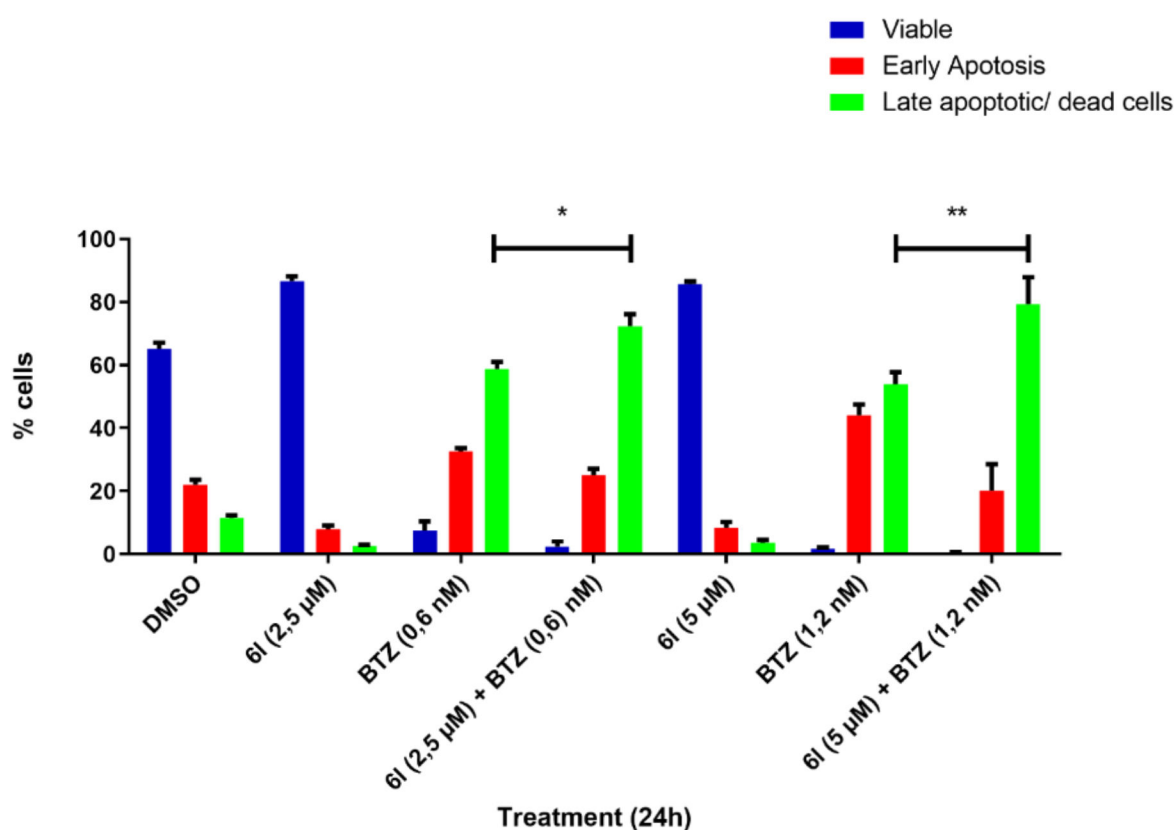
Figure 13: Enhanced effect of **6l** in combination with proteasome inhibitor bortezomib. Annexin-PI staining of HL60 cells exposed to compound **6l** alone, BTZ alone and compound **6l** and BTZ in combination at the indicated concentration for 24 h (n=3). Significance analyses of normally distributed data with variance similar between groups used paired, two-tailed Student's t-test. * < P 0.05, ** < P 0.005.
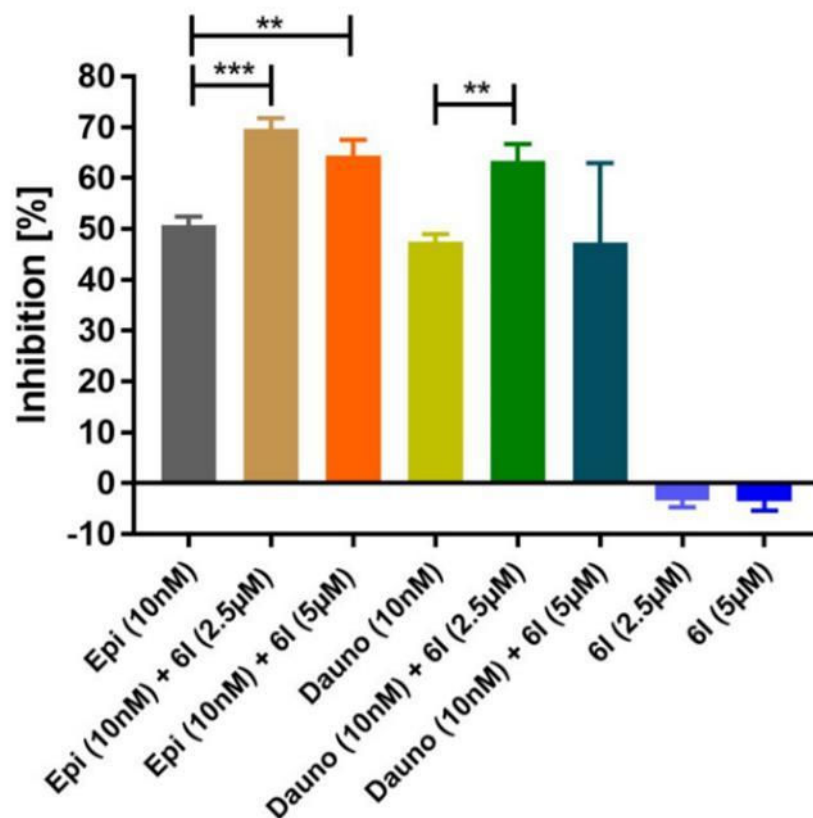
Figure 14. Combination analysis with **6l** and chemotherapeutic compounds. Cytotoxicity of compound **6l** alone or in combination with epirubicin (Epi) and daunorubicin (Dauno) against the T-cell acute lymphoblastic leukemia (T-ALL) cell line HSB-2. Significance analyses of normally distributed data (n=3) with variance similar between groups used unpaired, two-tailed Student's t-test. * < P 0.05, ** < P 0.005.

3.3 *In vitro* characterization of Nexturastat A analogs: preferential HDAC6 inhibitors

In the next section, derivatives of the HDAC6 selective inhibitor nexturastat A (fig. 15) were developed by the working group of Prof. Dr. T. Kurz (Institut für Pharmazeutische und Medizinische Chemie Heinrich-Heine-Universität Düsseldorf). Based on their finding that the functional group (CU) that connects the linker and the cap group can affect the isozyme profile of HDACi, derivatives of Nexturastat A were designed with an alkoxyurea-based connecting unit. Nexturastat A and their described derivates are still HDAC6 selective inhibitors but compared to compound **6l**, which was described before, they are less specific using isozyme profiling (Table 18). The data in this section are taken from our publication: *Oxa Analogues of Nexturastat A Demonstrate Improved HDAC6 Selectivity and Superior Antileukaemia Activity. ChemMedChem* **16**, *1798– 1803 (2021).*
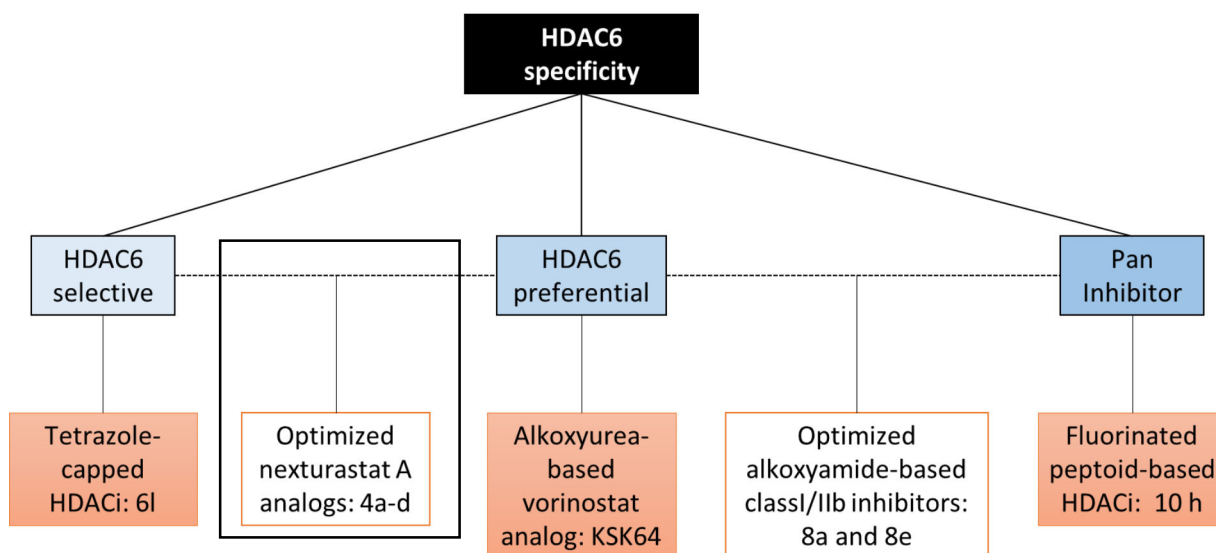
Figure 15: Overview of different HDAC inhibitors evaluated in this thesis. The black box highlights the inhibitor that will be described in this section.

The series of Nexturastat A analogous was modified by the introduction of a hydroxylamine-based connecting unit (CU) and analyzed for the HDAC inhibitory potential by a cell-free HDAC1-3/6 isozyme profiling for the evaluation of their HDAC6 selectivity and compared to nexturastat A (table 18). Nexturastat A showed a selectivity index of 24 for HDAC6 over HDAC1. This is in sharp contrast to the reported 600-fold selectivity of HDAC6 over HDAC1. Interestingly the hydroxylamine derivate **4a** showed a 1.5-, 1.7- 1.3 – fold higher SI 1/6, SI2/6, and SI 3/6 compared to nexturastat A, respectively.

Table 18: HDAC 1-3/6 isozyme profiling of compounds **4a-b**. The presented data are the result of N ≥ 2, each in duplicate.
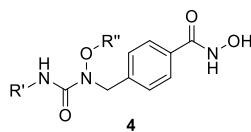
	R'	R''	HDAC1 IC_{50} [µM]	HDAC2 IC_{50} [µM]	HDAC3 IC_{50} [µM]	HDAC6 IC_{50} [µM]	SI 1/6	SI 2/6	SI 3/6
4a	phenyl	propyl	0.742 ± 0.039	1.42 ± 0.082	0.902 ± 0.008	0.020 ± 0.003	37	71	45
4b	3,5-dimethylphenyl	propyl	0.299 ± 0.057	0.515 ± 0.043	0.375 ± 0.084	0.014 ± 0.002	21	37	27
4c	4-(dimethylamino)phenyl	propyl	0.715 ± 0.010	1.14 ± 0.074	0.972 ± 0.064	0.022 ± 0.002	33	52	44
4d	3,5-dimethylphenyl	benzyl	2.89 ± 0.125	3.59 ± 0.410	3.12 ± 0.578	0.341 ± 0.021	8.5	11	9.2
Nexturastat A			0.504 ± 0.033	0.861 ± 0.008	0.730 ± 0.033	0.021 ± 0.001	24	41	35

To analyze the anti-cancer effects of the branched alkoxyurea-based hydroxamic acids, drug-screening with four different alkoxyurea-based hydroxamic acids along with nexturastat A as reference inhibitors in 6 different leukemic cell lines HAL-01, SUP-B15, K562, Jurkat, HL60, MOLM13 was performed (fig. 16, A). Compound **4b** showed the highest efficacy with the lowest IC_{50} across all tested cell lines. In the AML cell lines HL60 and MOLM13, **4b** demonstrated IC_{50} values of 0.44 µM and 0.11 µM, respectively. Against the other tested leukemic entities, **4b** exhibited antiproliferative activities in the micromolar range from 1.6 µM for K562 to 3.0 µM for Jurkat. The superior activity against the AML cell lines was a common feature shared by all four derivatives except for **4c**, which showed a generally weak efficacy against all cell lines compared to the other tested compounds. In this respect, **4a** demonstrated the highest selectivity towards AML cell lines amongst the tested alkoxyurea-based hydroxamic acid derivatives. **4a** and **4d** showed a higher efficacy in the AML cell line HL60 and MOLM13 than nexturastat A, whereby **4a** showed a similar antiproliferative profile to nexturastat A across all tested cell lines. Inhibitor **4b**, as the HDAC6 selective inhibitor with the most pronounced antiproliferative effect, and **4a**, with the most HDAC6

preferential isozyme profile (SI 1/6 = 37, SI 2/6 = 71, SI 3/6 = 45), with nexturastat A, as a reference, were further evaluated regarding its properties to induce α-tubulin acetylation (fig. 16, B). HL60 (AML) cells were treated with **4a**, **4b** and nexturastat A
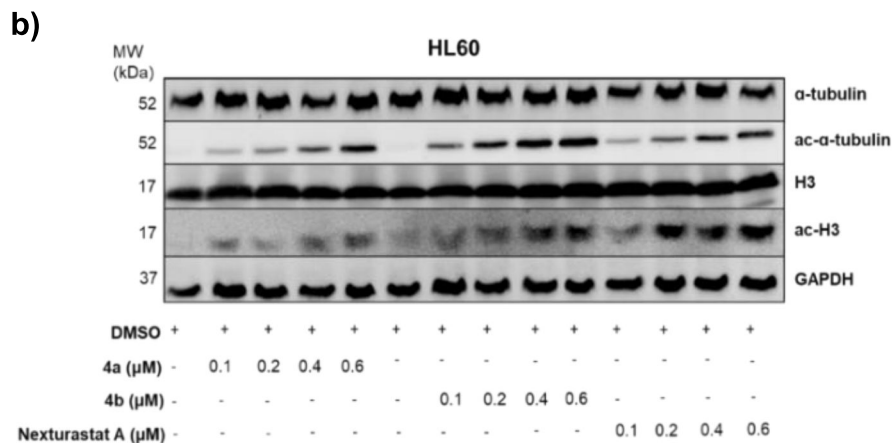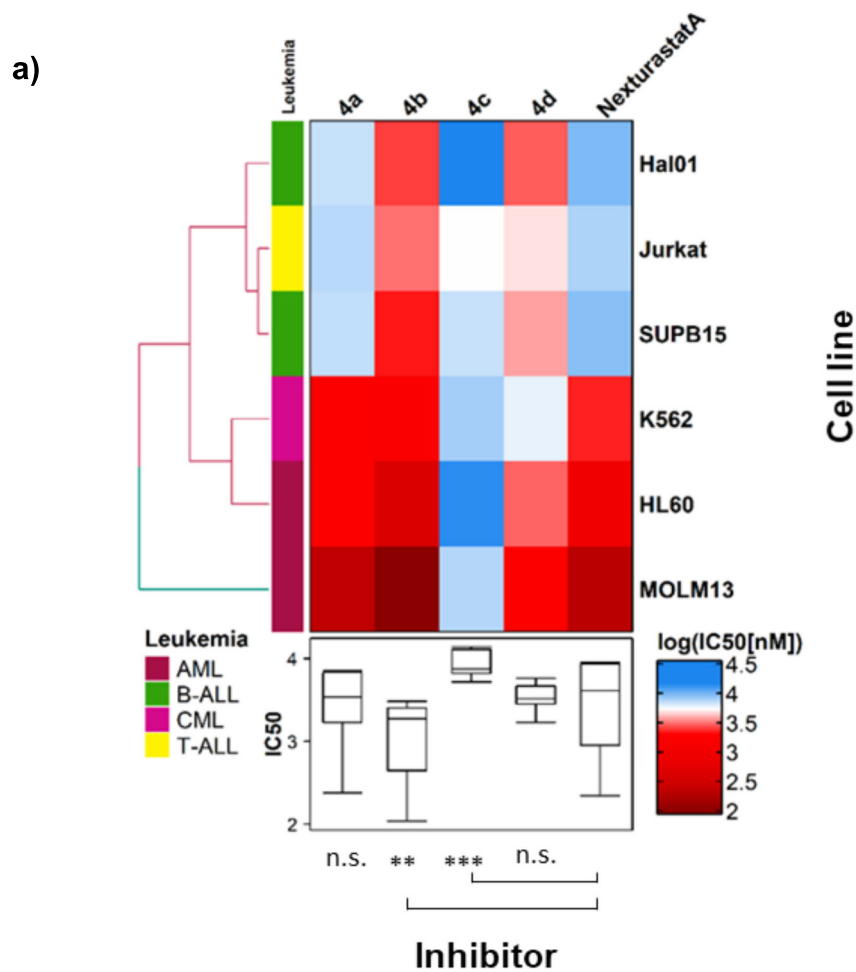
Figure 16. Cytotoxic and target specificity analysis **a)** Comparative cellular viability (log IC$_{50}$ nM) of different sub-groups of leukemic cell lines (HAL-01, Jurkat, SUP-B15, K562, HL60, MOLM13), after exposure of **4a, 4b, 4c** and **4d** in comparison to, nexturastat A. The IC$_{50}$ data are plotted as a clustered heat map, followed by unsupervised hierarchical clustering. The vertical axis of the dendogram exemplifies the dissimilarity between clusters, whereas the colour of the cell is related to its position along a log IC$_{50}$ (nM) gradient. The boxplot shows the median IC$_{50}$ (log IC$_{50}$ nM) of the respective inhibitor across all tested leukemic cell lines. **b)** HL60 cells were treated with **4a**, **4b** and nexturastat A for 24 h with the indicated concentrations. Afterwards, cell lysates were immunoblotted with anti-acetyl-α-tubulin, acetyl-histone H3, total α-tubulin, and total histone H3 antibodies. GAPDH was used as a loading control.

with the $IC_{12.5}$, IC_{25}, IC_{50}, and IC_{75} concentrations to compare the induction of the acetylation. The degree of acetylation, induced by **4a** and **4b**, was in good agreement with the isozyme profiling, as the strongest acetylation of α-tubulin, as a marker for HDAC6 inhibition, was observed with **4b** and weakest with nexturastat A. Total α-tubulin expression was not affected by the treatment. However, nexturastat A showed higher levels of H3 acetylation compared to **4b**, even though **4b** showed a lower IC_{50} for HDAC1 in the isozyme analysis. Total H3 expression was not affected by the treatment.

3.4 *In vitro* characterization of the alkoxyurea-based Vorinostat analog KSK64, a preferential HDAC6 inhibitor
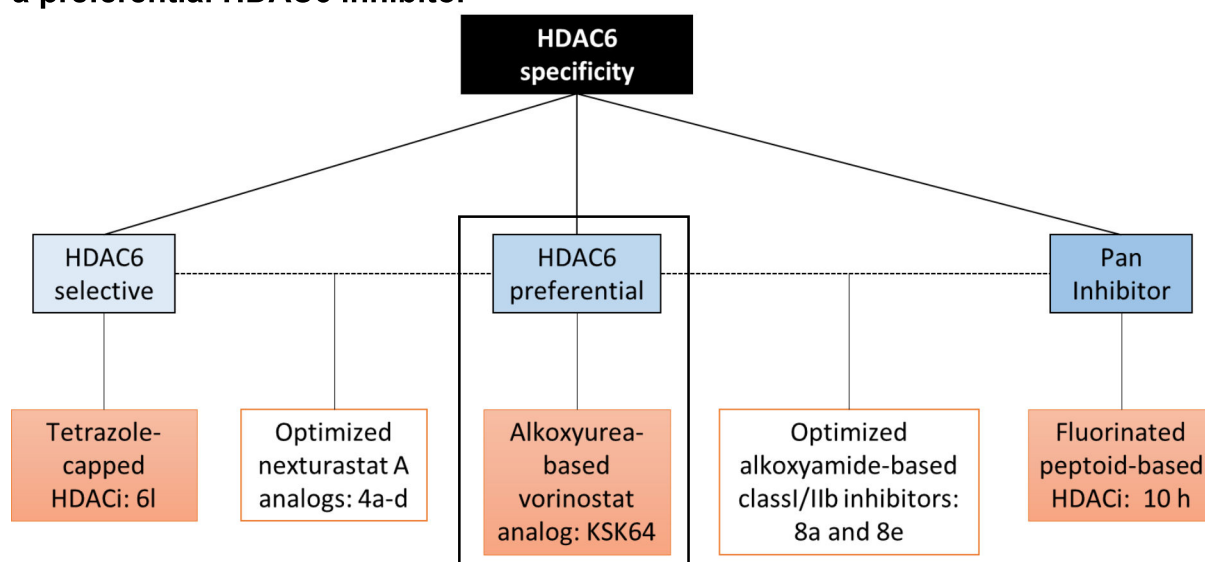
Figure 17: Overview of different HDAC inhibitors evaluated in this thesis. The black box highlights the inhibitor that will be described in this section.

The experimental inhibitor **KSK64** (fig. 17), developed by the working group of Prof. Dr. T. Kurz (Institut für Pharmazeutische und Medizinische Chemie Heinrich-Heine-Universität Düsseldorf), was chosen as HDAC inhibitor for the analysis of its anti-cancer properties in leukemia as previously published data showed that **KSK64** showed IC_{50} values in the sub-µM range and was able to enhance the cisplatin sensitivity in the cisplatin-resistant human squamous carcinoma cell line Cal27CisR[125]. Based on the cell-free isoform profiling analysis[125], **KSK64** showed an IC_{50} of 2.8 nM for HDAC6, 43.2 nM for HDAC1 (SI 1/6 = 15.4) and 1540 nM for HDAC8 (SI 8/6 = 550) and is, therefore, less specific compared to the selective HDAC6 inhibitor **6l** and the

Nexturastat A analogs that were previously described. Although **KSK64** still shows a preference for HDAC6 compared to other HDAC isoforms and is therefore referred to as a preferential HDAC6 inhibitor. Encouraged by the previous findings and its HDAC6 preferential isoform profile, further high-throughput drug screens with **KSK64** were performed in a large panel of leukemic cell lines (n=22) and compared it to the reference inhibitor ricolinostat ($SI^{1/6}$:11) (fig. 18). In all tested cell lines **KSK64** showed IC_{50} values in the nanomolar range in contrast to the IC_{50} values of ricolinostat that are in µM range. Encouraged by the potency of **KSK64** in various leukemic cell lines, especially in the *TCF3-HLF* fusion-oncogene harbouring cell line HAL-01, that represents a therapy resistant form of leukemia and is associated with a poor prognosis, its functional specificity and analysed its potential to induce α-tubulin hyperacetylation was investigated. Therefore, HAL-01 (BCP-ALL, *TCF3-HLF*) and 697 (BCP-ALL, *TCF3-PBX1*) were treated for 24 h with their IC_{50} and IC_{100} of **KSK64** and ricolinostat and subsequently immunoblotted for acetyl-α-tubulin and acetyl-H3 (fig. 19a). DMSO (vehicle) treated HAL-01 and 697 cells served as negative control. The IC_{50} concentration of **KSK64** did not induce acetylation of H3 and only slightly of α-tubulin in the HAL-01 cell line. In 697 cell line the IC_{50} concentrations of **KSK64** as well as ricolinostat induced hyperacetylation of α-tubulin and H3. As expected, both inhibitors induced the acetylation of α-tubulin and H3 at their IC_{100} concentration. Venetoclax was used as negative control and did not altered the acetylation levels of α-tubulin nor H3 in the HAL-01 cell line. In the 697 cell line, it appeared that the acetylation of H3 is slightly stronger in the venetoclax treated cells compared to the DMSO control. Next, **KSK64** was subjected to a cellular-based activity assay for HDAC class I/IIb and class IIa, using the HL60 cell line (fig. 19b). Ricolinostat served as a reference inhibitor. As expected, **KSK64** was able to deacetylate class I/IIb specific substrates with < 1 µM concentrations. Class IIa substrates were not altered and remained deacetylated. The IC_{50} for HDAC class I/IIb activity for **KSK64** was 91.03 nM and for ricolinostat 881.2 nM. These data were complemented with cell viability data (IC_{50}) and was done by incubating HL60 cells at the same time point with the respective inhibitors for 72 h. In this screen **KSK64** showed an IC_{50} of 658.9 nM and ricolinostat <10000 nM.
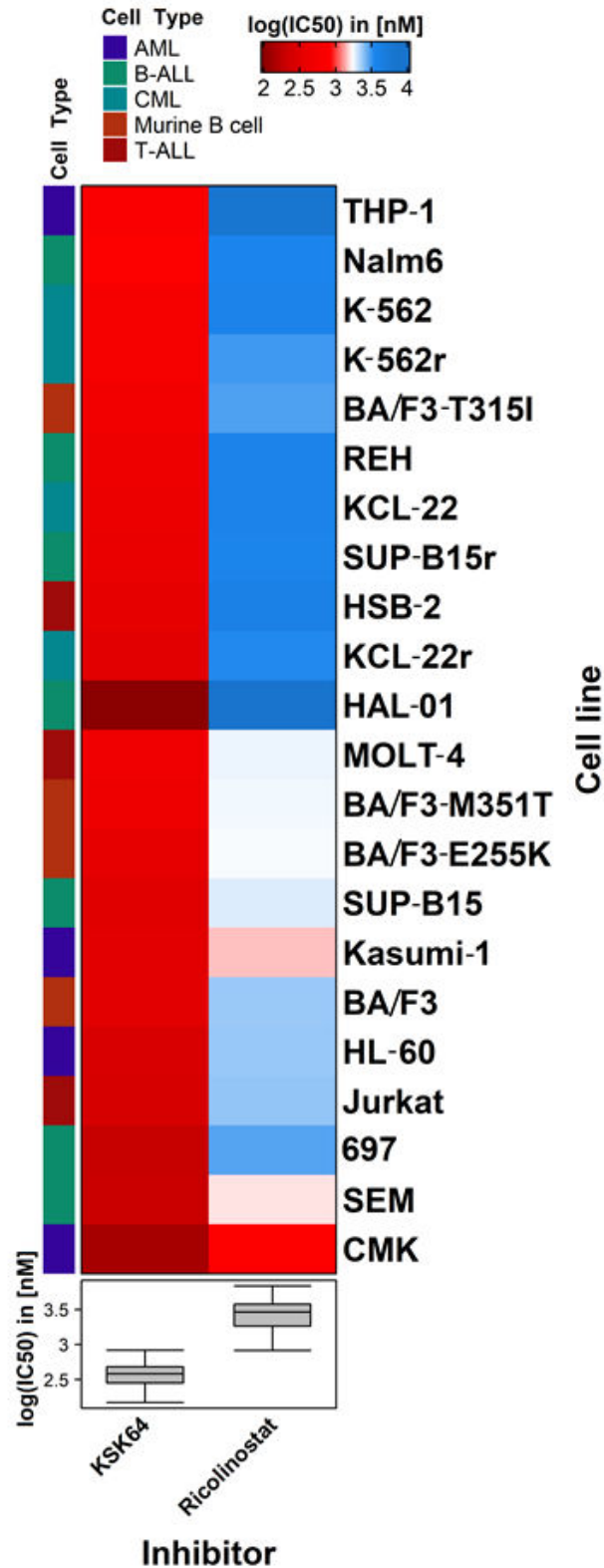
Figure 18. Comparative cellular viability (log IC$_{50}$ nM) of different sub-groups of human and mouse leukemic cell lines after exposure of **KSK64** and ricolinostat. The IC$_{50}$ data are plotted as a clustered heat map. The boxplot shows the median IC$_{50}$ (log IC$_{50}$ nM) of the respective inhibitor across all tested leukemic cell lines.
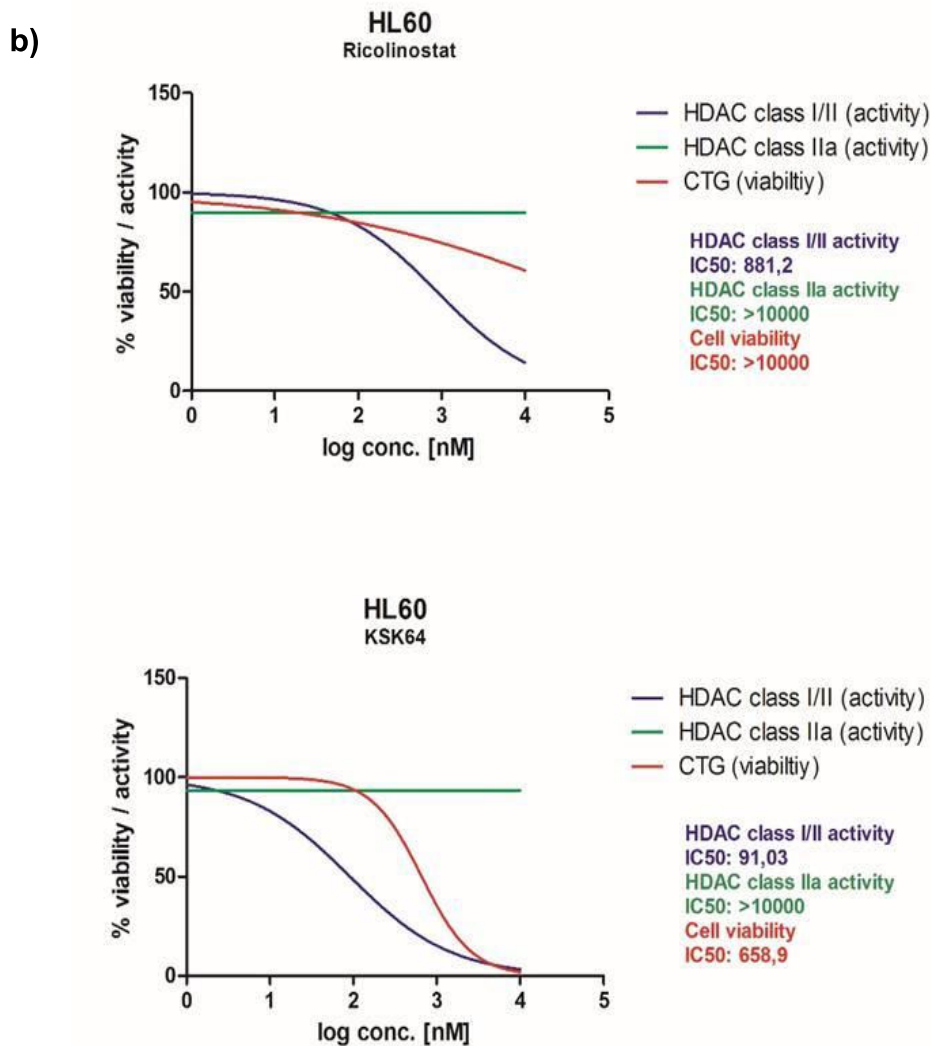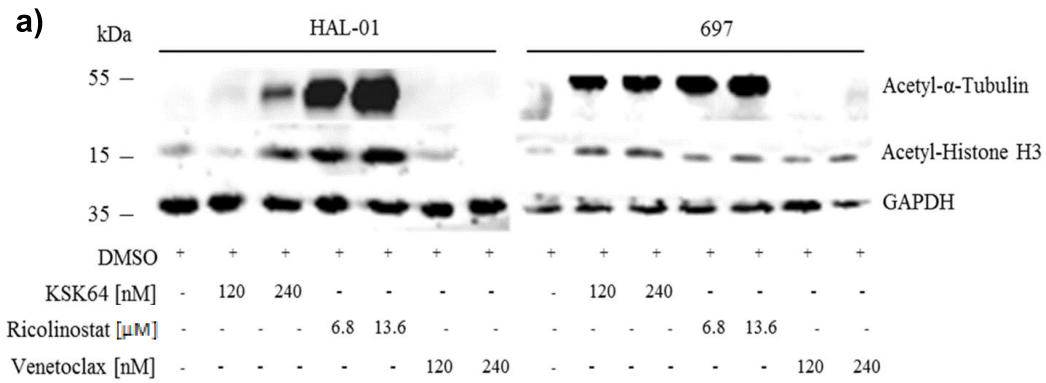
Figure 19: Functional specificity of **KSK64**. **a)** HAL-01 and 697 cells were treated with **KSK64**, Ricolinostat and Venetoclax for 24 h with the indicated concentrations. Afterwards, cell lysates were immunoblotted with anti-acetyl-α-tubulin, acetyl-histone H3 antibodies. GAPDH was used as a loading control. **b) KSK64** and ricolinostat inhibit class I and class IIb histone deacetylases (HDACs) at different drug concentrations. The activity of class IIa HDACs was not affected by drug treatment. The cytotoxicity was determined after 72 h of incubation with the inhibitors using the CellTiter-Glo (CTG) Luminescent Cell Viability Assay. Each data point represents three replicates and error bars are ± s.d. Curve-fits to determine IC_{50} values (sigmoidal dose-response, variable slope) were calculated using GraphPad Prism.

Furthermore, a broad drug screen with different commercially available selective and preferential HDAC6 inhibitors in a selection of leukemic cell lines (SUP-B15, SUP-B15-IMr, KCl22, KCL22-IMr, HL60, HL60-BTZr, THP1-BTZr, Jurkat, MOLT4 and SEM (fig. 20a). **KSK64** was the most potent inhibitor across all tested cell lines with IC_{50}
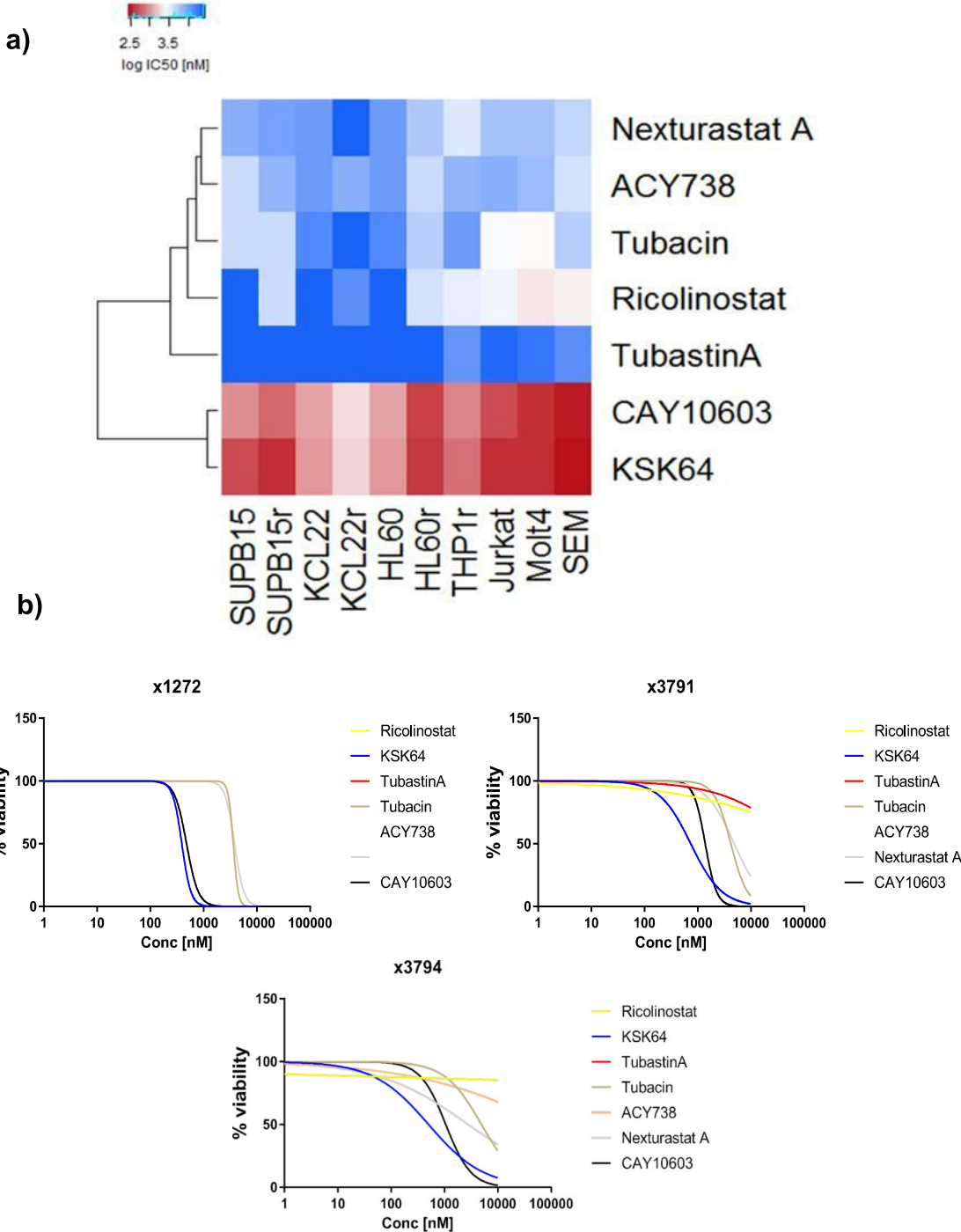
Figure 20: Cytotoxic analysis of **KSK64** vs. commercial available HDAC6i. **a)** Leukemic cell lines were treated for 72 h with the depicted inhibitors. Seven concentration were tested ranging from 10 nM to 10.000 nM in a logarithmic distribution. Log transformed IC_{50} values were used for visualization. Unsupervised clustering was used to cluster the different HDAC6i. **b)** TCF-HLF+ patient derived BCP-ALL cells (x1272, x3791, and x3794) were treated for 72 h with the depicted HDAC6i. Seven concentrations were tested ranging from 10 nM to 10.000 nM in a logarithmic distribution.

concentrations in the nanomolar range. CAY10603 was comparable potent to **KSK64**, however, all other tested inhibitors (nexturastat A, ACY738, tubacin, ricolinostat, and tubastatin A) showed IC$_{50}$ values in the micromolar range. Based on the results of the initial screen in the 23 leukemic cell lines, HAL-01 showed the lowest IC$_{50}$ concentration of all tested cell lines. Encouraged by that, three patient samples were tested that also harbor the *TCF3-HLF* fusion gene: x1272, x3791, and x3794 (fig.20b). Also in these primary patient samples, **KSK64** was found as the most potent HDAC6 preferential inhibitor.

Next, to determine the interplay between HDAC6 and HSP90[89], a luciferase refolding assay was performed. HL60 cells were incubated with increasing concentrations of **KSK64** and the reference inhibitor ricolinostat for 6 h. Before the incubation, cells were heated for 5 min at 50 C° to induce reversible denaturation of luciferase (fig. 21). However, in the case of **KSK64** and ricolinostat luciferase activity was not inhibited by both of the inhibitors, and the luciferase was completely refolded by chaperone proteins.
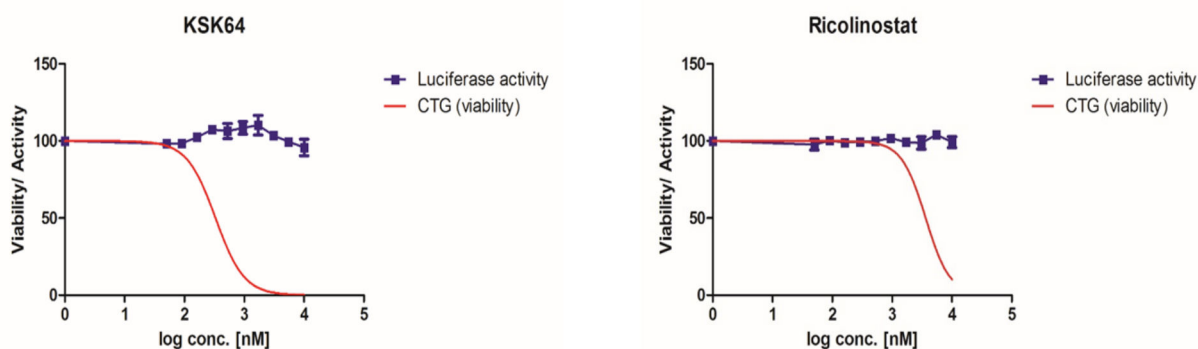
Figure 21: HL60 cells were heated to 50 °C for 5 min and afterwards subjected to either **KSK64** or ricolinostat treatment. Both of the inhibitors did not changed the capacity of the chaperone proteins to refold the luciferase.

Recent studies showed that HDA6i when combined with proteasome inhibitors exhibits promising anti-cancer properties[124]. Therefore, **KSK64** was screened against increasing concentrations of the proteasome inhibitors bortezomib (10 x 10 dose-response matrices) in the HL60 and SUP-B15 cell lines using a semi-automated drug screening platform (fig. 22). In line with the previous studies, the significant synergistic interaction of **KSK64** and bortezomib in both of the tested cell line was detected, using Bliss synergy analysis.
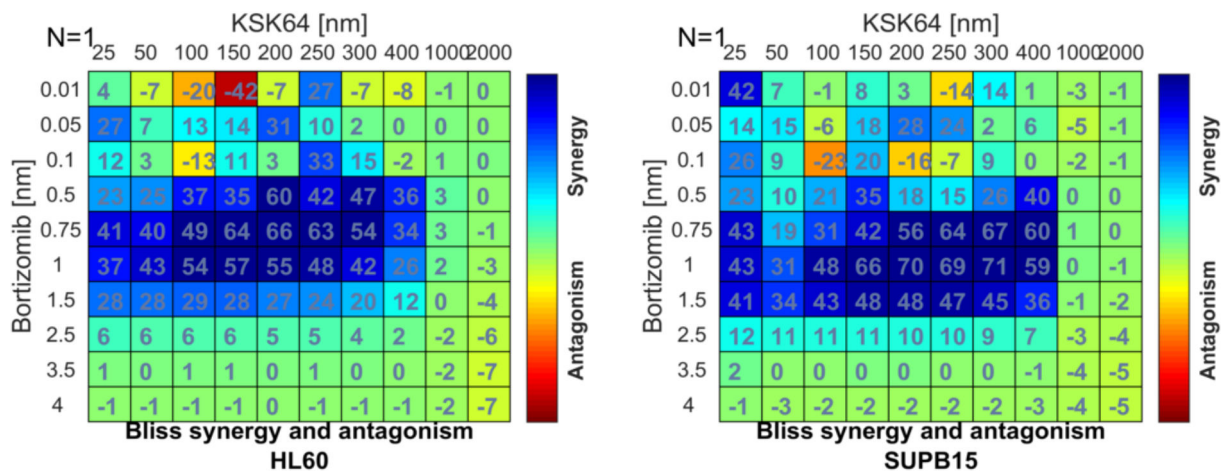
Figure 22: Synergistic effect of HDAC6i and Proteasome Inhibitors: HL60 and SUPB15 cell lines were treated for 72 h with different combinations of **KSK64** and bortezomib concentrations. The Bliss synergy model was used for analysis of the synergistic effects.
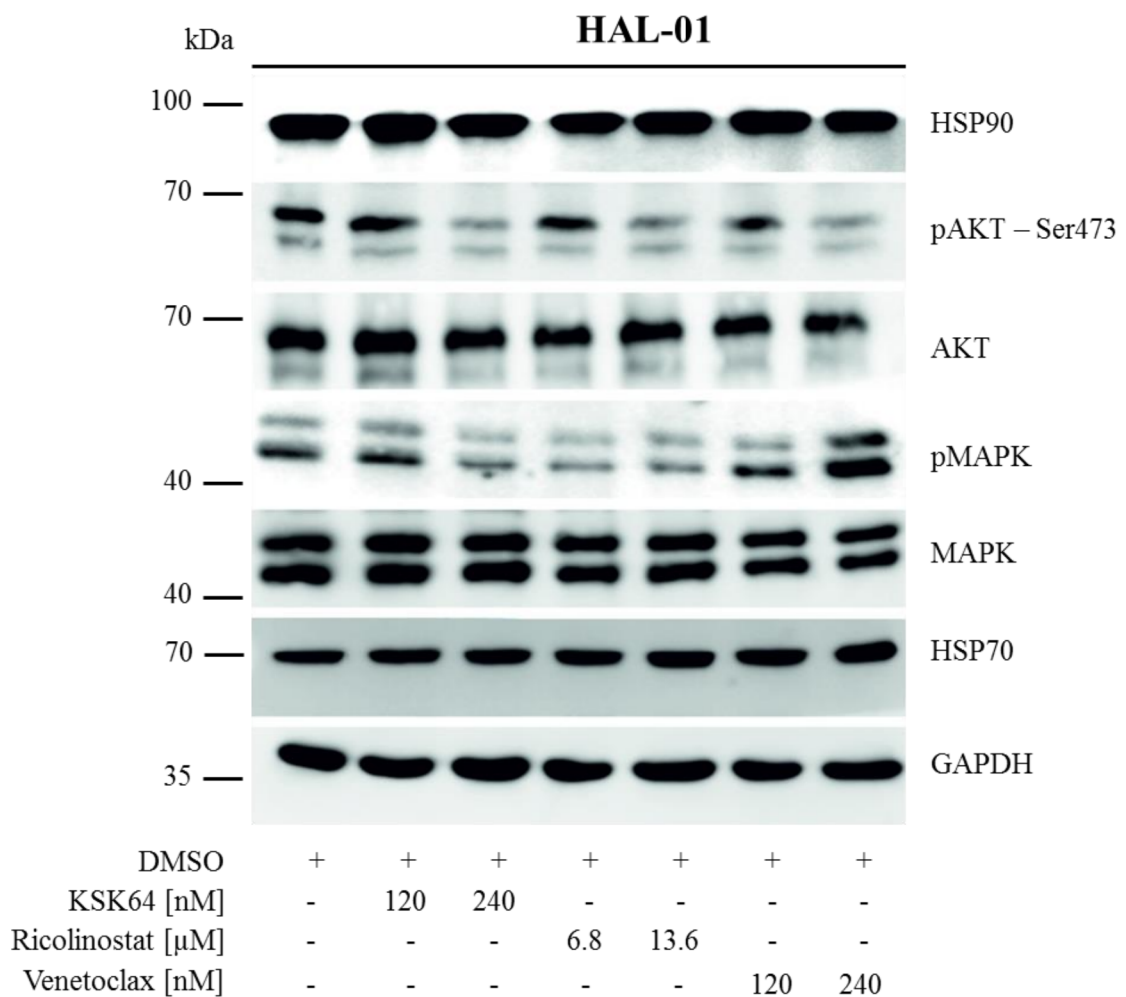

Figure 23: Immunoblot analysis of downstream targets of the HAL-01 cell line after exposure to **KSK64** for 24 h. Cancer related kinases such as (p)AKT and (p)MAPK were analyzed as well as the heat shock proteins HSP90 and HSP70.

Next, to assess the downstream signaling related to HDAC inhibition evoked by **KSK64**, HAL-01 cells were incubated with 120 nM or 240 nM of **KSK64** for 24 h (fig. 23). Interestingly, western blot analysis revealed that the phosphorylation status of AKT (Ser473) was reduced after the treatment of **KSK64** (240 nM). The same effect was observed after the treatment of ricolinostat (13.6 µM). Furthermore, the phosphorylation of MAPK was reduced after the treatment of **KSK64** (240 nM) and ricolinostat (6.8 µM and 13.6 µM).

3.5 *In vitro* characterization of the HDAC class I/IIb inhibitors 8e and 8a

After evaluating relatively selective or preferential HDAC6 inhibitors, HDAC class I/IIb targeting inhibitors with comparatively low HDAC6 selectivity were next tested (fig. 24). The data of this section are taken from our publication: *Synergistic induction of apoptosis in resistant head and neck carcinoma and leukemia by alkoxyamide-based histone deacetylase inhibitors. Eur. J. Med. Chem. 211, 113095 (2021)*.
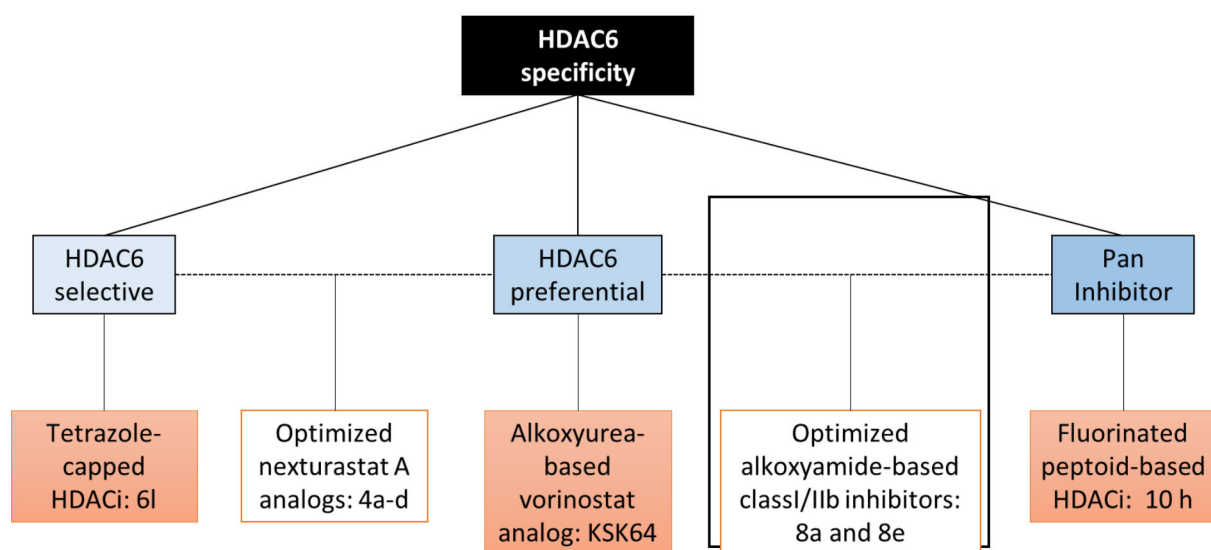
Figure 24: Overview of different HDAC inhibitors evaluated in this thesis. The black box highlights the inhibitor that will be described in this section.

In previously reported studies it was found that the cap group of the classical HDACi pharmacophore model is important for the cytotoxic effects of alkoxyamide-based HDACi. Therefore, new alkoxyamide-based class I/IIb HDAC inhibitors were developed with bicyclic (hetero)aromatic cap groups by the working group of Prof. Dr.
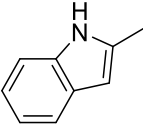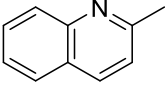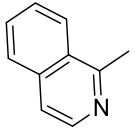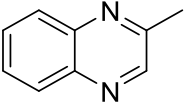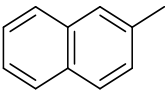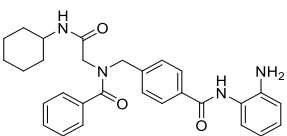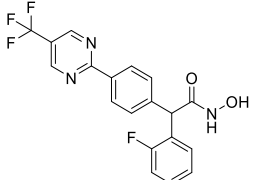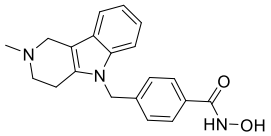
T. Kurz (Institut für Pharmazeutische und Medizinische Chemie Heinrich-Heine-Universität Düsseldorf) and characterized for their *in vitro* activity in leukemic cell lines. First, isozyme profiling was performed to analyze the selectivity of the newly designed alkoxyamide-based HDACi for the different HDAC classes. The compounds were tested against recombinant HDAC2, 4, 6, and 8, which represent class I (HDAC2, 8), IIa (HDAC4), and IIb (HDAC6). Vorinostat (pan HDACi), compound 2a (class I selective HDACi), CHDI00390576 (class IIa selective HDACi), and tubastatin A (class IIb selective HDACi) served as reference controls (table 19). All selected HDACi, except for vorinostat, 2a and 8c, show IC_{50} values for HDAC2 in the nanomolar range. The HDAC6 inhibition showed even lower IC_{50} for compound 6c, 8a, 8c, 8d and **8e**. Hence, compounds 6c, 8a, 8c, 8d, and **8e** are potent HDAC class I/IIb inhibitors, with a preference for HDAC6. The IC_{50} values for HDAC8 were relatively weak for all tested compounds as they were in the µM range. Furthermore, all compounds showed weak HDAC4 inhibition, except for the class IIa selective reference inhibitor CHDI00390576. Next, compounds **8a** and **8e** were chosen as lead compounds for further analysis of the functional specificity and efficacy in leukemic cell lines from different leukemic entities. Therefore, the specificity of the compounds **8a** and **8e** against different HDAC classes were analyzed with a cellular-based (HDAC class I/IIb and HDAC class IIa) activity assay using the HL60 cell line and the reference inhibitors CAY10603 and ricolinostat as controls (fig. 25 a). As expected, based on the isozyme profile, compounds **8a** and **8e** were able to deacetylate class I/IIb substrates in the nanomolar range but were unable to deacetylate class IIa specific substrates. The IC_{50} values for HDAC class I/IIb activity for **8a** and **8e** (73.2 nM and 85.1 nM, respectively) were comparable to the HDAC class IIb selective inhibitor CAY10603, whereas ricolinostat showed a significantly higher IC_{50} of 902 nM. The cellular HDAC inhibition data were further complemented with cell viability analysis, which was performed by incubating the HL60 cells with the respective inhibitors at the same time point, later the cell viability was measured using the ATP-based CellTiter-Glo luminescent cell viability assay. Based on the superior activity of **8a** and **8e**, these compounds were further tested against a panel of commercially available preferential and selective HDAC6i in different leukemic cell lines and four primary leukemic patient samples (Fig 26 a). Again, compound **8a** was the most potent inhibitor with IC_{50} values in the nanomolar range (data is shown in a clustered map), similar to **8e** and CAY10603. All other tested inhibitors showed IC_{50} values in the micromolar range. Based on the potent anti-
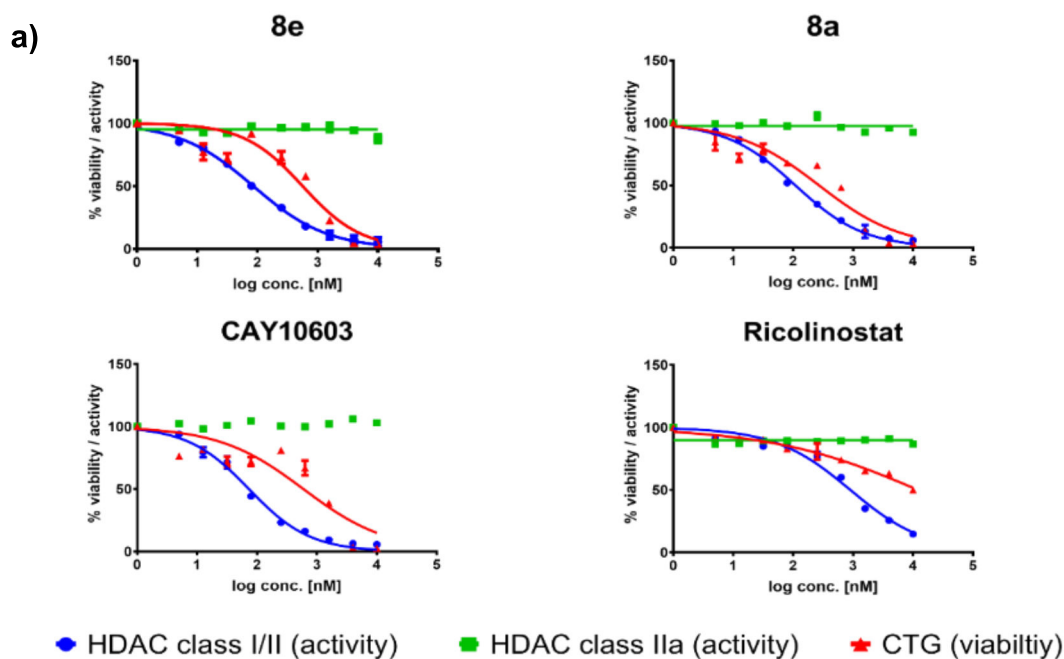
leukemic activity of compound **8a**, its induction of apoptosis was further analyzed with an enzyme-dependent caspase 3/7 assay. Therefore, HL60 cells were treated with the IC_{50} and IC_{75} concentration of compound **8a** and a 10-fold higher concentration of ricolinostat as a positive control for 48 h. Compound **8a** significantly induces apoptosis on both tested concentrations, similar to ricolinostat, however, with a 10-fold higher concentration (Fig. 26b) The potent cytotoxic activity and apoptosis induction of **8a** encouraged us to test for potential synergistic combination partners. In recent studies, it was shown that HDACi showed promising anti-cancer properties when combined with proteasome inhibitors[113,124]. Therefore, increasing concentrations of compound **8a** against increasing concentrations of the proteasome inhibitors bortezomib and carfilzomib were screened in the same set of leukemic cells that were used in the prior experiments (HAL-01 (B-ALL), Jurkat (T-ALL) and HL60 (AML)) using a semi-automated drug screening platform (fig. 27). Significant synergistic interactions of compound **8a** and bortezomib or carfilzomib were found in all three tested cell line. Especially, in the HL60 and Jurkat cell lines strong fields of synergy were detected. Next, the same kind of synergy screen for the reference inhibitor vorinostat was performed against the proteasome inhibitors bortezomib in the HL60 and Jurkat cell lines. No synergistic interaction between proteasome inhibitors and vorinostat in the Jurkat cell line and only minor synergistic effects in the HL60 cell line (fig. 28) were found, showing the superiority of our experimental inhibitor compared to vorinostat for the combinational treatment of proteasome inhibitors and HDAC inhibitors in leukemic cell lines.

Table 19: Inhibition of human HDAC 2, 4, 6 and HDAC8 by 6c, 8a, 8c-e and reference compounds vorinostat, 2a, CHDI00390576, Tubastatin A.
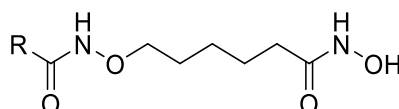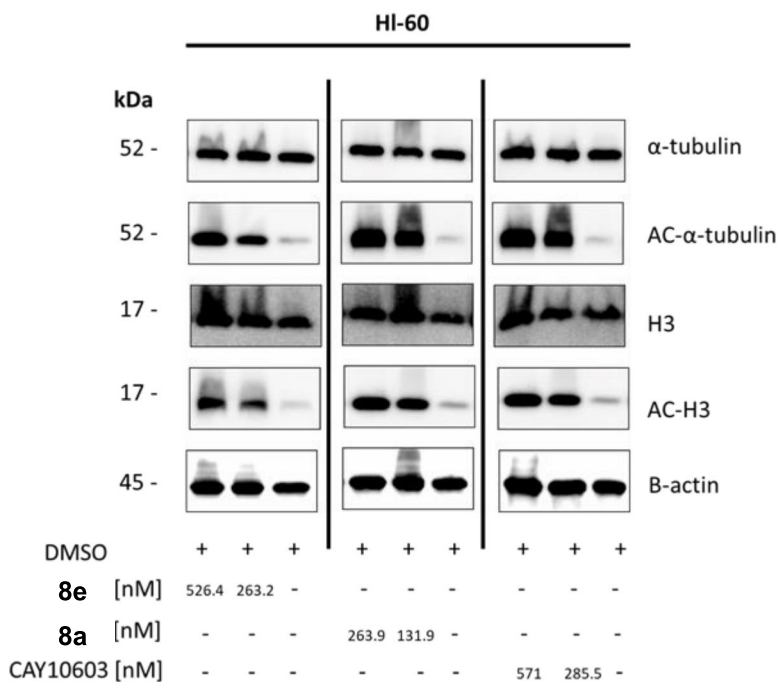

Compound	IC_{50} (µM)			
	HDAC2[a]	HDAC4[a]	HDAC6[a]	HDAC8[a]

|				
6c	0.057	55.7	0.013	10.3
8a	0.092	>100	0.025	9.78 (±1.45)
8c	0.759	>100	0.173 (±0.033)	12.4
8d	0.044 (±0.005)	60.8	0.018	7.95
8e	0.041	51.8	0.011	3.79
Vorinostat	0.107	47.8 (±6.68)	0.024 (±0.003)	2.26 (±0.35)
2a	0.283	>10	>10	9.21
CHDI00390576	ND	0.450	ND	ND
Tubastatin A	ND	ND	0.118	ND

Figure 25. a) Compounds **8a** and **8e** inhibit class I and class IIb histone deacetylases (HDACs) at different drug concentrations. The activity of class IIa HDACs was not affected by drug treatment. The cytotoxicity was determined after 72 h of incubation with the inhibitors using the CellTiter-Glo (CTG) Luminescent Cell Viability Assay. Each data point represents three replicates and error bars are ± s.d. Curve-fits to determine IC_{50} values (sigmoidal dose-response, variable slope) were calculated using GraphPad Prism. **b)** HL-60 cells were treated with compound **8e** and **8a** and CAY10603 for 24 h with the indicated concentrations. Afterwards, cell lysates were immunoblotted with acetyl-α-tubulin, acetyl-histone H3, α-tubulin and histone H3 antibodies. B-actin was used as loading control was used as a loading control.
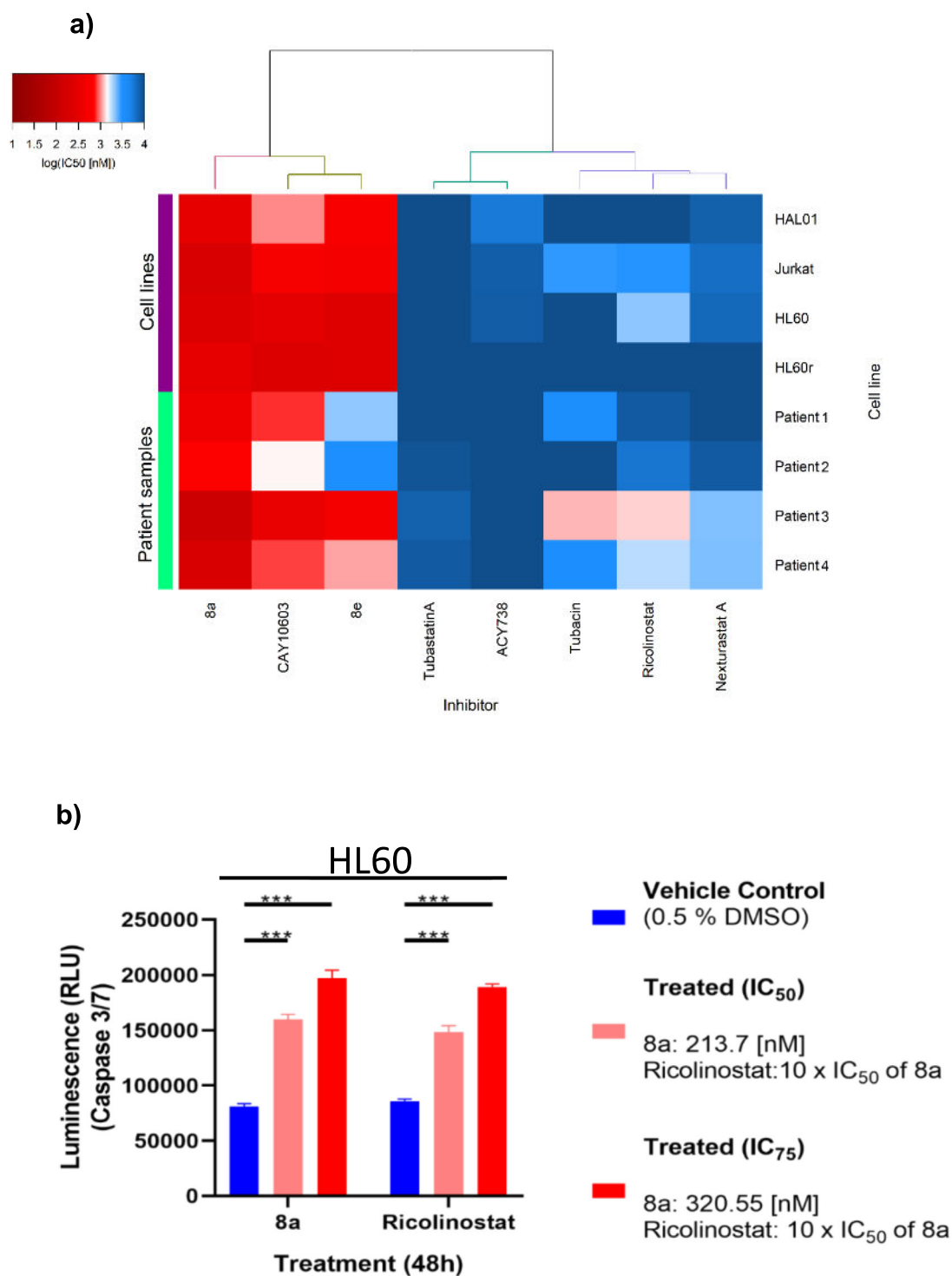
Figure 26: Cytotoxic analysis of compound **8a** and **8e**. **a)** Comparative IC_{50} (log IC_{50} nM) of different sub-groups of leukemic cell lines (HAL-01, HL60 and Jurkat), a bortezomib resistant form of HL60 (HL60-BTZr) and primary leukemic patient samples plotted as heatmap, after exposure of **8a** and **8e** in comparison to commercially available selective HDAC6 inhibitors tubastatin A, ACY-738, nexturastat A, ricolinostat, tubacin and CAY-10603. The IC_{50} data plotted as a clustered heat map, followed by unsupervised hierarchical clustering. The horizontal axis of the dendogram exemplifies the dissimilarity between clusters, whereas the color of the cell is related to its position along with a (log IC_{50} (nM) gradient. **b)** Compound **8a** induces caspase 3/7 activation in HL60 cells. HL60 cells were treated for 48 h with either **8a** (IC_{50} and IC_{75}) or Ricolinostat (10 x IC_{50} of **8a** and 10 x IC_{75} of **8a**) and subsequently analyzed for caspase 3/7 activation.
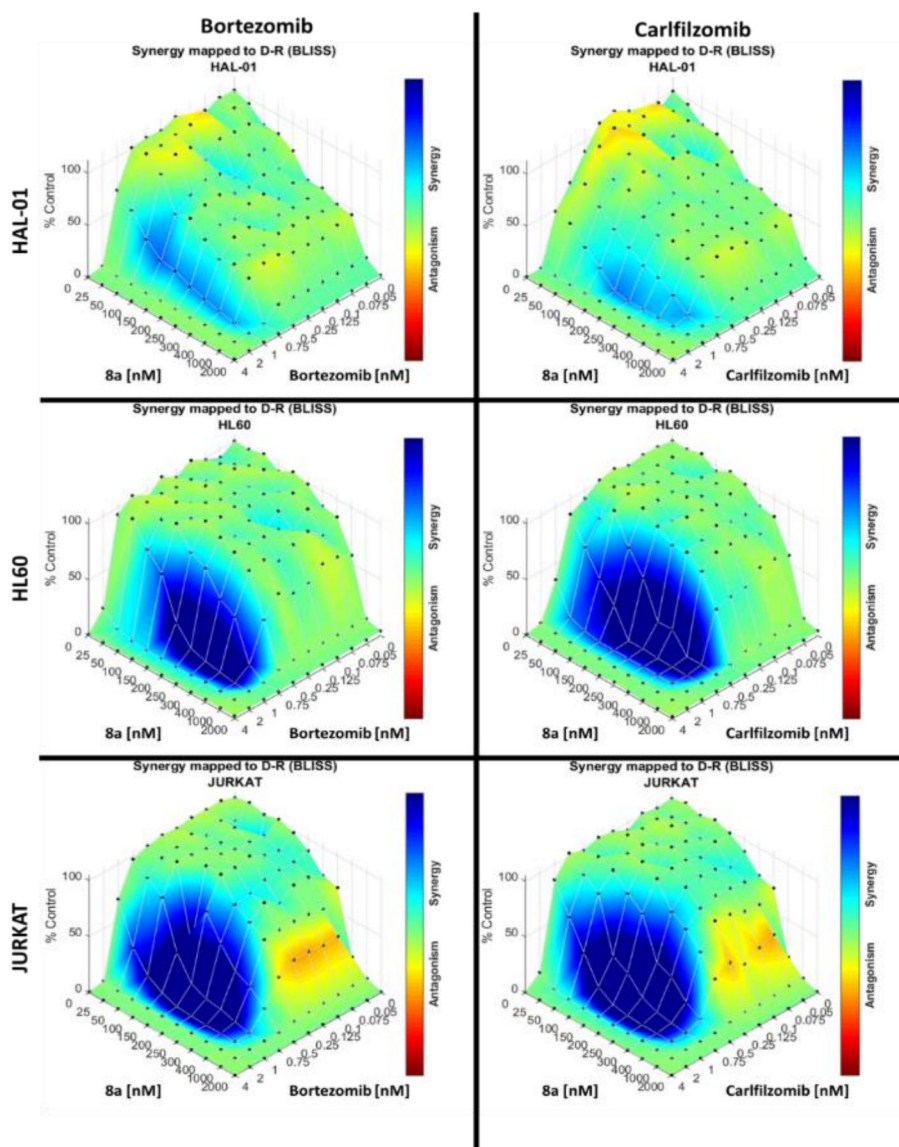
Figure 27: Compound **8a** synergizes with proteasome inhibitors. Bliss synergy plots of compound **8a** in combination with bortezomib or carfilzomib in HAL-01 (top), HL60 (mid), and Jurkat leukemic (bottom) cell lines (n=3). The Bliss synergy analysis and visualization were performed using the Combenefit software.
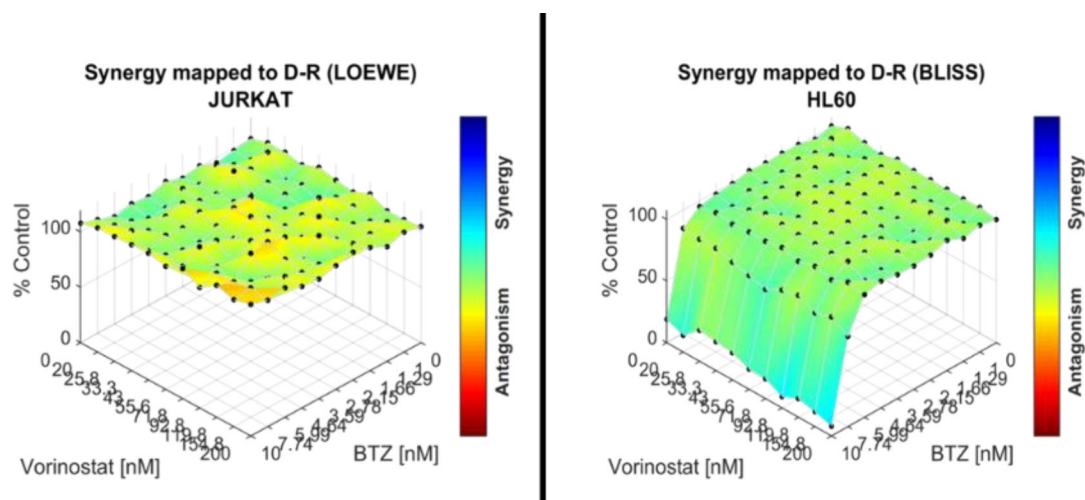
Figure 28: Vorinostat does not synergize with the proteasome inhibitor bortezomib. Bliss synergy plots of vorinostat in combination with bortezomib in Jurkat (left) and HL60 (right) cell lines (n=3). The Bliss synergy analysis and visualization were performed using the Combenefit software.

3.6 *In vitro* characterization of the peptoid-based pan HDAC inhibitor 10h

A new series of fluorinated peptoid-based HDACi (fig. 29) were synthesized by our collaborators, the working group of Prof. Dr. F. K. Hansen (Pharmaceutical and Cell Biological Chemistry, Pharmaceutical Institute, University of Bonn). These compounds were assessed concerning their HDAC inhibitory properties and selectivity. Two
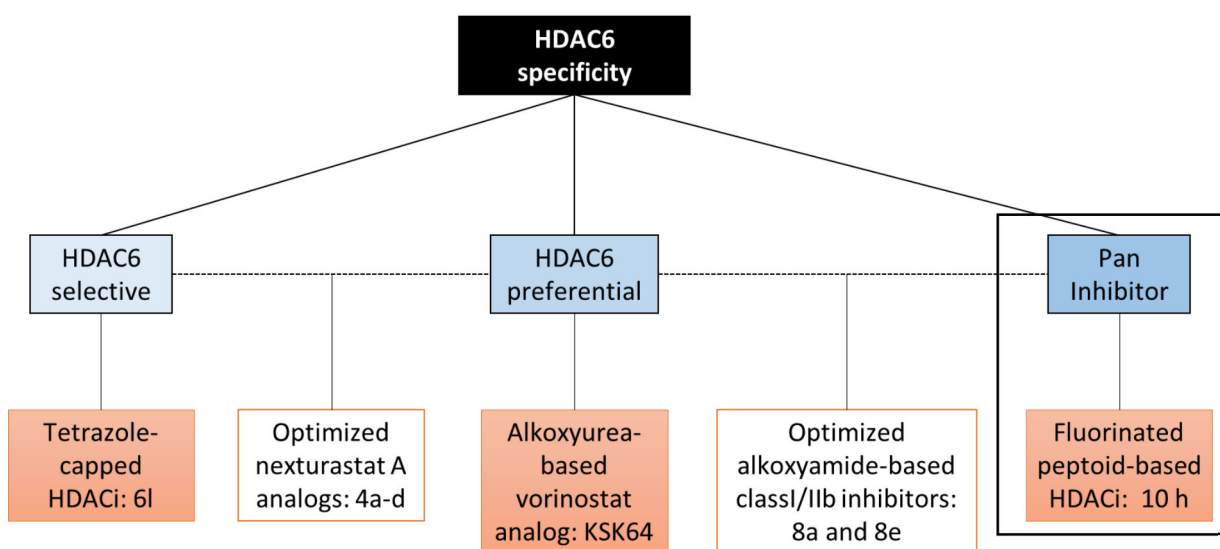
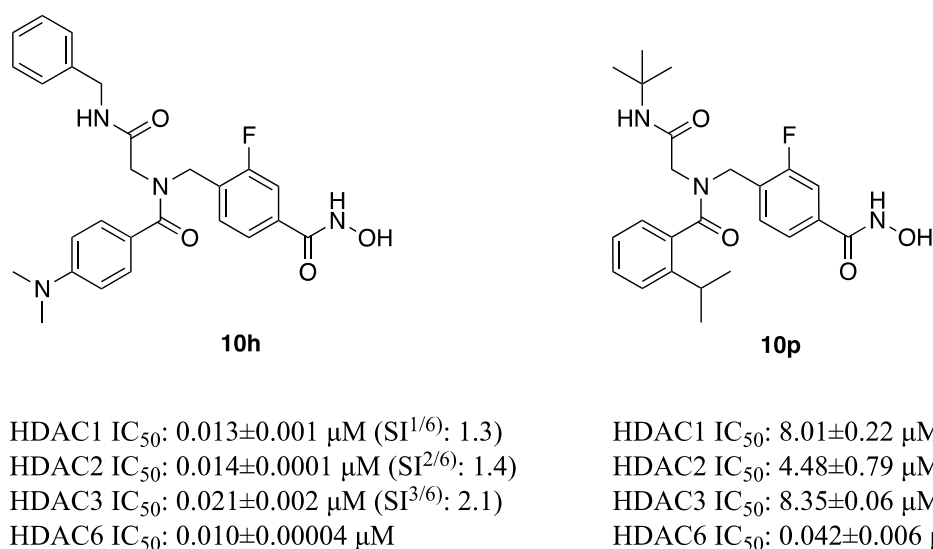**Figure 29:** Overview of different HDAC inhibitors evaluated in this thesis. The black box highlights the inhibitor that will be described in this section.

compounds came up as lead compounds based on their HDAC inhibition profile (fig. 30). Compound **10h** is classified as pan-HDACi based on their selectivity profile for HDAC1 (IC$_{50}$: 0.013 µM (SI 1/6 = 1.3), HDAC2 (IC$_{50}$: 0.014 µM (SI 2/6 = 1.4), HDAC3

(IC$_{50}$: 0.021 µM (SI 3/6 = 2.1), and HDAC6 (IC$_{50}$: 0.010 µM). Compound **10p** was chosen as the lead compound for further experimental investigation because of its selectivity profile (SI 1/6 = 191) which exceeded the selectivity profile of the reference HDAC6i tubastatin A (SI 1/6 = 172).

First, a drug screen was performed against a selection of leukemic cell lines (HAL-01, K562, Jurkat, MOLM13, HL60, MV4-11) to determine its cytotoxic effects on leukemic cell lines (fig. 30a). As expected, the pan-HDACi **10h**, showed low IC$_{50}$ values in the nanomolar range in nearly all tested cell lines, except for HAL-01. The lowest IC$_{50}$ was observed in the AML cell lines MOLM13 with 100 nM. In sharp contrast, the selective HDAC6i

10h

10p

HDAC1 IC$_{50}$: 0.013±0.001 µM (SI$^{1/6}$: 1.3)
HDAC2 IC$_{50}$: 0.014±0.0001 µM (SI$^{2/6}$: 1.4)
HDAC3 IC$_{50}$: 0.021±0.002 µM (SI$^{3/6}$: 2.1)
HDAC6 IC$_{50}$: 0.010±0.00004 µM

HDAC1 IC$_{50}$: 8.01±0.22 µM (SI$^{1/6}$: 191)
HDAC2 IC$_{50}$: 4.48±0.79 µM (SI$^{2/6}$: 107)
HDAC3 IC$_{50}$: 8.35±0.06 µM (SI$^{3/6}$: 199)
HDAC6 IC$_{50}$: 0.042±0.006 µM

Figure 30: Inhibition of HDACs 1-3 and HDAC6 by the selected hit compounds **10h** and **10p**. Selectivity index (SI = IC$_{50}$ (HDAC1)/IC$_{50}$ (HDAC6)).

10p, showed high IC$_{50}$ values in all tested cell lines (> 20µM). The reference inhibitors CI-994 and ricolinostat showed moderate IC$_{50}$ values in the low µM range. Interestingly ricolinostat and CI-994 were generally lower in the AML cell lines (MV4-11, HL60, and MOLM13).
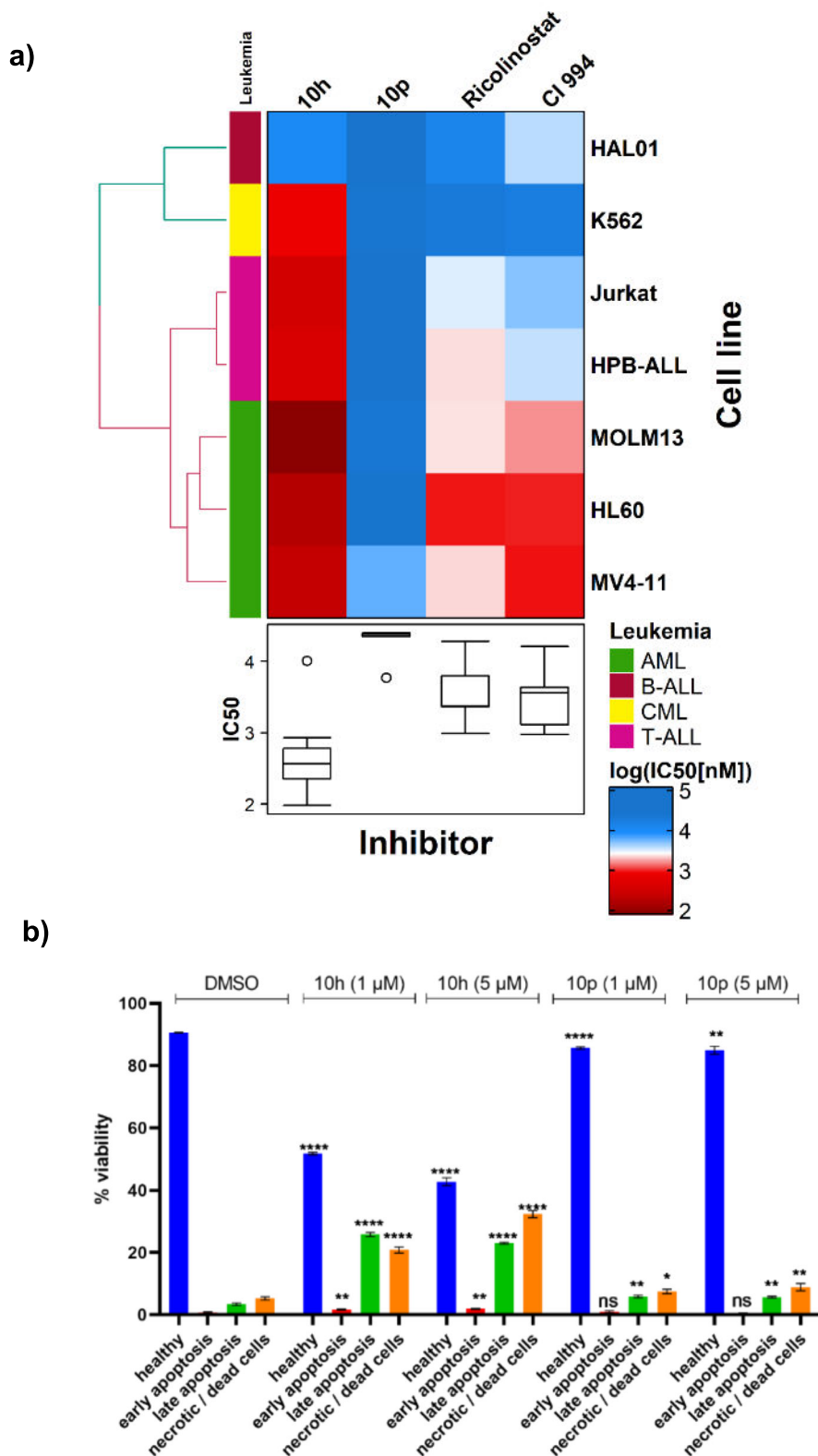
Figure 31: Cytotoxic and target specificity analysis of compounds **10h** and **10p a)** Comparative cellular viability (log IC$_{50}$ nM) of different sub-groups of leukemic cell lines (K562, Jurkat, HAL-01, MV4-11, HL60 and MOLM13), after treatment with **10h** and **10p** in comparison to the commercially available selective HDAC6 inhibitors ricolinostat and HDAC class I inhibitor CI-994. The IC$_{50}$ data plotted as a clustered heat map, followed by unsupervised hierarchical clustering. The horizontal axis of the dendogram exemplifies the dissimilarity between clusters, whereas the color of the cell is related to its position along with a log IC$_{50}$ (nM) gradient. **b)** Annexin-PI staining of HL60 cells exposed to **10p** and **10h** at 1 µM and 5 µM after 48 h (n=3).

To elucidate the cytotoxic effects of **10h** and **10p**, the induction of apoptosis was determined following their treatment in HL60 cells. HL60 cells were treated with 1 µM or 5 µM of **10h** and **10p** for 48 h, stained with annexin V and propidium iodide, and analyzed by flow cytometry (fig. 31b). There was a significant ($p < 0.0001$) increase in apoptotic cells observed after the treatment with the unselective inhibitor **10h** at 1 µM as well as 5 µM, indicating that induction of apoptosis is involved in the antitumoral effects of **10p**. There was also a significant increase in apoptosis after the treatment with the HDAC6 selective inhibitor **10p** at 1 µM or 5 µM observed ($p < 0.05$), but to a lesser extent compared to the unselective inhibitor **10h**. To further assess the *in-vitro* characteristics of **10h** and **10p**, the target specificity of the respective inhibitors was analyzed. Therefore, HL60 cells were treated with the respective $IC_{12.5}$, IC_{25}, IC_{50}, and IC_{75} concentrations of the inhibitors **10h** and **10p** for 24 h, were subsequently immunoblotted, and compared to HL60 cells treated for 24 h with the reference inhibitor ricolinostat at its IC_{50} concentration (fig. 32). After the treatment with the unselective HDACi **10p**, a concentration-dependent increase in the acetylation of α-tubulin and H3 was observed. After the treatment with the selective HDAC6i **10h** only the acetylation of α-tubulin was induced but not the acetylation of H3. Ricolinostat-treated cells also induced the acetylation of α-tubulin but also the acetylation of H3, however, compared to the **10p** treated cells, ricolinostat showed lower levels of H3 acetylation.

												Acetyl-α-tubulin
												Acetyl-H3
												GAPDH
DMSO	+	+	+	+	+	+	+	+	+	+	+	
10h (nM)	-	49	99	197	296	-	-	-	-	-	-	
10p (µM)	-	-	-	-	-	-	6	12	24	36	-	
Ricolinostat (µM)	-	-	-	-	-	-	-	-	-	-	0.9	
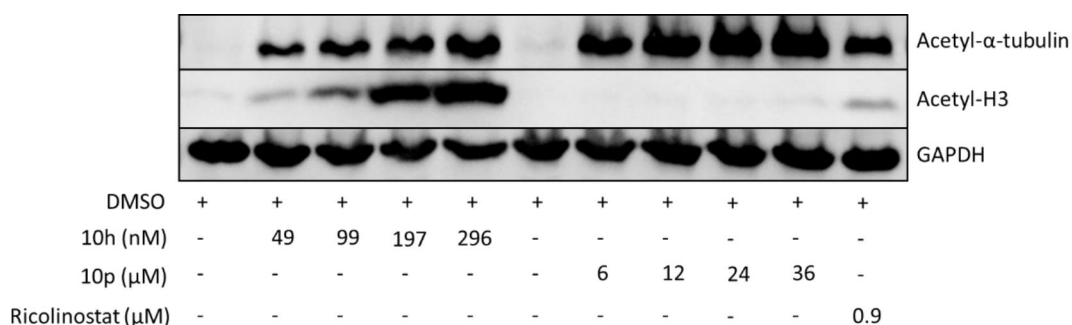
Figure 32: Immunoblot of HL60 cells after 24 h treatment with **10h**, **10p** and ricolinostat at the indicated concentrations. Cell lysates were immunoblotted with anti-acetyl-α-tubulin, acetyl-histone H3 antibodies. GAPDH was used as a loading control.

Based on the potent cytotoxic effects of **10h,** it was tested together with the DNA methyltransferase inhibitor decitabine as a potential synergistic combination partner. In a recent study, it was shown that HDAC inhibitors synergistically interact with decitabine, which motivated me to analyze its effect in combination with **10h**[126].

Increasing concentrations of **10h** (0.1 – 2 µM) against increasing concentrations of decitabine (0.25 – 10 µM) in different subsets of leukemic cell lines from different entities HL60 (AML), MOLM13 (AML), Jurkat (T-ALL) and HAL-01 (B-ALL) using 10 x 10 dose-response matrices was next tested (fig. 32). A strong synergistic interaction of compound **10h** and decitabine in the AML cell lines (HL60, MOLM13) was found, in contrast to other two tested non-AML cell lines (Jurkat (T-ALL) and HAL-01 (B-ALL). Next, HL60 cells were treated with 200 nM or 400 nM of **10h** or decitabine alone and in combination with each other for 24 h. Immunoblot analysis identified that **10h** alone or in combination with decitabine was able to induce acetyl-α–tubulin acetylation, whereas decitabine alone was not able to induce acetyl-α-tubulin expression. Slight acetyl-H3 induction was observed after treatment with **10h** alone and decitabine alone. Interestingly, hyperacetylation of α-tubulin was only observed in the combination of decitabine and **10h**.
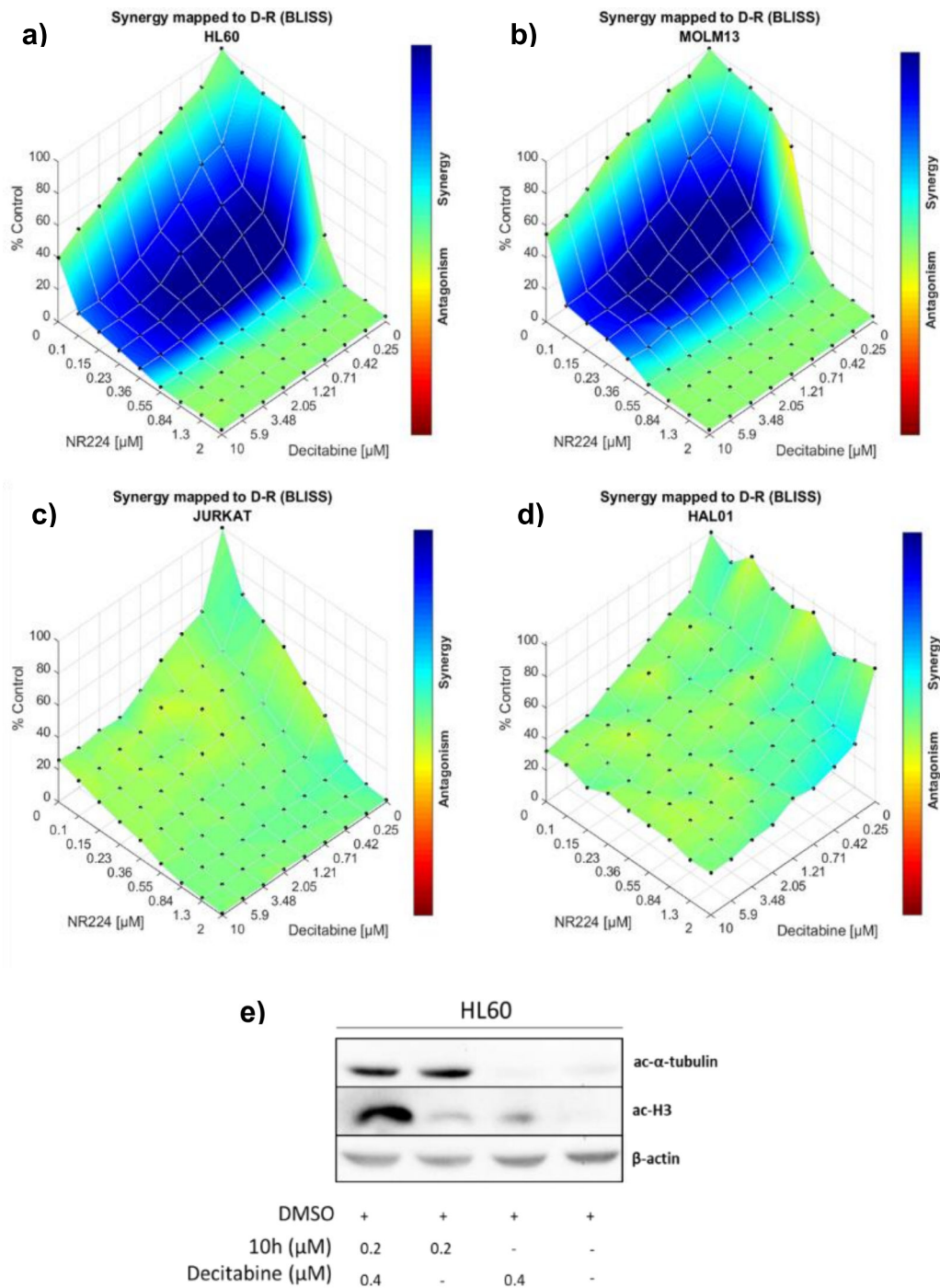
Figure 33: Compound **10h** synergizes with the DNA methyltransferase inhibitor decitabine in AML cell lines. **a)** Bliss synergy plot of compound **10h** in combination with decitabine in the HL60 cell line (AML). (n=3) **b)** Bliss synergy plot of compound **10h** in combination with decitabine in the MOLM13 (AML). (n=3) **c)** Bliss synergy plot of compound **10h** in combination with decitabine in the HAL-01 cell line (BCP-ALL cell line). (n=3) **d)** Bliss synergy plot of compound **10h** in combination with decitabine in the Jurkat cell line (T-ALL). (n=3) The Bliss synergy analysis and visualization were performed using the Combenefit software. **e)** Immunoblot of HL60 cells after 24 h of treatment with **10h** alone and in combination with decitabine with the indicated concentrations. Afterwards, cell lysates were immunoblotted with anti-acetyl-α-tubulin, acetyl-histone H3 antibodies. β-actin was used as a loading control.

3.6.1 Pilot study: Evaluation of *in vivo* activity of 10h

To further analyze the therapeutic potential of **10h** a pilot *in-vivo* study was performed in a xenograft mouse model of the HPBALL (T-ALL) cell line. HBP-ALL cells expressing stable GFP and luciferase were injected into the tail vein of 10 NSG (NOD SCID gamma) mice. The tumor engraftment and tumor burden over time were measured by

a)

T: Treatment

V: Vehicle

- : Exculded

b)
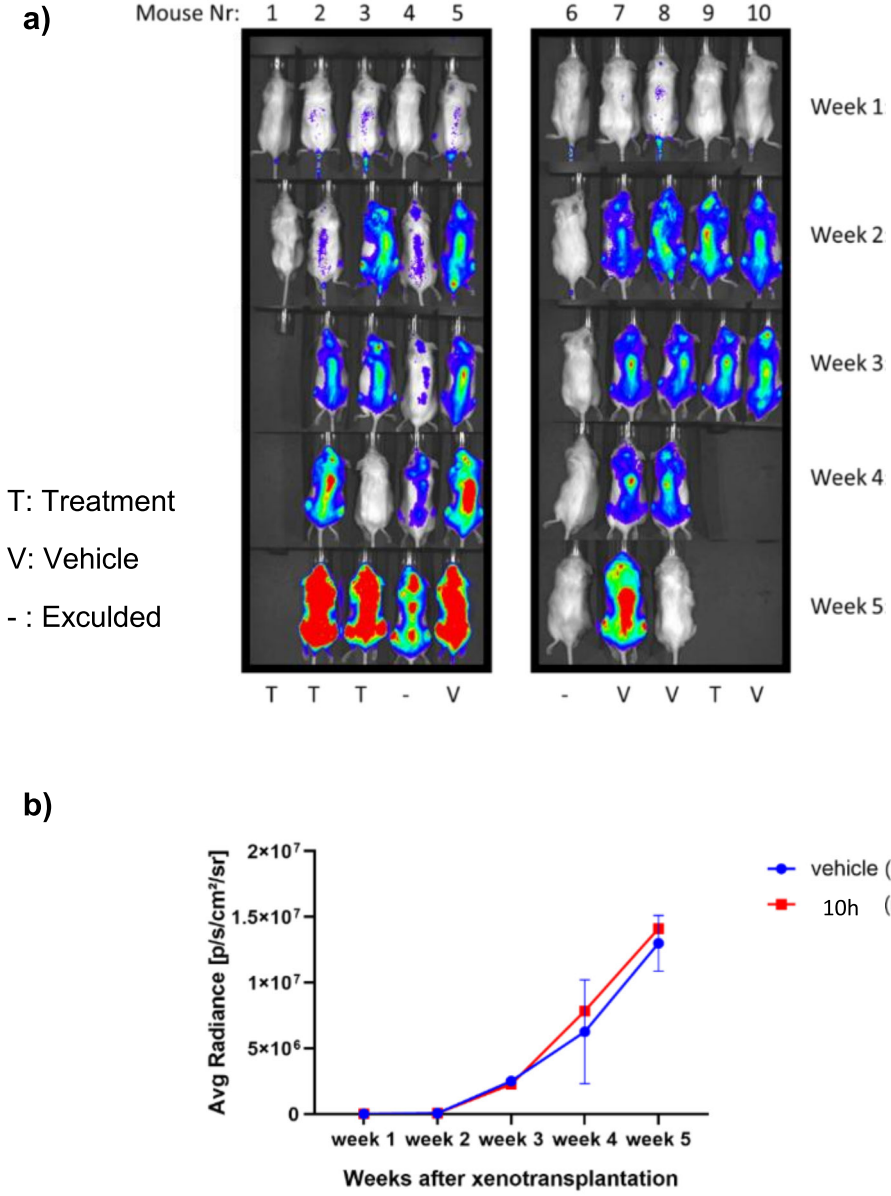
Figure 34: a) Bioluminescence imaging of HPB-ALL xenograft mice post vehicle or **10h** treatment. Mice were treated twice a week with either 100 mg/kg or vehicle for two consecutive weeks. IVIS pictures of the respective treatment groups and the day post transfection. The scaling was adjusted for each measurement time point and is used to compare the intensities between the individual treatment groups of the specific day. **b)** Average ROI measurements of the different mice groups (treated vs. vehicle) of each measured time point.

bioluminescence imaging three days after injection. Subsequently, mice that were positive for the luciferase-bearing HPB-ALL cells were treated twice a week with 100 mg/kg of **10h** or vehicle control for two consecutive weeks. Four weeks after the injection of the cells 6 mice were alive, two vehicle control mice, two treated mice, and two mice that were initially excluded from treatment or vehicle group as they were defined as negative for the HPB-ALL cells, three days after injection. No difference in tumor burden was detected between the treatment group and vehicle group based on the bioluminescence data (fig. 34). Mouse 7 (vehicle group) appeared to have fewer tumor cells compared to mouse 2 or mouse 3 (treatment group). Next to bioluminescent data, the weight of the mice was monitored weekly, and found no significant differences between the treated and vehicle group except for mouse 1 (treatment group) which lost a significant amount of weight during week 1 and also died after week 1 during the anesthesia (fig. 35). Four days after the last bioluminescence measurement, retrobulbar bleeding was performed to analyze the proportions of human cells compared to mice cells in the blood of the mice (fig. 36). In mouse 2 and 3 (treatment group), 3.31 % and 4.87 % human cells were observed, respectively. In mice 5 and 7 (vehicle group) 2.34 % and 0.86 % human cells were found, respectively. After sacrificing the mice, the spleen was analyzed regarding the proportions of human to mouse cells. In mice 2 and 3 (vehicle group) 7.35 % and 6.99 % of human cells were found, respectively. In mice 5 and 7 (vehicle group) 11.98 % and 1.83 % of human cells were found, respectively. Next to this, the liver, kidney, and spleen were isolated and compared among the mice (fig. 37). No obvious difference between treated or vehicle mice was detected and all organs looked normal and healthy.
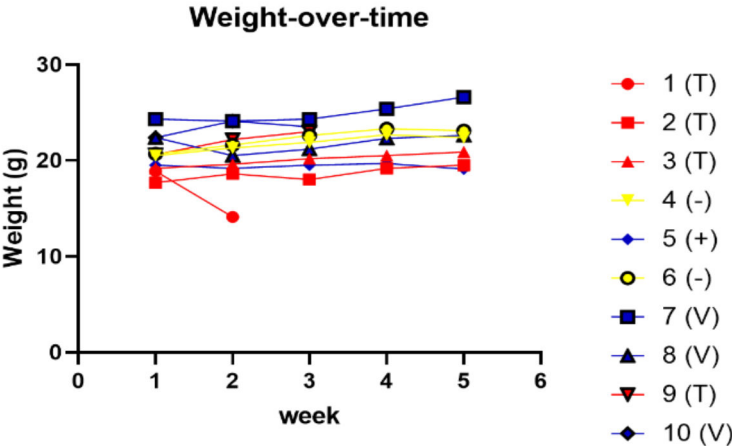

Figure 35: Weekly weight measurements of HPB-ALL xenograft mice.
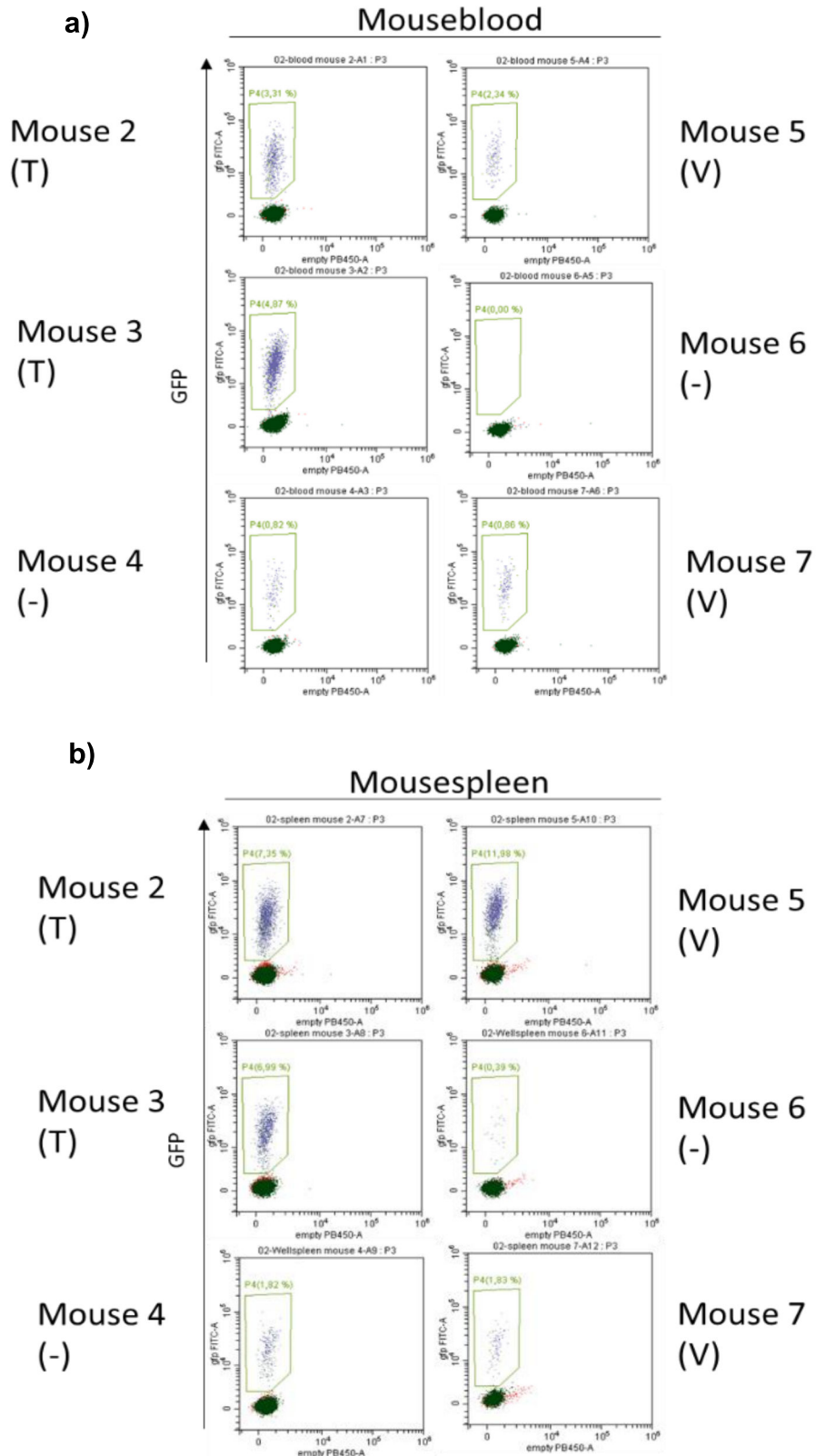
Figure 36: FACS analysis of mouse blood and mouse spleen after week5 for the proportion of mouse to human cells. **a)** The blood of two mice of the treatment arm, two mice of the vehicle arm and two mice that were initially excluded from the experiment were analyzed for the proportion of mouse to human cells. **b)** After sacrificing the mice, the spleen of the same mice that were used for the blood analysis were used to analyze to proportions of mouse to human cells in the spleen.
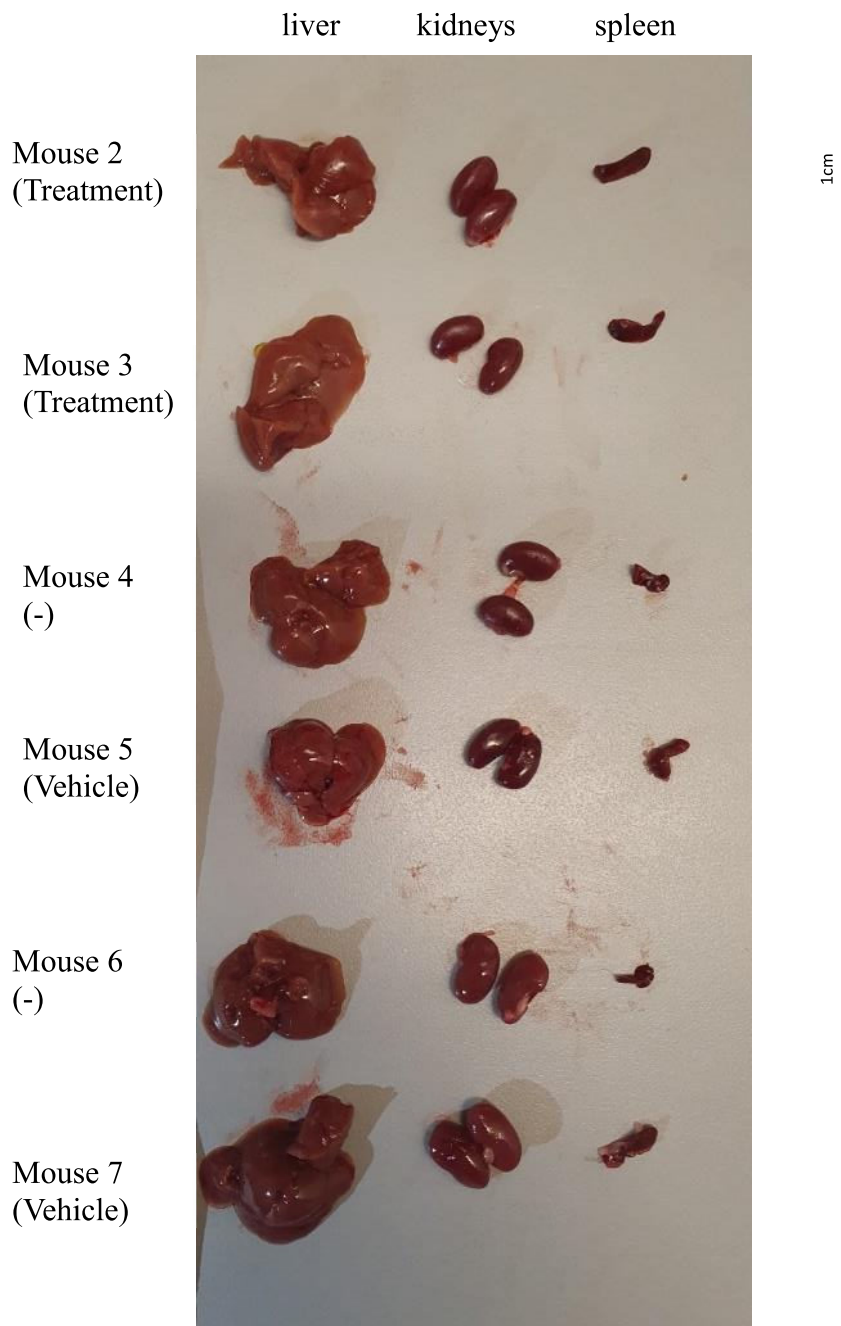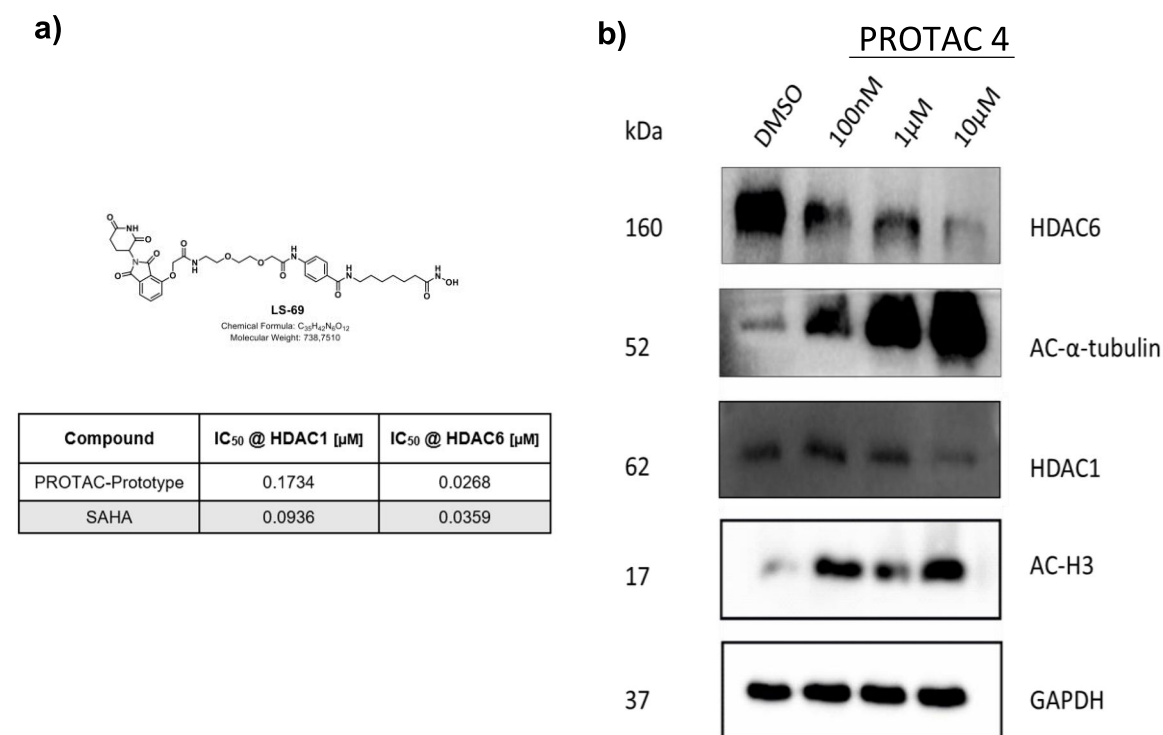
Figure 37: Comparison of liver, kidneys and spleen of mice that were either treated, received the vehicle or that were initially excluded from the experiment.

3.7 In vitro characterization of the proteolysis targeting chimera (PROTAC) PROTAC 4

Our collaborators, the working group of Prof. Dr. F. K. Hansen (Pharmaceutical and Cell Biological Chemistry, Pharmaceutical Institute, University of Bonn), developed an efficient solid-phase synthesis protocol using hydroxamic acids immobilized in resins (HAIR) to prepare the HDAC degrader **PROTAC 4**. The data of this section are taken from our publication*: Sinatra, L. et al. Hydroxamic Acids Immobilized on Resins (HAIRs): Synthesis of Dual-Targeting HDAC Inhibitors and HDAC Degraders (PROTACs). Angew. Chemie - Int. Ed. **59**, 22494–22499 (2020).* Cell-free isozyme profiling showed that **PROTAC 4** inhibits HDAC1 with 0.17 µM and HDAC6 with 0.027 µM. To characterize the bioactivity of **PROTAC 4**, HL60 cells were

a)

| Compound	IC$_{50}$ @ HDAC1 [µM]	IC$_{50}$ @ HDAC6 [µM]
PROTAC-Prototype	0.1734	0.0268
SAHA	0.0936	0.0359

b)

Figure 38: Analysis of target specificity of **PROTAC 4**: **a)** Isoform profiling of **PROTAC 4** and the reference inhibitor SAHA (vorinostat) for HDAC1 and HAC6. **b)** Immunoblot analysis of HL60 cells treated for 24 h with increasing concentration of **PROTAC 4**. The cell lysates were immunoblotted with HDAC6, anti-acetyl-α-tubulin, HDAC1 and acetyl-histone H3 antibodies. GAPDH was used as a loading control.

treated with three different concentrations of **PROTAC 4** (0.1 µM, 1 µM, and 10 µM) for 24 h. Afterward, whole cell lysates were analyzed by immunostainings, and the concentration-dependent degradation of HDAC1 and especially HDAC6 was validated (fig. 38). Furthermore, the treatment with the **PROTAC 4** induced hyperacetylation of

α-tubulin (a marker for reduced HDAC6 activity) and H3 (a marker of reduced HDAC 1-3 activity). Hence, these results confirm **PROTAC 4** as an efficient HDAC degrader that is suitable for the chemical knock-down of histone deacetylases.

Next, drug screens were performed to determine the IC_{50} of PRTOAC 4 but found that **PROTAC 4** was not affecting the cell viability after 72 h incubation with a concentration of up to 25 μM. An enzymatic caspase 3/7 assay was performed to determine the induction of caspase-dependent apoptosis (fig. 39). Neither 1 μM nor 10 μM of the **PROTAC 4** was enough to induce apoptosis in the 697 (TCF3-PBX1) cell line after 48 h of incubation. Ricolinostat-treated cells served as control and caspase 3/7 dependent induction of apoptosis was detected with ricolinostat at 2.1 μM.
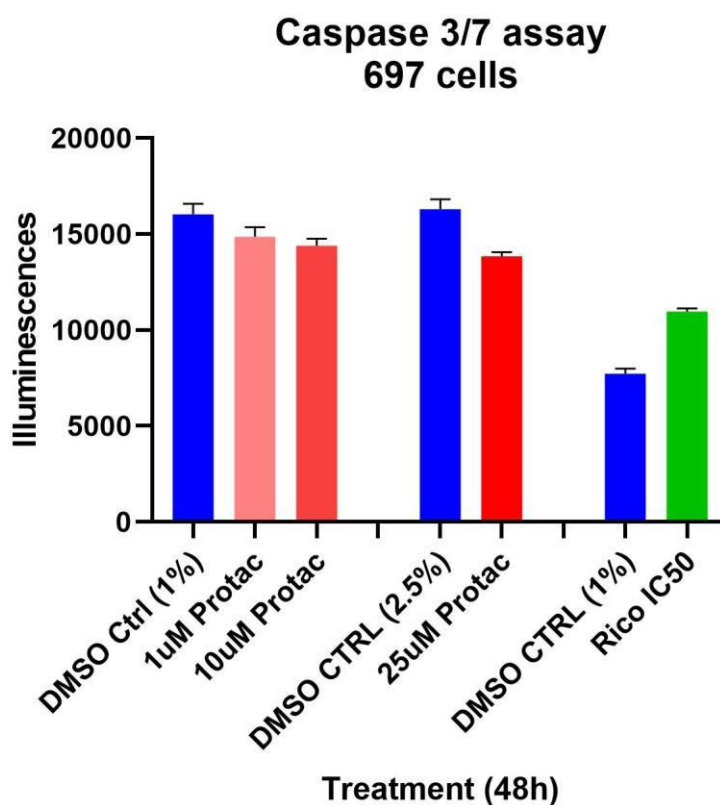
Figure 39: Caspase 3/7 assay of 697 cells treated with **PROTAC 4** with the indicated concentrations. Ricolinostat treated cells served as positive control.

Part 2: The molecular mechanism of HDAC6 inhibition and its biological relevance

### 3.8 The molecular mechanism of preferential HDAC6 inhibitors

Based on the assessed inhibitors in part 1, it was observed that preferential HDAC6 inhibitors, like **KSK64**, were showing relatively low IC_{50} values compared to the selective HDAC6 inhibitors (**6l, 10p**). Furthermore, **KSK64** showed a particularly low IC_{50} value in the resistant subgroup of leukemia, mainly the TCF3-HLF+ HAL-01 cell line. To identify the molecular mechanism behind the **KSK64** activity, HAL-01 and 697 cells were treated with **KSK64** and ricolinostat at their IC_{50} concentrations for 8 and 24 h and subjected to RNA sequencing (RNAseq) analysis. Principal coordinates analysis (PCoA) was used to control for the quality of the triplicates of the RNAseq samples (fig. 40). All samples from the same condition cluster together and thus the overall quality was suited for further analysis.

The next step was to analyze the differentially expressed genes (DEGs) after the treatment with a preferential HDAC6 inhibitor (**KSK64**). It was chosen to analyze the DEGs after 8 h because those genes can be more considered direct target genes in contrast to the gene expression after 24 h, as many indirect target genes will be altered as well. The DEGs were visualized with a volcano plot, whereby each dot represents a gene. The red and blue dots need to fulfill two requirements, a –log10 false discovery rate (FDR) of at least 1.3 (0.05% FDR) and log2 fold change in expression of at least 1 or -1 (fig. 40). Light blue and pink dots represent down or upregulated genes with a low read coverage. The grey dots represent genes that had a too-low fold change and the black dots represent genes that showed a too-high FDR and were not used for further analysis. The DEGs with the overall highest significance are highlighted by their names. In the HAL-01 cell line after 8 h of **KSK64** treatment, the most significant upregulated genes are RIMS3, SAMHD1, STK17B, PRKCB, SNN, ITM2C, and COTL1 and the most significant downregulated genes IGL1, TRIMM22, and GRK2. The most significantly upregulated genes in the 697 cell line are RASSF4, CREG1, IRGM, JUN, SAMHD1, STIM1, CFH, FOS, and BMF and the most downregulated DEG is UTP20. The most significant changes in expression in both cases were upregulated genes. The next step was to interpret and identify the biological processes based on the altered gene expression. Therefore, gene set enrichment analysis (GSEA) was performed, which focuses on the coordinated differential expression of gene groups,

or gene sets and produces results that can be interpreted in terms of biological processes. Specifically, two different gene set collections were used for further analysis. First, the hallmark gene set collection, which consists of genes that display coordinate expression and represent well-defined biological processes. Second, the curated gene set, which are gene sets that are manually curated by investigators and are thus experimentally validated gene sets. Interestingly, both cell lines showed a similar pattern of downregulated hallmark gene sets (fig. 42) after 8 h of **KSK64** treatment. The color of the dot represents its FDR, whereby red means low FDR and blue high FDR. In both cell lines the G2M checkpoints, E2F target, and myc targets hallmark gene sets were downregulated. In the 697 cell line, the hallmark gene sets for hypoxia and allograft rejection were upregulated. The number of up and down-regulated curated gene sets is higher compared to the hallmark gene sets as it consists of many gene sets compared to the number hallmark gene sets (fig. 43) (50 gene sets and 6366 gene sets respectively). However, two gene sets (HELLER_HDAC_TARGETS_UP and HELLER_HDAC_TARGETS_SILENCED_BY_METHYLATION_UP) are specifically interesting as they represent gene sets that are based on multiple myeloma cell lines that were treated with TSA only and TSA together with decitabine, respectively. Clusterprofiler was further used to analyze and visualize functional genes and gene clusters (fig. 44). In the HAL-01 cell line the upregulated gene clusters were involved in morphological changes, cell signaling, muscle and blood biology, neuronal synapse formation, and immune repose regulation. Down-regulated gene clusters were involved in mRNA regulation, tRNA regulation, methylation, and acetylation biology (fig. 44 a). In the 697 cell line upregulated gene clusters were involved in G protein-coupled receptor signaling, immune response, exocytosis, muscle and blood regulation, and neuronal synapse regulation. Downregulated gene clusters have a function in mitochondrial translation, acetylation, methylation, tRNA, rRNA, mRNA, and general RNA biology (fig. 44 b).
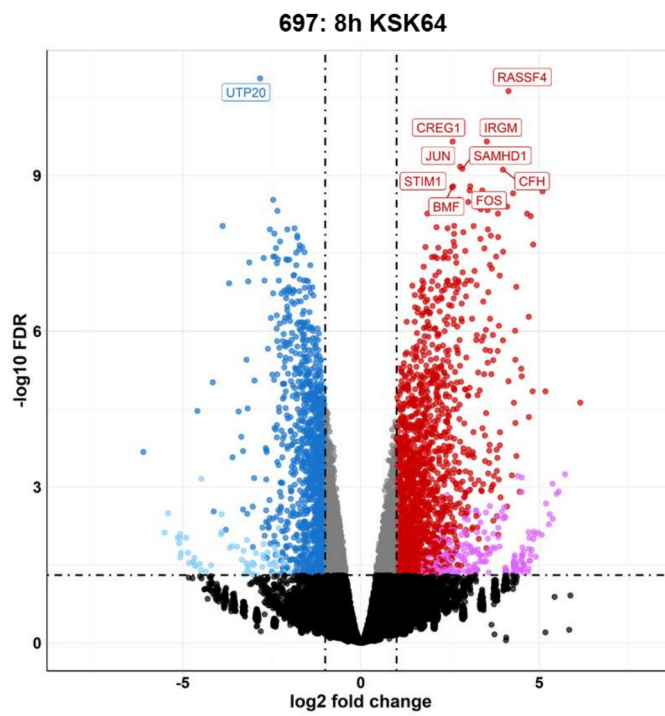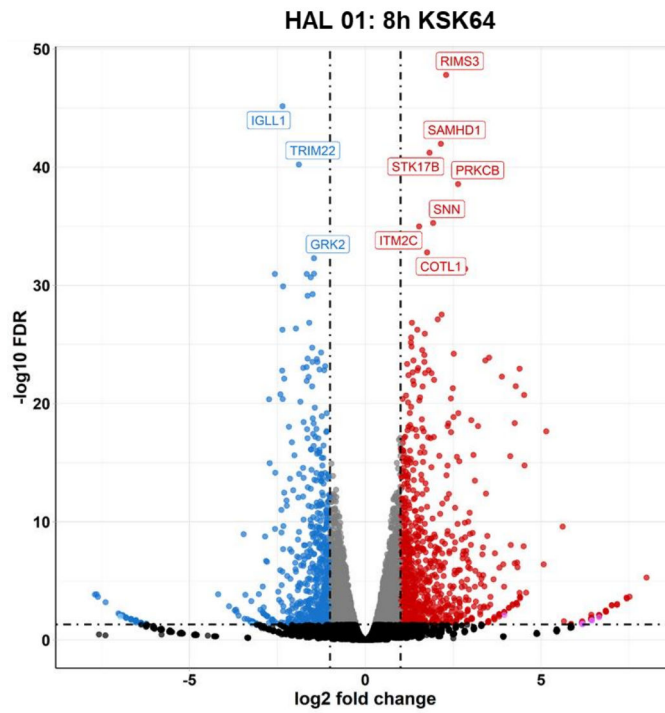
Figure 41: Volcano plots of DEG's after 8 h of **KSK64** treatment. **a)** Hall-01 cell line, **b)** 697 cell line
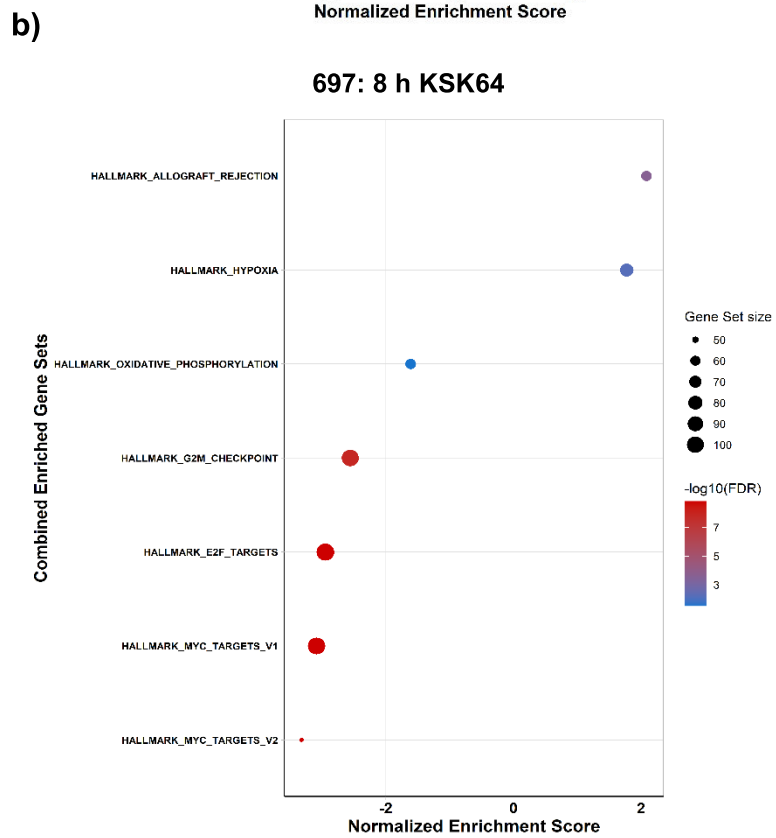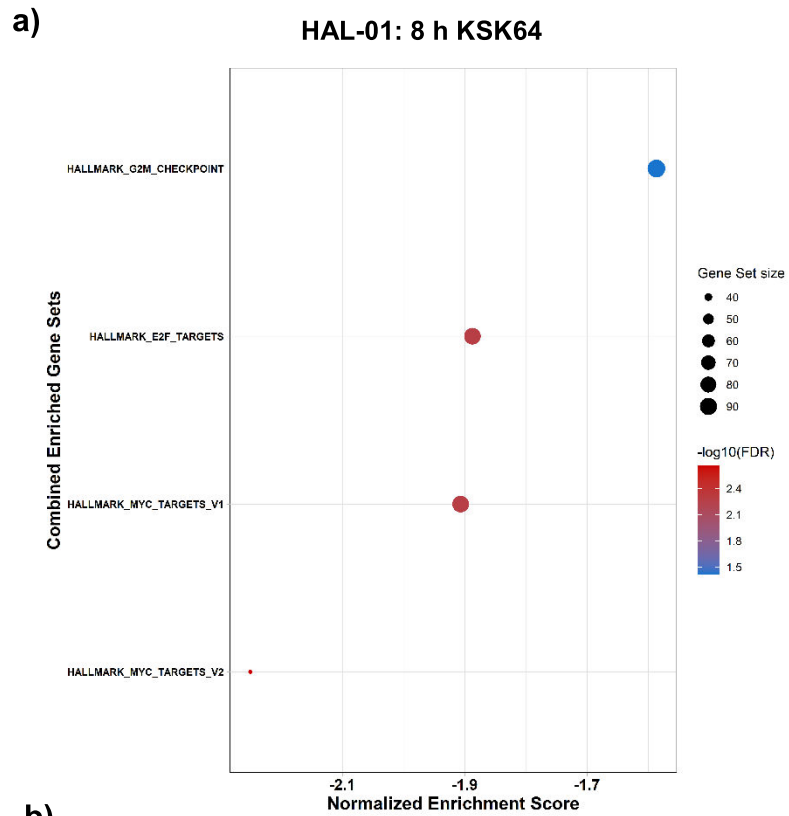
Figure 42: Enriched Hallmark gene sets in the **a)** HAL-01 cell line and **b)** 697 cell line after 8 h of **KSK64** treatment.
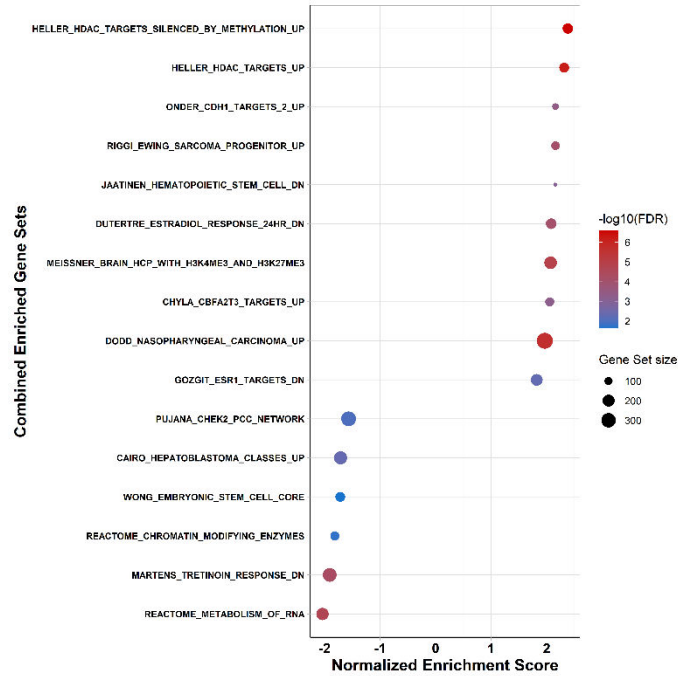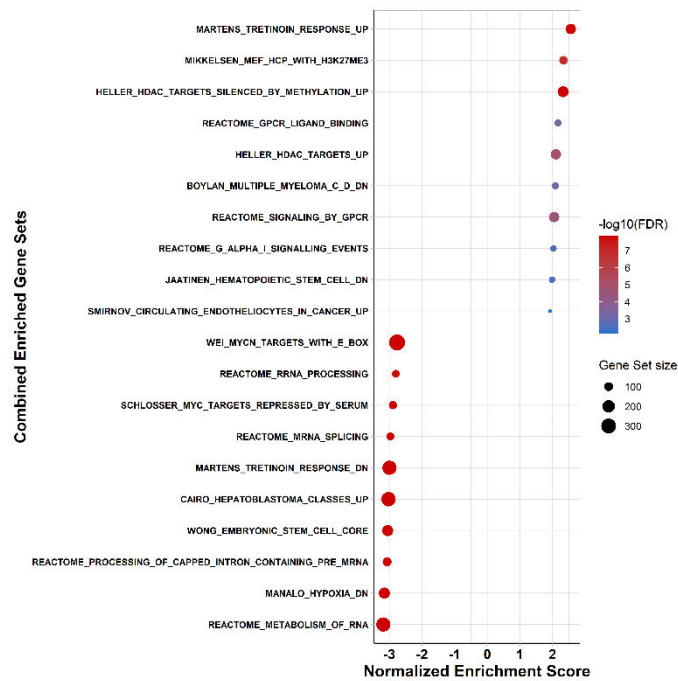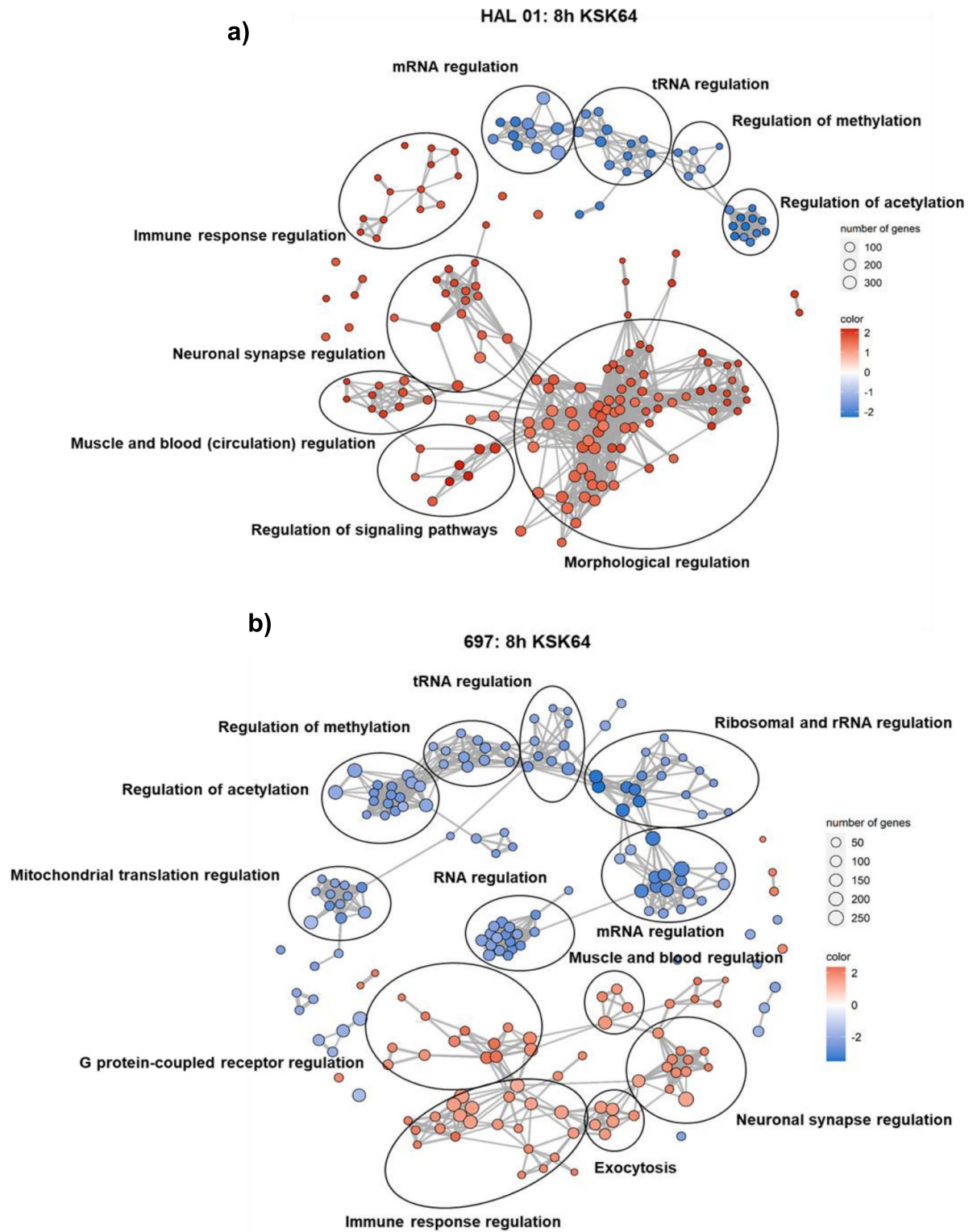
Figure 43: Enriched curated gene sets in the **a)** HAL-01 cell line and **b)** 697 cell line after 8 h of **KSK64** treatment.

Figure 44: Cluster GSEA analysis of DEGs after 8 h of **KSK64** treatment in **a)** HAL-01 and **b)** 697 cell line. Clusters were manually curated.

3.9 The biological relevance of HDAC6 as a target for precision cancer therapy

Selective HDAC6i was unable to induce apoptosis in leukemic cell lines. To further analyze the biological role of HDAC inhibition, conditional genetic HDAC6 knockdown models were developed. Furthermore, a stable HDAC6 knock-out cell line (K562) was generated and later tested on our in-house high-throughput drug screening library. The library comprises 181 compounds, whereby most of which are commercially available compounds that entered clinical trials already or are already FDA/EMA approved compounds. The result of such a drug screen could be used to find compounds that could be used for combinational therapy as compounds that show stronger cytotoxic effects in the HDAC6 KO K562 cells compared to the wild-type K562 could hint towards a synergistic interaction between HDAC6 and the tested compounds.

To study the relevance of HDAC6 as a molecular target for cancer therapy, a conditional genetic knockdown cell line model in the HL60 cell line was generated. HL60 cells were created with sh-RNA targeting HDAC6 under the control of a doxycycline promotor. Based on the RT-qPCR and western-blot analysis of the HL60 cell line after 24 h of doxycycline treatment, construct B3 was chosen for further analysis as it showed the most pronounced knockdown of HDAC6 of all tested constructs (fig. 43). Next, a drug screen was performed of doxycycline-treated HL60 cells (B3 +) as well as non-doxycycline treated cells (B3 -) to analyze the effects of **KSK64**, CAY10603, ricolinostat and compound **8e** (fig. 44). The IC_{50} concentration of the indicated compounds showed no differences (**8e**: B3+: 315 nM, B3-: 311.1 nM; **KSK64**: B3+: 290.8 nM, B3-: 268 nM; CAY10603: B3+: 353.6 nM, B3-: 356.6 nM; ricolinostat: B3+: 3274 nM, B3-: 3147 nM).

Next to this, genetically stable HDAC6 knockout cells were created, using the CRISPR-Cas9 technology. Two different sgRNAs against HDAC6 were used (G1, G2) to guide Cas9 to the corresponding genomic HDAC6 location and to induce DNA double-strand breaks and thereby removing the gene. As seen by western blot analysis (fig. 47b), G1 and G2 were able to remove HDAC6 efficiently. Normal K562 cells and Cas9-expressing K562 cells that were transfected with an empty vector were used as control and showed clear HDAC6 expression. After having created the stable HDAC6 knockout K562 cells, these cells were tested on our manually curated high-throughput drug screen library (fig. 45). The results are presented in the heatmap and each row represents the IC_{50} values (log nM) for each of the tested drugs from the library of the specific cell line used. The patterns of the heatmaps are very similar to each other,

meaning that there are only a few drugs that show a changed IC_{50} concentration between the control and the HDAC6 KO cells. Three drugs came up, especially in the G2 K562 cells, that showed a lower IC_{50} in the knock-out cells compared to the control K562 cells. These drugs are clofarabine, aurora A inhibitor, and gemcitabine (black box fig. 45).

a)
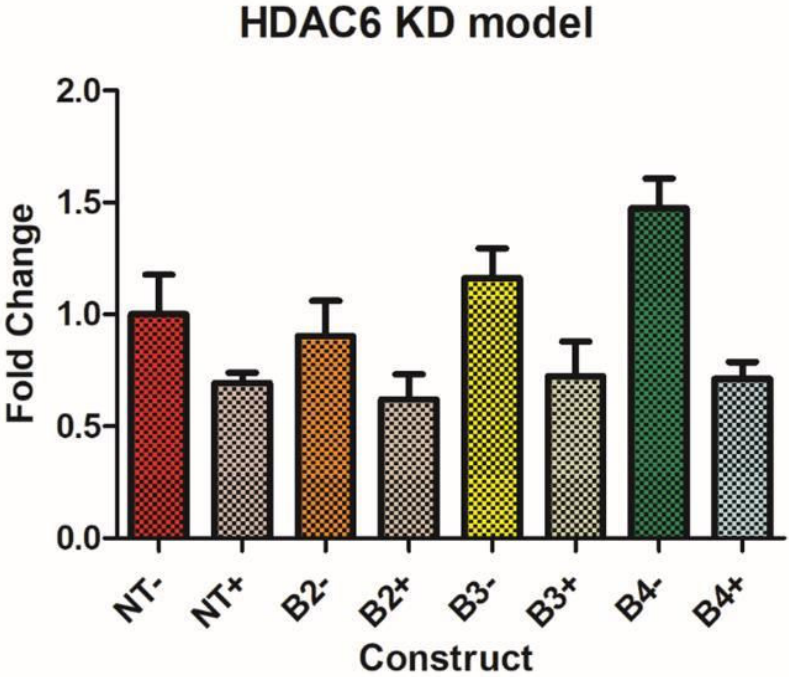
b)
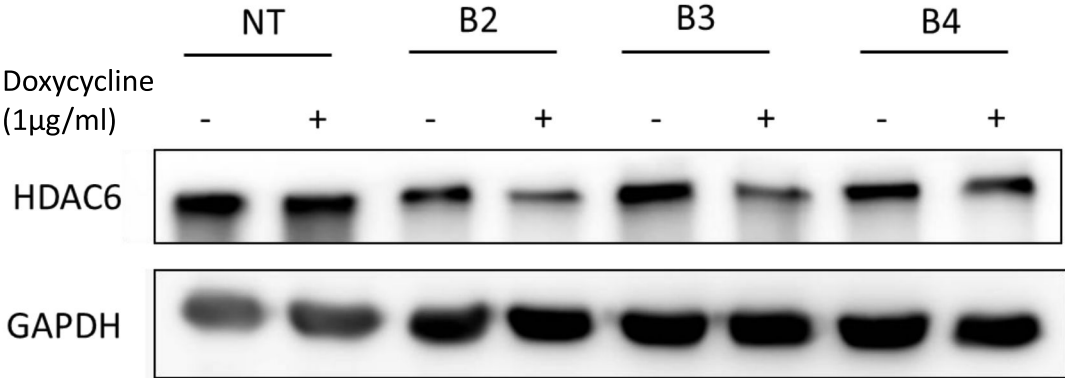
Figure 45: Validation of the conditional knockdown models of HL60 cells after 24 h treatment with doxycycline. **a)** RT-qPCR analysis of the non-targeting control and three different sh-RNA constructs. **b)** Western-blot analysis of the non-targeting control and three different sh-RNA constructs after 24 h of exposure to doxycycline.
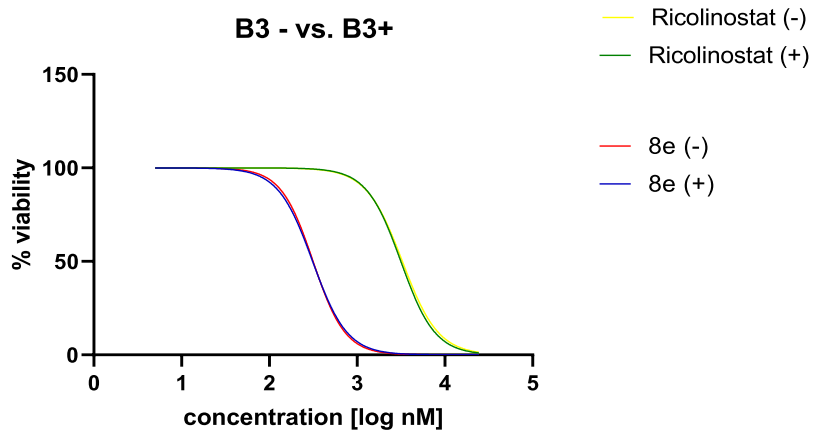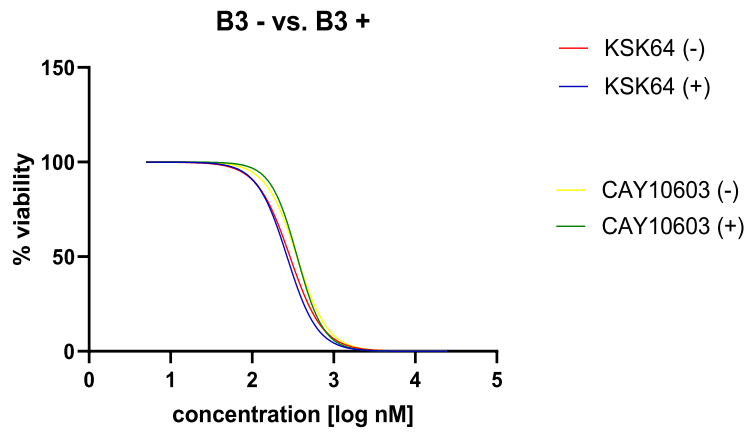
Figure 46: HL60 cells, that were transfected with a conditional sh-RNA construct targeting HDAC6 under a doxycycline promotor, were treated with different HDACi after exposure to doxycycline and compared to HL60 that were not exposed to doxycycline.
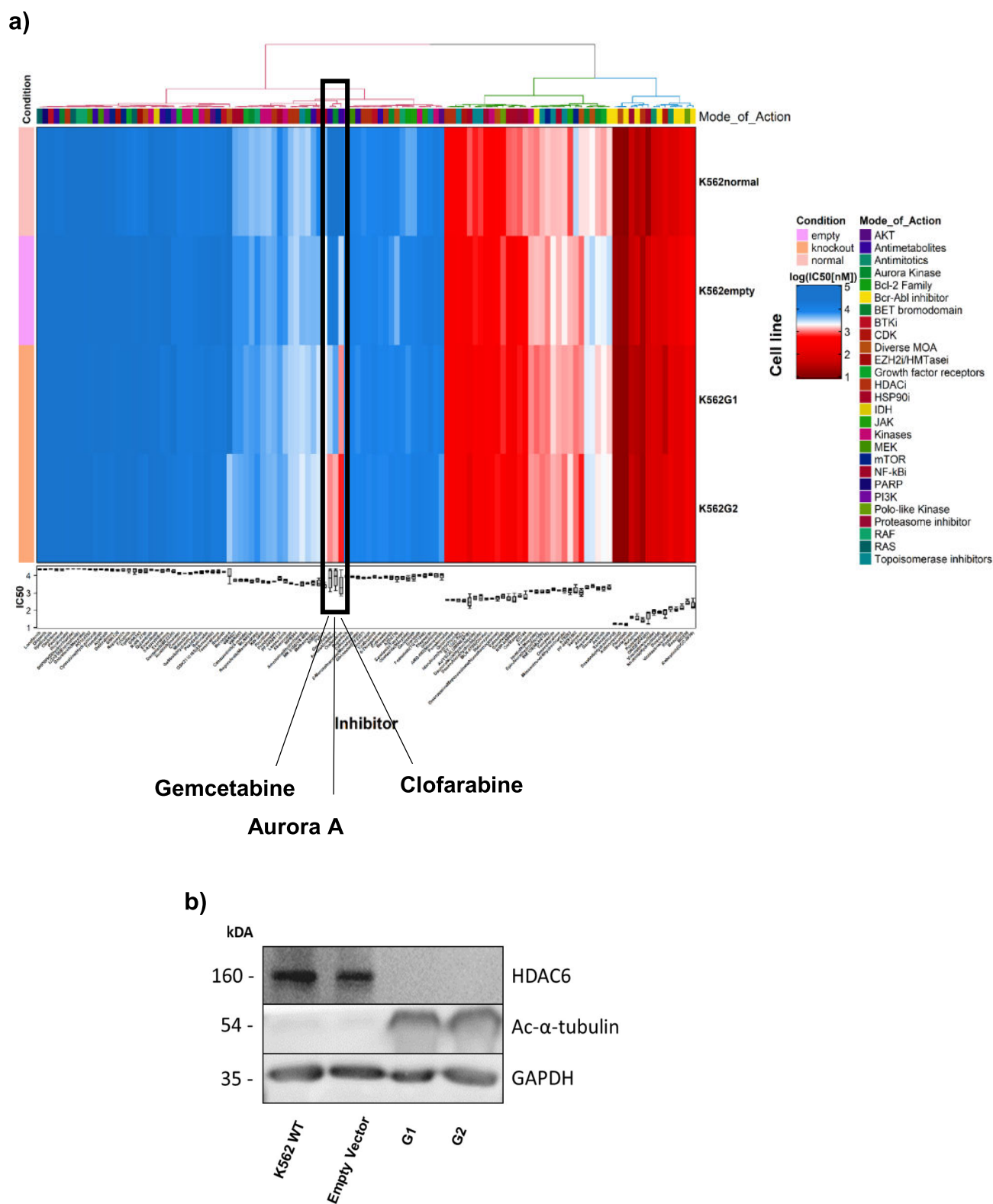
Fig. 47: a) High-throughput drug screen of HDAC6 KO K562 cells and compared to normal empty vector control K562 cells. The black box shows inhibitors that have different effect on the HDAC6 KO K562 cells compared to the control K562 cells. These inhibitors are gemcitabine, aurora A inhibitor and clofarabine. **b)** Western blot analysis of HDAC6 KO K562 cells (G1, G2) compared to wild-type K562 and K562 cells transfected with an empty vector.

4. Discussion:

Even though the event-free survival of pediatric leukemia has improved up to 85-90%, the therapy can be traumatizing and can have long-term health consequences for the child due to the intense use of chemotherapeutics[127]. Moreover, some leukemia subtypes are still associated with poor prognosis e.g. the TCF3-HLF+ BCP-ALL. Pan-HDAC inhibitors, like panobinostat, romidepsin, vorinostat, or belinostat are already applied in the clinic against hematological malignancies[16,127–130]. However, pan-HDACi are often associated with side effects in the clinics, and therefore to mitigate them, I have focused on targeting isoform-specific HDAC6 inhibitors. In theory, HDAC6 is an attractive molecular target as it is widely expressed across the tested leukemia cell lines (fig. 8,9). HDAC6 is localized in the cytoplasm of the cells, making it more accessible for inhibitors as they don't have to reach the nucleus, where most of the other HDAC isoforms are localized. HDAC6 has two catalytic domains (CD1 and CD2), and confirmed substrates of CD2 include α-tubulin, cortactin, tau, and the chaperone protein HSP90[62,131,132]. Furthermore, HDAC6 is unique by possessing a ubiquitin-binding domain that is involved in the regulation of the aggresome-autophagy pathway, an important protein degradation mechanism next to the 26S proteasome. Therefore, HDAC6i are known to enhance the effect of proteasome inhibitors by promoting proteotoxic stress and apoptosis in fast-growing cells[108,113,124].

4.1 Selective HDAC6 inhibition shows low cytotoxic effects on leukemic cells

The HDAC6 selective inhibitor **6l** showed outstanding selectivity for HDAC6 over class I isoforms ($SI^{1/6}$: 172), which outperformed the selectivity of ricolinostat ($SI^{1/6}$: 11) (fig. 11a). The chemical selectivity data were confirmed by enzymatic- and cell-based assays and show that compound **6l** is only acetylating α-tubulin but not H3 with relevant concentrations (fig. 11b). However, **6l** exhibited only low cytotoxicity as a single agent against a wide range of leukemic cell lines (fig. 12a). In line, similar results were found in other studies, which also showed that HDAC6 has no or very minor cytotoxic effects[133]. It is hypothesized that the cytotoxic effects of HDAC6 inhibitors are due to their unselective binding at higher concentrations and the observed anticancer properties are evoked by HDAC class I inhibition, as HDAC class I inhibition has an important role in inducing cytotoxicity[134–136]. However, it was found that compound **6l**, with a concentration at which only HDAC6 inhibition was observed, in combination with

proteasome inhibitor bortezomib evoked a stronger apoptosis induction compared to bortezomib alone (fig.13). Therefore, **6l** could still be used in combination with proteasome inhibitors to reduce the concentration of a proteasome inhibitor and thereby reducing the side effects evoked by proteasome inhibitors. Moreover, compound **6l** enhanced the cytotoxicity significantly of the anthracyclines epirubicin and daunorubicin (fig. 14). Anthracyclines are regularly used as chemotherapeutics in cancer treatment protocols but is often accompanied by serious side effects such as neuronal toxicity, cardiomyopathy, and resistance[137,138]. Selective HDAC6 inhibitors, such as compound **6l**, could be used in combination with anthracyclines to reduce the severe side effects of anthracyclines by lowering the doses needed for successful therapy on the one hand and the other hand lowering the chance for the development of resistance against anthracyclines[139,140]. Concluding, compound **6l**, can be seen as a very useful tool compound with very high selectivity towards HDAC6 and potentially as a compound for combinational therapies.

4.2 Improving the HDAC6 selective compound Nexturastat A

Nexturastat A is classified as a selective HDAC6 inhibitor, which shows its activity in the low-nanomolar range. It is reported to possess 600-fold selectivity for HDAC6 over HDAC1[141] (table 18). However, the reported selectivity could not be reproduced in our enzyme assays, which showed a selectivity index of 24. Other groups also found a lower selectivity index of 84 compared to the initially reported 600- fold[142] and thus agrees with the selectivity index found by our assays (fig. 16). The pharmacophore model for HDAC6 selective inhibitors, in contrast to the classical pharmacophore model (ZBG, linker, cap), consists of the ZBG, linker and a sterically demanding cap group (S-CAP)[95]. HDAC6 has, compared to HDAC1, a much wider shallower entrance tunnel making it accessible for the S-CAP group, whereby HDAC1, with a much more narrow entrance cannot be reached by bulky or branched S-CAP groups. Nexturastat A possesses such a branched S-CAP group. To alter the isozyme profile of Nexturastat A by making it more selective towards HDAC6, our collaborators, the working group of Prof. Dr. T. Kurz (Institut für Pharmazeutische und Medizinische Chemie Heinrich-Heine-Universität Düsseldorf), rationally designed analogs of Nexturastat A by the introduction of an alkoxyurea-based connecting unit. They could already show before that altering the connecting unit (CU), which connects the linker and the cap group, of

pan-HDACi, such as vorinostat or panobinostat significantly alters the isoform profile of these unselective HDACi[143,144]. The resulting alkoxyamide and alkoxyurea derivates of the pan-HDACi showed a higher preference for HDAC6. And indeed, also for nexturastat A analogs, it was proven to be a successful approach to enhance the selectivity of hydroxamic acids by the instruction of alkoxyurea-based connection units, which resulted in a 1.5-fold higher selectivity index (**4a**) compared to nexturastat A, while it still maintaining its potency. Interestingly, compound **4b** ($SI^{1/6}$:21) showed a similar selectivity compared to nexturastat A ($SI^{1/6}$:24) but showed more pronounced antiproliferative activity across all tested cell lines than nexturastat A (fig. 16). Thus altering the connecting unit to enhance selectivity and altering its antiproliferative effects is a successful approach for the rational design of more potent and more selective HDAC6 inhibitors.

4.3 The alkoxyurea-based Vorinostat analog and preferential HDAC6 inhibitor KSK64

The HDAC6 preferential inhibitor **KSK64**[125] was very active in the low nanomolar range against a variety of leukemic cell lines (fig. 18). In all tested cell lines **KSK64** outperformed the HDAC6 preferential inhibitor ricolinostat regarding their IC_{50} values, which currently is tested in clinical trials[96]. This is surprising as **KSK64** shows a $SI^{1/6}$ of 15.4 and ricolinostat 11, meaning that ricolinostat is less specific for HDAC6 compared to **KSK64**. However, **KSK64** showed overall stronger HDAC class I/II inhibition in a cellular enzymatic compared to ricolinostat (fig. 19b), making it a more efficient HDACi at lower concentrations, which can explain its superior anticancer properties at lower concentrations. The superior cytotoxic activity of **KSK64** was further validated in a comparative drug screen, in which **KSK64** was tested against a broad range of commercially available HDAC6 inhibitors against a selection of leukemic cell lines (fig. 20a). Overall, **KSK64** was the most active compound and its ability to synergize with proteasome inhibitors was shown, a hallmark of HDAC6 inhibitors[113] (fig. 22). Especially interesting was the finding that **KSK64** was very effective against the TCF3-HLF+ cell line HAL-01 (fig. 18), which is associated with a poor prognosis and accounted incurable. We hypothesized that by inhibiting HDAC6 also the chaperone function of HSP90 could be inhibited due to their functional interplay[132]. However, the functional impairment of HSP90 after **KSK64** or ricolinostat treatment

was not detected (fig. 21). However, further analysis into the interplay of HDAC6 inhibition and HSP90 function is needed.

To further understand the molecular mechanism of a preferential HDAC6 inhibitor (**KSK64),** HAL-01 (TCF3-HLF+) and 697 (TCF3-PBX1+) cell lines were treated with **KSK64** at its IC_{50} concentration and afterward subjected to RNA sequencing. The HAL-01 and 697 cell lines are both pro-B cells and both showed to be particularly sensitive to the treatment with **KSK64** (fig. 18), which is interesting as TCF3-HLF+ cells are associated with a poor prognosis as these cells are hard to treat. To understand the cellular events after the treatment with a preferential HDAC6 inhibitor, the differential expressed genes (DEGs) after 8 h of **KSK64** treatment were analyzed. After 8 h the DEGs are more likely to be direct target genes of the treatment. In both cell lines highly significant DEGs were found after the 8 h treatment (fig. 41, table 20). In the HAL-01 cell line after 8 h of **KSK64** treatment, the most significant upregulated genes are RIMS3, SAMHD1, STK17B, PRKCB, SNN, ITM2C, and COTL1 and the most significant downregulated genes IGL1, TRIMM22 and GRK2 (fig. 41a). The upregulated gene PRKCB is an interesting gene as it is a serine- and threonine-specific kinase and a member of protein kinase C family that is reported to be involved in B-cell activation and apoptosis induction[107]. Another interesting gene is the downregulated IGL1 gene, which encodes for the preB cell receptor, which is found on proB and preB cells and involved in the signal transduction for cell proliferation[145].

Table 20: List of DEGs in the HAL-01 cell line after 8 h of **KSK64** treatment

Gene (upregulated)	Function
RIMS3 (Regulating Synaptic Membrane Exocytosis 3)	Predicted to be involved in calcium ion-regulated exocytosis of neurotransmitters; modulation of chemical synaptic transmission; and regulation of synapse organization.[146]
SAMHD1 (SAM Domain And HD Domain-Containing Protein 1)	May play a role in the regulation of the innate immune response. Upregulated in response to viral infection and may be involved in the mediation of tumor necrosis factor-alpha proinflammatory responses.[141]
STK17B	Enables ATP binding activity and protein serine/threonine kinase activity. Involved in intracellular signal

(Serine/Threonine Kinase 17b)	transduction; positive regulation of fibroblast apoptotic process; and protein phosphorylation.[147]
PRKCB (Protein Kinase C Beta)	Family of serine- and threonine-specific protein kinases that can be activated by calcium and second messenger diacylglycerol. Involved in B cell activation by regulating BCR-induced NF-kappa-B activation, apoptosis induction, and endothelial cell proliferation.[148]
SNN (Stannin)	Enables metal ion binding activity. Predicted to be involved in response to a toxic substance.[149]
ITM2C (Integral Membrane Protein 2C)	Enables amyloid-beta binding activity. Involved in negative regulation of neuron projection development and neuron differentiation.[150]
COTL1 (Coactosin Like F-Actin Binding Protein 1)	Encodes for an actin-binding protein that regulates the actin cytoskeleton. This protein binds F-actin and also interacts with 5-lipoxygenase, which is the first committed enzyme in leukotriene biosynthesis.[151]
Gene (downregulated)	
IGL1 (Immunoglobulin Lambda-Like Polypeptide 1)	Involved in the transduction of signals for cellular proliferation, and differentiation from the proB cell to the preB cell stage.[145]
TRIMM22 (Tripartite Motif Containing 22)	The protein is involved in innate immunity against different DNA and RNA viruses.[152]
GRK2 (G Protein-Coupled Receptor Kinase 2)	Predicted to be involved in embryonic development, heart function, and metabolism.[153]

The most significantly upregulated genes in the 697 cell line are RASSF4, CREG1, IRGM, JUN, SAMHD1, STIM1, CFH, FOS, and BMF and the most downregulated DEG is UTP20 (fig. 41b, table 21). Ras Associated Domain Family Member 4 (RASSF4) is an interesting gene as it is a potential effector protein of Ras and is involved in the induction of apoptosis and cell cycle arrest[154,155]. Next to this, BMF is an interesting gene, specifically known to bind other BCL-2 proteins and thereby function as an apoptotic activator[156]. Furthermore, JUN and FOS are two interesting hits as well. FOS genes encode for leucine zipper proteins and can form dimers with proteins of the JUN family to form the transcription factor complex AP-1, which is involved in the regulation of apoptosis[157,158].

Table 21: List of DEG's in the 697 cell line after 8 h of **KSK64** treatment

Gene (upregulated)	Function
RASSF4 (Ras Association Domain Family Member 4)	Potential effector protein of Ras and involved in the induction of apoptosis and cell cycle arrest.[154]
CREG1 (Cellular Repressor Of E1A Stimulated Genes 1)	May contribute to the transcriptional control of cell growth and differentiation.[159]
IRGM (Immunity Related GTPase M)	May play a role in the innate immune response by regulating autophagy formation in response to an intracellular pathogen.[160]
JUN (Transcription Factor AP-1 Subunit Jun)	Heterodimerizes with proteins of the FOS family to form an AP-1 transcription factor that is involved in the regulation of activation-induced cell death.[158]
SAMHD1 (SAM Domain And HD Domain-Containing Protein 1)	May play a role in the regulation of the innate immune response. The encoded protein is upregulated in response to viral infection and may be involved in the mediation of tumor necrosis factor-alpha proinflammatory responses.[161]

STIM1 (Stromal Interaction Molecule 1)	Mediates Ca2+ influx after depletion of intracellular Ca2+ stores by gating of store-operated Ca2+ influx channels.[162]
CFH (Complement Factor H)	A glycoprotein that modulates complement activation. Acts as a soluble inhibitor of complement, where it's binding to self markers such as glycan structures prevents complement activation and amplification on cell surfaces.[163]
FOS (Transcription Factor AP-1 Subunit C-Fos)	FOS proteins have been implicated as regulators of cell proliferation, differentiation, and transformation. In some cases, expression of the FOS gene has also been associated with apoptotic cell death. [157]
BMF (Bcl2 Modifying Factor)	Belongs to the BCL2 protein family and has been shown to bind BCL2 proteins and function as an apoptotic activator.[156]
Gene (downregulated)	
UTP20 (UTP20 Small Subunit Processome Component)	Involved in 18S pre-rRNA processing.[164]

The enrichment of two gene sets (HELLER_HDAC_TARGETS_UP and HELLER_HDAC_TARGETS_SILENCED_BY_METHYLATION_UP) further validates that **KSK64** is acting through HDAC inhibition as these gene sets are based on experiments of multiple myeloma cell lines that were treated with the HDAC6 specific inhibitor TSA alone or together with decitabine, respectively[165] (fig. 42b). Furthermore, the cluster GSEA showed, especially in the HAL-01 cell line, gene cluster involved in morphological regulation of the cells was upregulated as a result of **KSK64** treatment (fig. 44 a). In view of HDAC6 as a regulator of the cytoskeleton by actin and tubulin regulation, this was an expectable finding. Furthermore, in the line with the HDAC inhibition the cellular acetylation, as well as methylation processes, were down-regulated. It is known that HDAC6 is also involved in neuronal diseases and also has a role in regulating the immune response[73,166], therefore it is interesting that in both cell

lines neuronal synapse regulation, as well as processes of the immune response were upregulated. However, all the observations gained from the RNA-sequencing cannot be regarded as effects of HDAC6 inhibition alone. **KSK64** is a preferential HDAC6 inhibitor and therefore, it is likely that other HDAC isoforms are inhibited as well. Therefore, for future experiments, it would interesting to compare the results of **KSK64** treatment to the RNA sequencing results of clean HDAC6 knock cell lines cells or cells treated with a highly selective HDAC6i, such as compound **6l**. This way the effects of HDAC6 inhibition alone could be analyzed on the transcriptional level.

4.4 Alkoxyamide-based preferential HDAC6 inhibitors with bicycle (hetero) aromatic cap groups are very active at a low nanomolar range

The alkoxyamide-based HDAC class I/IIb inhibitors **8a** and **8e** are other examples of inhibitors that were optimized by small chemical modifications to enhance their potency. Both of the compounds are derivates of vorinostat-type inhibitors with a modified bicycle (hetero) aromatic cap groups. Based on the western blot and cellular enzymatic assays both of the inhibitors target HDAC6 (fig. 25), as seen by the acetylation of α-tubulin, as well as HDAC1 based on the acetylation of H3. They still have a preference for HDAC6 over HDAC2, 4, and 8 based on the isozyme profile (table 19). In contrast to vorinostat, these compound show synergistic interaction with the proteasome inhibitors bortezomib and carfilzomib (fig. 27), which is again a hallmark for HDAC6 inhibition. In comparison to other commercially available HDAC6 inhibitors, they show very low IC_{50} values (fig. 26a), which is not surprising as compounds **8a** and **8e** are less selective for HDAC6 and also target class I HDACs, which are well known for their cytotoxic properties. Additionally, **8a** induces apoptosis at a similar degree compared to ricolinostat, however, ricolinostat was used at 10x higher concentration compared to **8a** (fig. 26b). Together with the previous results from the other selective and preferential HDAC6 inhibitors it appears to be important to also inhibit class I HDAC isoforms to reach a potent level of anticancer properties.

4.5 The fluorinated HDAC inhibitors 10h and 10p show distinct cytotoxic profiles that are in line with their isozyme profiles.

Compound **10h** was chosen for further cellular analysis as it showed the strongest pan-HDAC inhibition ($SI^{1/6}$: 1.3) and compound **10p** showed the most selective HDAC6 inhibition ($SI^{1/6}$: 191) (fig.30). Following our previous data, compound **10p** showed also no or very minor cytotoxic properties as seen by the comparative drug screen with the HDAC class I selective inhibitor CI-994 and ricolinostat as controls against different subgroups of leukemic cells (fig. 31a). Also the apoptosis induction was very low compared to the pan-HDAC inhibitor **10h** (fig. 31b). This is in accordance with our previous data, which already showed that very selective HDAC6 inhibitors lack cytotoxic properties[167]. Compound **10h**, however, showed cytotoxic properties and a significant increase in apoptosis induction. This was also expected, as **10h** is a less selective HDAC6 inhibitor, thereby in line with showing stronger cytotoxic effects. Also, the western blot analysis showed clearly the selectivity of compound **10p** as strong acetylation of α-tubulin was observed but no acetylation of H3 (fig. 32). Compound **10h** showed strong levels of H3 and α-tubulin acetylation, which both is in accordance with their isozyme profiles (fig.32). HDACi as a monotherapy are facing often the problem of acquired resistance. To counter that effect, I looked out to find clinically relevant combination partners, that are often used in the clinic. Preclinical reports suggest that the combinations of DNA hypomethylating agents together with HDACis are working synergistically by disrupting the transcriptional repressor complex such as methyl-CpG binding proteins[126,168]. Therefore, the combination of decitabine and **10h** were tested and synergistic interaction in the AML cell line HL60 but not in the other leukemic subtypes such as B- and T-lymphoid lineages were found (fig. 33). The western blot analysis revealed higher levels of H3 acetylation compared to the treatment of **10h** alone, which could explain the higher anticancer properties of the combination (fig 33e). Taken together these data suggest therapeutic potential for the combination of **10h** or pan-HDACi together with decitabine to treat AML.

Importantly compounds **10h** and **10p** are both fluorinated compounds, an important feature in modern pharmaceuticals. Fluorination became an important feature to improve the bioavailability and pharmacodynamic properties of drugs[169]. Therefore, I went further to test the promising pan-HDACi **10h** in a xenograft mouse model. In our group, the engraftment of the T-cell line HBP-ALL was well established and was therefore used to test the anti-cancer properties of compound **10h**. The HBP-ALL cell

line was manipulated to stably express GFP and luciferase (GFP-Luc) to identify the in vivo engraftment of the leukemic cells using bioluminescent *in-vivo* imaging. After successful engraftment of the human leukemic cells either **10h** or a vehicle were injected twice a week with 100mg/kg for two consecutive weeks and tumor burden was measured over time. However, no significant differences in tumor burden between the treated vs. vehicle group were detected (fig.34). Furthermore, of the 10 mice used for the pilot study only 8 mice were determined to be positive for the HBP-ALL cell line. Thus it was decided to have two groups (treatment vs. vehicle), with each 4 mice. Of these 4 mice per group only 2 survived for 5 weeks and thus meaningful statistical analysis could not be applied. Compound **10h** was tolerated well by the mice as the weekly weight measurements didn't show any noticeable problems (fig. 35). Only mouse 1 died after the first administration of **10h**. One reason for this fast death could be a wrong injection of compound **10h** and thereby harming essential organs. The post-mortem analysis of the mice organs (liver, kidney, and spleen) showed no noticeable differences between the treated and control mice (fig. 37). Furthermore, there was also no noticeable trend recognized after post-mortem analysis of the blood and spleen of the mice regarding their proportion of engrafted human to mouse cells (fig. 36). More studies are needed to determine the pharmacodynamics and kinetics as well as bioavailability of compound **10h** before conducting statistically meaningful *in-vivo* experiments.

4.6 Protein targeting chimera (PROTAC) 4 is biochemical active but does induce apoptosis

Protein-targeting chimeras are bifunctional molecules that have a cap group to bind the protein of interest (POI) and are linked to a ligand of ubiquitin E3 ligase. This way the POI will be recruited to an E3 ligase, which will in turn induce polyubiquitylation of the POI and thereby mark it for proteasomal degradation[115,170]. The working group of Prof. Dr. F. K. Hansen (Pharmaceutical and Cell Biological Chemistry, Pharmaceutical Institute, University of Bonn) developed an efficient sold-phase supported protocol using hydroxamic acids immobilized on resins (HAIR) as building blocks for the preparation of functional HDACi. This approach was further used for the synthesis of a proof-of-concept PROTAC that degrades histone deacetylases, as the synthesis of HDAC PROTACs is usually cumbersome. The resulting **PROTAC 4** was then further investigated for its biological functioning to analyze its ability to degrade HDACs (fig.

38b). Indeed, a concentration-dependent degradation of HDAC6 and HDAC1 was observed, and also the concentration-dependent increase in α-tubulin and H3 acetylation was detected, which are markers for HDAC6 and HDAC1 inhibition, respectively. Surprisingly, induction of apoptosis was not detected when 697 cells were treated with 1, 10, or 25 µM of **PROTAC 4** (fig. 39). 697 cells treated with the IC_{50} concentration of ricolinostat served as positive control and showed, as expected, the induction of apoptosis. Based on the results from HDAC class I/IIb inhibitors (like compound **8a** or **KSK64,** that were previously described) it was expected that **PROTAC 4** would comparably induce apoptosis. The reason why **PROTAC4** does not induce apoptosis is unclear but one might speculate that there is a difference in the degradation of a protein compared to its inhibition. As opposed to inhibition, it could be possible that the degradation of a protein, like HDAC6 or HDAC1, initiates alternative pro-survival signaling pathways in the cells to counteract that protein degradation alternative pathways, which are unknown yet. However, the biological data suggest that HAIR methodology is a versatile method for the synthesis of HDACi-based PROTACs.

4.7 The cytotoxic effect of preferential HDAC6 inhibitor is independent of HDAC6 expression in the cells

HDAC inhibitors have arrived in the clinic, as seen by the FDA-approved pan-HDAC inhibitors vorinostat, belinostat, and panobinostat[128–130]. Even though they show high potential for cancer therapy, pan-HDACi are associated with adverse side effects. Therefore, isoform-selective HDAC inhibitors that offer better tolerability are needed. For the development of isoform-specific HDAC inhibitors, it needs to be investigated, which HDAC isoforms are best to target. HDAC6 offers some crucial advantages as a target for the development of such isoform-selective inhibitors as it offers some unique properties compared to the other isoform, such as structural distinctions in the entrance tunnel, that allows for the development of selective HDAC6 inhibitors[167,171]. Furthermore, it is localized in the cytoplasm and it was shown that HDAC6 KO mice have normal development, in contrast to other HDAC isoform[172]. Thus, the improved safety profile, the ability to selectively target HDAC6, and its involvement in several diseases, such as cancer, neurodegenerative diseases, and inflammation, make it a promising candidate for the development of isoform-selective inhibitors[98,166,173]. In this

thesis, several HDAC6 inhibitors were tested, ranging from very selective to pan-HDAC inhibitors. The two most selective inhibitors that were analyzed are compound **6l** and compound **10p**. They showed extraordinary selectivity profiles compared to other HDACi and especially in comparison to ricolinostat, an HDAC6 inhibitor in clinical trials. However, these inhibitors showed virtually no cytotoxic effect when cells were treated by these compounds alone. Furthermore, the knock-down of HDAC6 in HL60 did not influence the IC_{50} values of the preferential HDAC6 inhibitors (fig. 46), which are inhibitors that have a preference for HDAC6 but also target other isoforms, especially class I HDAC isoforms. This observation is also supported by previous reports as one study has shown that the cytotoxic potential of HDAC6 inhibitors occurs only when given at high concentrations at which unselective binding of these HDAC6 inhibitors takes place[133]. Another group has also investigated several anticancer therapeutics and analyzed their efficiency in killing cancer cells concerning their proposed mechanism of action (MOA). They used a CRISPR-Cas9 approach to knock out the proposed targets of the cancer therapeutics and then reevaluated the cytotoxic potential of the analyzed drug candidates. In this study ricolinostat was reevaluated in TOV-21G cells, an ovarian cancer cell line, that was genetically manipulated to not express HDAC6 anymore. However, these cells were still sensitive to ricolinostat, similar to the wild-type cells. Thus, the authors concluded that the proposed MOA is wrong and there need to be other targets responsible for the anticancer effects of ricolinostat[134]. This is also following our finding that HDAC6 preferential inhibitors kill cells, independent of the HDAC6 expression. Therefore, selective HDAC6i as monotherapy is not an effective approach for the treatment of cancer and more specifically leukemia. However, selective HDAC6 inhibitors, when combined with e.g. anthracyclines, such as daunorubicin and epirubicin raise the cytotoxic potential of these anthracyclines significantly. This is important information as there is the potential of selective HDAC6 inhibitors to reduce the amount of anthracyclines, thereby making the therapy potentially more tolerable for the patient. Furthermore, proteasome inhibitors such as bortezomib and carfilzomib, both FDA-approved for the treatment of hematological malignancies are used in the clinic and often face the problem of acquired resistance[174]. To counteract the development of resistance and to reduce the doses of proteasome inhibitors, the combination with HDAC6 inhibitors could be a promising approach for the treatment of hematological malignancies.

4.8 HDAC6 knockout (KO) and inducible knockdown (KD) cell line models for target validation and finding new drug combinations

To investigate the role of HDAC6 as a drug target the development of HDAC6 knockdown and knockout cell lines offer some strong advantages. HL60 cells were chosen as cell lines model for the inducible knockdown approach, as it was used in a variety of previous drug-screens. In this case sh-RNA was used against HDAC6, which was under the control of doxycycline inducible promotor. The qPCR and western blot data showed that the expression of HDAC6 was reduced in all sh-RNA constructs targeting HDAC6 (fig. 45). The strongest downregulation of HDAC6 was observed with sh-RNA construct B3. Therefore, the HL60 cells that were transduced with construct B3 were further used for a drug screen against a variety of HDACi. Strikingly there was virtually no change in IC$_{50}$ values of the tested HDACi between doxycycline treated and non-treated HL60 cells (fig.46). One explanation for this could be that the knockdown was not efficient enough, meaning that the leftover HDAC6 protein expression was still enough for the cells to not make a difference in cell viability under HDACi treatment. Another explanation could be that the tested inhibitors are not acting through HDAC6, or at least are not influencing cell viability through HDAC6. Next to the inducible HDAC6 KD cell line model, a genetic CRISPR-Cas9 mediated HDAC6 knockout model was established. K562 cells were transduced to express Cas9 and were further transduced with sgRNA's targeting the HDAC6 gene. After monocolonal selection, a clean HDAC6 KO were created in K562 cells (fig. 47b). As seen before, HDAC6 KO alone was not sufficient to induce cell death. However, it was shown that in combination with bortezomib or with the anthracycline epirubicin and daunorubicin selective HDAC6i had beneficial effects on the efficiency of these drugs. By combining HDAC6i with these drugs, the side effects of e.g. anthracycline can be lowered by lowering their dose. Another potential advantage of drug combination is to counteract the development of resistance to e.g. proteasome inhibitors such as bortezomib. Therefore, the HDAC6 KO model was next tested on our in-house drug screen library, consisting of 180 pre-clinical and clinical used drugs printed on one 1536-well drug screen plate. To analyse the cell viability of genetic KO models and compare them to empty vector control K562 cells and wild-type K562 cells, ATP-based glo assay was used. Three potential hits came up in the high-throughput drug screen, which are clofarabine, aurora A inhibitor and gemcitabine (fig. 47a). These drugs need to be carefully investigated for their potential to be combined with HDAC6i.

4.9 Conclusion and outlook

In this work, several different HDAC inhibitors were developed ranging from very selective HDAC6 inhibitors towards less specific, so called preferential HDAC6 inhibitors, and finally also a pan-HDAC inhibitor. All of the developed HDAC inhibitors were pre-clinically tested in our in-house drug screening facility against a variety of leukemic cell lines and further subjected to a variety of molecular techniques to further validate their properties and selectivity. It was found that very selective HDAC6 inhibitors are not cytotoxic even at high concentrations. In contrast, less selective, so called preferential inhibitors, were effective as monotherapy in the low nanomolar concentration range. Preferential HDAC6 inhibitors, as seen by the results for **KSK64**, **8a** and **8e** are potent against cancer cells but it is questionable to what extent this is dependent on HDAC6 inhibition. Therefore, it is important in the future to decipher the overall HDAC isozyme inhibition profile inside cells that results in anticipated anticancer effects and direct the development of HDAC inhibitors accordingly. Furthermore, RNA sequencing of cells treated with preferential HDAC6 inhibitors revealed the upregulation of pro-apoptotic genes. However, the pan-HDAC inhibitor with the highest cytotoxic profile but failed as a monotherapy in the initial leukemia xenograft mouse model to reduce tumor burden.

However, several beneficial combination partners of HDAC6 selective inhibitors, such as anthracycline epirubicin and daunorubicin, were found. The selective HDAC6 inhibitor significantly enhanced the cytotoxicity the anthracycline making it an interesting partner for combinational therapy, with the aim to reduce the concentration of anthracycline, which are known for their harsh-side effects and the development of resistance. Furthermore, it was shown that HDAC6 selective inhibitors enhanced the apoptosis induction, it used in combination with the clinically used proteasome inhibitor bortezomib, which is also known to have severer side effects and acquired resistances. Furthermore, HDAC6 KO cells were screened on our in-house drug-screen library, consisting of a mixture of approved and clinically established drugs, used against haematological malignancies as well as experimental inhibitors. It was found that HDAC6 KO cells were sensitive to clofarabine, aurora A inhibitor and gemcitabine, in contrast to the wild type cell line, making these inhibitors interesting for future combination experiments.

Furthermore, in this thesis the experimental inhibitors were analyzed for their potential to kill leukemic cells and it was found that the developed selective HDAC6i are not

effective as monotherapy. However, HDAC6 is involved in other diseases as well, such as neurodegenerative diseases, inflammation, or the process of metastasis[166,173,175]. The developed HDAC6i have the potential to be possible treatment strategies for such malignancies other than leukemia.

5. References

1. Birbrair, A. & Frenette, P. S. Niche heterogeneity in the bone marrow. *Ann. N. Y. Acad. Sci.* **1370**, 82–96 (2016).

2. Morrison, S. J. & Kimble, J. Asymmetric and symmetric stem-cell divisions in development and cancer. *Nature* **441**, 1068–1074 (2006).

3. Ketley, N. J. & Newland, A. C. Haemopoietic growth factors. *Postgrad. Med. J.* **73**, 215–221 (1997).

4. CARCHARHINI, H. & OCEAN, P. The Journal of the American Society of Parasitologists. *J. Parasitol* **98**, 333–340 (2012).

5. Schuldiner, M., Yanuka, O., Itskovitz-eldor, J., Melton, D. A. & Benvenisty, N. Effects of eight growth factors on the differentiation of cells derived from human embryonic stem cells. **97**, 11307–11312 (2000).

6. Jopling, C., Boue, S., Carlos, J. & Belmonte, I. regeneration. *Nat. Publ. Gr.* **12**, 79–89 (2011).

7. O'Brien, P., Morin, P., Ouellette, R. J. & Robichaud, G. A. The Pax-5 gene: A pluripotent regulator of B-cell differentiation and cancer disease. *Cancer Res.* **71**, 7345–7350 (2011).

8. American Cancer Society. About Childhood Leukemia What Is Childhood Leukemia ?Cancer. 1–11 (2019).

9. Winther, J. F. & Schmiegelow, K. How safe is a standard-risk child with ALL? *The Lancet Oncology* (2014) doi:10.1016/S1470-2045(14)70294-3.

10. Essig, S. *et al.* Risk of late effects of treatment in children newly diagnosed with standard-risk acute lymphoblastic leukaemia: A report from the Childhood Cancer Survivor Study cohort. *Lancet Oncol.* (2014) doi:10.1016/S1470-2045(14)70265-7.

11. Greaves, M. A causal mechanism for childhood acute lymphoblastic leukaemia. *Nature Reviews Cancer* (2018) doi:10.1038/s41568-018-0015-6.

12. Greaves, M. Europe PMC Funders Group Europe PMC Funders Author Manuscripts A causal mechanism for childhood acute lymphoblastic leukaemia. **18**, 471–484 (2020).

13. Schäfer, D. *et al.* Five percent of healthy newborns have an ETV6-RUNX1 fusion as revealed by DNA-based GIPFEL screening. *Blood* **131**, 821–826 (2018).

14. Martín-Lorenzo, A. *et al.* Infection exposure is a causal factor in B-cell precursor acute lymphoblastic leukemia as a result of Pax5-inherited susceptibility. *Cancer Discov.* **5**, 1328–1343 (2015).

15. Rodríguez-Hernández, G. *et al.* Infection exposure promotes ETV6-RUNX1 precursor B-cell leukemia via impaired H3K4 demethylases. *Cancer Res.* **77**, 4365–4377 (2017).

16.   Greaves, M. Darwinian medicine: A case for cancer. *Nat. Rev. Cancer* **7**, 213–221 (2007).

17.   Wills-Karp, M., Santeliz, J. & Karp, C. L. The germless theory of allergic disease: Revisiting the hygiene hypothesis. *Nat. Rev. Immunol.* **1**, 69–75 (2001).

18.   Gilham, C. *et al.* Day care in infancy and risk of childhood acute lymphoblastic leukaemia: Findings from UK case-control study. *Br. Med. J.* **330**, 1294–1297 (2005).

19.   Amitay, E. L. & Keinan-Boker, L. Breastfeeding and childhood leukemia incidence: A meta-analysis and systematic review. *JAMA Pediatr.* **169**, 1–9 (2015).

20.   Marcotte, E. L. *et al.* Caesarean delivery and risk of childhood leukaemia: A pooled analysis from the Childhood Leukemia International Consortium (CLIC). *Lancet Haematol.* **3**, e176–e185 (2016).

21.   Dockerty, J. D., Draper, G., Vincent, T., Rowan, S. D. & Bunch, K. J. Case-control study of parental age, parity and socioeconomic level in relation to childhood cancers. *Int. J. Epidemiol.* **30**, 1428–1437 (2001).

22.   Program, T. O. *et al.* An intact gut microbiome protects genetically predisposed mice against leukemia. (2021).

23.   Iacobucci, I. & Mullighan, C. G. Genetic basis of acute lymphoblastic leukemia. *Journal of Clinical Oncology* (2017) doi:10.1200/JCO.2016.70.7836.

24.   Belver, L. & Ferrando, A. The genetics and mechanisms of T cell acute lymphoblastic leukaemia. *Nature Reviews Cancer* (2016) doi:10.1038/nrc.2016.63.

25.   Papaemmanuil, E. *et al.* Genomic Classification and Prognosis in Acute Myeloid Leukemia. *N. Engl. J. Med.* (2016) doi:10.1056/nejmoa1516192.

26.   O'Brien, M. M., Seif, A. E. & Hunger, S. P. Acute lymphoblastic leukemia in children. *Wintrobe's Clin. Hematol. Fourteenth Ed.* 4939–5015 (2018) doi:10.1056/nejmra1400972.

27.   Dworzak, M. N. *et al.* AIEOP-BFM consensus guidelines 2016 for flow cytometric immunophenotyping of Pediatric acute lymphoblastic leukemia. *Cytom. Part B - Clin. Cytom.* **94**, 82–93 (2018).

28.   Bartram, C. R., Schrauder, A., Köhler, R. & Schrappe, M. Akute lymphoblastische Leukämie bei Kindern: Therapiesteuerung durch den Nachweis von MRD (minimal residual disease). *Dtsch. Arztebl. Int.* **109**, 652–658 (2012).

29.   Stanulla, M. & Schrappe, M. Treatment of Childhood Acute Lymphoblastic Leukemia. *Semin. Hematol.* **46**, 52–63 (2009).

30.   Pinkel, D. Five-Year Follow-Up of "Total Therapy" of Childhood Lymphocytic Leukemia. *JAMA J. Am. Med. Assoc.* **216**, 648–652 (1971).

31.   Pui, C. & Evans, W. E. TRATAMIENTO LLA nejm pui2006. *Th e new engl J. Med. Rev.* **354**, 166–178 (2006).

32.   Balduzzi, A. *et al.* Chemotherapy versus allogeneic transplantation for very-high-risk childhood acute lymphoblastic leukaemia in first complete remission: Comparison by genetic randomisation in an international prospective study. *Lancet* **366**, 635–642 (2005).

33.   Matteo, P. S. & Gerardo, O. S. The Ne w E n g l a nd Jo u r n a l o f Me d ic i ne OUTCOME OF TREATMENT IN CHILDREN WITH PHILADELPHIA. (2000).

34.   Specialist, I. Long-Term and Late Effects of Treatment for Childhood Leukemia or Lymphoma Facts. 1–8 (2013).

35.   Padma, V. V. An overview of targeted cancer therapy. *Biomed.* **5**, 1–6 (2015).

36.   Iqbal, N. & Iqbal, N. Imatinib: A Breakthrough of Targeted Therapy in Cancer. *Chemother. Res. Pract.* (2014) doi:10.1155/2014/357027.

37.   Xu, G. & Mcleod, H. L. Strategies for Enzyme / Prodrug Cancer Therapy 1. **7**, 3314–3324 (2001).

38.   Vander Velde, R. *et al.* Resistance to targeted therapies as a multifactorial, gradual adaptation to inhibitor specific selective pressures. *Nat. Commun.* (2020) doi:10.1038/s41467-020-16212-w.

39.   Moore, A. R., Rosenberg, S. C., McCormick, F. & Malek, S. RAS-targeted therapies: is the undruggable drugged? *Nature Reviews Drug Discovery* (2020) doi:10.1038/s41573-020-0068-6.

40.   Liu, P., Wang, Y. & Li, X. Targeting the untargetable KRAS in cancer therapy. *Acta Pharmaceutica Sinica B* (2019) doi:10.1016/j.apsb.2019.03.002.

41.   Waddington, C. H. The epigenotype. 1942. *Int. J. Epidemiol.* (2012) doi:10.1093/ije/dyr184.

42.   Holliday, R. & Ho, T. DNA methylation and epigenetic inheritance. *Methods* (2002) doi:10.1016/S1046-2023(02)00072-5.

43.   Quina, A. S., Buschbeck, M. & Di Croce, L. Chromatin structure and epigenetics. *Biochem. Pharmacol.* **72**, 1563–1569 (2006).

44.   Allis, C. D. & Jenuwein, T. The molecular hallmarks of epigenetic control. *Nat. Rev. Genet.* **17**, 487–500 (2016).

45.   Peters, J. The role of genomic imprinting in biology and disease: An expanding view. *Nat. Rev. Genet.* **15**, 517–530 (2014).

46.   Okamoto, I., Otte, A. P., Allis, C. D., Reinberg, D. & Heard, E. Epigenetic Dynamics of Imprinted X Inactivation during Early Mouse Development. *Science (80-.).* **303**, 644–649 (2004).

47.   Ghosh, S., Sinha, J. K. & Raghunath, M. Epigenomic maintenance through dietary intervention can facilitate DNA repair process to slow down the progress of premature aging. *IUBMB Life* 717–721 (2016) doi:10.1002/iub.1532.

48.   Wong, K. K., Lawrie, C. H. & Green, T. M. Oncogenic Roles and Inhibitors of DNMT1 , DNMT3A , and DNMT3B in Acute Myeloid Leukaemia. (2019) doi:10.1177/1177271919846454.

49.   Wouters, B. J. & Delwel, R. Epigenetics and approaches to targeted epigenetic therapy in acute myeloid leukemia. *Blood* **127**, 42–52 (2016).

50.   Campos, E. I. & Reinberg, D. Histones : Annotating Chromatin. 559–601 (2009) doi:10.1146/annurev.genet.032608.103928.

51.   Muntean, A. G. & Hess, J. L. Epigenetic Dysregulation in Cancer. *Am. J. Pathol.* **175**, 1353–1361 (2009).

52.   Ho, T., Chan, A. & Ganesan, A. Thirty years of HDAC inhibitors : 2020 hindsight Thirty years of HDAC inhibitors : 2020 hindsight. 0–111 (2020) doi:10.1021/acs.jmedchem.0c00830.

53.   Kelly, R. D. W. & Cowley, S. M. Biochemical Society Annual leading parts. 741–749 (2013) doi:10.1042/BST20130010.

54.   Emmett, M. J. & Lazar, M. A. Integrative regulation of physiology by histone deacetylase 3. *Nat. Rev. Mol. Cell Biol.* **1**, (2000).

55. Chakrabarti, A. *et al.* HDAC8 : a multifaceted target for therapeutic interventions. *Trends Pharmacol. Sci.* **36**, 481–492 (2015).

56. Asfaha, Y. *et al.* Recent advances in class IIa histone deacetylases research. *Bioorg. Med. Chem.* 115087 (2019) doi:10.1016/j.bmc.2019.115087.

57. Li, T. *et al.* Histone deacetylase 6 in cancer. **1**, 1–10 (2018).

58. Koeneke, E., Witt, O. & Oehme, I. *HDAC Family Members Intertwined in the Regulation of Autophagy: A Druggable Vulnerability in Aggressive Tumor Entities.* (2015). doi:10.3390/cells4020135.

59. Kutil, Z. *et al.* Histone deacetylase 11 is a fatty-acid deacylase. (2018) doi:10.1021/acschembio.7b00942.

60. Roma, J., Serrador, J. M. & Sa, F. HDAC6 : a key regulator of cytoskeleton , cell migration and cell – cell interactions. 291–297 (2008) doi:10.1016/j.tcb.2008.04.003.

61. Miyake, Y. *et al.* deacetylation and its selective inhibition. *Nat. Publ. Gr.* (2016) doi:10.1038/nchembio.2140.

62. Zhang, X. *et al.* Article HDAC6 Modulates Cell Motility by Altering the Acetylation Level of Cortactin. 197–213 (2007) doi:10.1016/j.molcel.2007.05.033.

63. Kovacs, J. J. *et al.* HDAC6 Regulates Hsp90 Acetylation and Chaperone-Dependent Activation of Glucocorticoid Receptor. **18**, 601–607 (2005).

64. Li, Y., Shin, D. & Kwon, S. H. Histone deacetylase 6 plays a role as a distinct regulator of diverse cellular processes. *FEBS J.* **280**, 775–793 (2013).

65. Khochbin, S., Verdel, A., Lemercier, C. & Seigneurin-Berny, D. Functional significance of histone deacetylase diversity. *Curr. Opin. Genet. Dev.* **11**, 162–166 (2001).

66. Seigneurin-Berny, D. *et al.* Identification of Components of the Murine Histone Deacetylase 6 Complex: Link between Acetylation and Ubiquitination Signaling Pathways. *Mol. Cell. Biol.* **21**, 8035–8044 (2001).

67. Boyault, C. *et al.* HDAC6-p97/VCP controlled polyubiquitin chain turnover. *EMBO J.* **25**, 3357–3366 (2006).

68. Qui, L. *et al.* Structure and function of the PLAA/Ufd3-p97/Cdc48 complex. *J. Biol. Chem.* **285**, 365–372 (2010).

69. Boyault, C. *et al.* HDAC6 controls major cell response pathways to cytotoxic accumulation of protein aggregates. 2172–2181 (2007) doi:10.1101/gad.436407.HDAC6.

70. Kwon, S., Zhang, Y. & Matthias, P. The deacetylase HDAC6 is a novel critical component of stress granules involved in the stress response. 3381–3394 (2007) doi:10.1101/gad.461107.lates.

71. Kawaguchi, Y. *et al.* The Deacetylase HDAC6 Regulates Aggresome Formation and Cell Viability in Response to Misfolded Protein Stress. **115**, 727–738 (2003).

72. Losson, H., Schnekenburger, M., Dicato, M. & Diederich, M. HDAC6—an emerging target against chronic myeloid leukemia? *Cancers (Basel).* **12**, 1–31 (2020).

73. Seidel, C., Schnekenburger, M., Dicato, M. & Diederich, M. Histone deacetylase 6 in health and disease. *Epigenomics* **7**, 103–118 (2015).

74. Featherstone, C. & Jackson, S. P. Ku, a DNA repair protein with multiple cellular functions?

Mutat. Res. - DNA Repair **434**, 3–15 (1999).

75. Subramanian, C., Jarzembowski, J. A., Opipari, A. W., Castle, V. P. & Kwok, R. P. S. HDAC6 deacetylates Ku70 and regulates Ku70-Bax binding in neuroblastoma. *Neoplasia* **13**, 726–734 (2011).

76. Parmigiani, R. B. *et al.* HDAC6 is a specific deacetylase of peroxiredoxins and is involved in redox regulation. *Proc. Natl. Acad. Sci. U. S. A.* **105**, 9633–9638 (2008).

77. Bazzaro, M. *et al.* NIH Public Access. **14**, 7340–7347 (2009).

78. Bradbury, C. A. *et al.* Histone deacetylases in acute myeloid leukaemia show a distinctive pattern of expression that changes selectively in response to deacetylase inhibitors. *Leukemia* **19**, 1751–1759 (2005).

79. Kanno, K. *et al.* Overexpression of histone deacetylase 6 contributes to accelerated migration and invasion activity of hepatocellular carcinoma cells. *Oncol. Rep.* **28**, 867–873 (2012).

80. Lee, Y. *et al.* The Cytoplasmic Deacetylase HDAC6 Is Required for Efficient Oncogenic Tumorigenesis. 7561–7570 (2008) doi:10.1158/0008-5472.CAN-08-0188.

81. Lee, Y. S. *et al.* The cytoplasmic deacetylase HDAC6 is required for efficient oncogenic tumorigenesis. *Cancer Res.* **68**, 7561–7569 (2008).

82. Putcha, P. *et al.* Erratum to : HDAC6 activity is a non- oncogene addiction hub for inflammatory breast cancers. 13058 (2017) doi:10.1186/s13058-017-0841-6.

83. Wickström, S. A., Masoumi, K. C., Khochbin, S., Fässler, R. & Massoumi, R. CYLD negatively regulates cell-cycle progression by inactivating HDAC6 and increasing the levels of acetylated tubulin. *EMBO J.* **29**, 131–144 (2010).

84. Woan, K. V. *et al.* Targeting histone deacetylase 6 mediates a dual anti-melanoma effect: Enhanced antitumor immunity and impaired cell proliferation. *Mol. Oncol.* **9**, 1447–1457 (2015).

85. Lienlaf, M. *et al.* Essential role of HDAC6 in the regulation of PD-L1 in melanoma. *Mol. Oncol.* **10**, 735–750 (2016).

86. Yu, H., Pardoll, D. & Jove, R. 乳鼠心肌提取 HHS Public Access. *Physiol. Behav.* **176**, 139–148 (2016).

87. Liu, Y., Peng, L., Seto, E., Huang, S. & Qiu, Y. Modulation of histone deacetylase 6 (HDAC6) nuclear import and tubulin deacetylase activity through acetylation. *J. Biol. Chem.* **287**, 29168–29174 (2012).

88. Ryu, H.-W. *et al.* HDAC6 deacetylates p53 at lysines 381/382 and differentially coordinates p53-induced apoptosis. *Cancer Lett.* **391**, 162–171 (2017).

89. Krämer, O. H., Mahboobi, S. & Sellmer, A. Drugging the HDAC6-HSP90 interplay in malignant cells. *Trends Pharmacol. Sci.* **35**, 501–509 (2014).

90. Bali, P. *et al.* Inhibition of histone deacetylase 6 acetylates and disrupts the chaperone function of heat shock protein 90: A novel basis for antileukemia activity of histone deacetylase inhibitors. *J. Biol. Chem.* **280**, 26729–26734 (2005).

91. Rao, R. *et al.* HDAC6 inhibition enhances 17-AAG–mediated abrogation of hsp90 chaperone function in human leukemia cells. *Blood* **112**, 1886–1893 (2008).

92. Bamodu, O. A. *et al.* HDAC inhibitor suppresses proliferation and tumorigenicity of drug-

resistant chronic myeloid leukemia stem cells through regulation of hsa-miR-196a targeting BCR/ABL1. *Exp. Cell Res.* **370**, 519–530 (2018).

93.   Vanhaecke, T., Papeleu, P., Elaut, G. & Rogiers, V. Trichostatin A - like Hydroxamate Histone Deacetylase Inhibitors as Therapeutic Agents: Toxicological Point of View. *Curr. Med. Chem.* **11**, 1629–1643 (2012).

94.   Zhang, M. C. *et al.* Clinical efficacy and molecular biomarkers in a phase II study of tucidinostat plus R-CHOP in elderly patients with newly diagnosed diffuse large B-cell lymphoma. *Clin. Epigenetics* **12**, 1–11 (2020).

95.   Melesina, J., Praetorius, L., Simoben, C. V., Robaa, D. & Sippl, W. Design of selective histone deacetylase inhibitors: Rethinking classical pharmacophore. *Future Med. Chem.* **10**, 1537–1540 (2018).

96.   Zhang, X. H. *et al.* A Review of Progress in Histone Deacetylase 6 Inhibitors Research: Structural Specificity and Functional Divefile:///C:/Users/Melf/Downloads/kuendgen2008.pdfrsity. *J. Med. Chem.* **64**, 1362–1391 (2021).

97.   Shah, R. R. Safety and Tolerability of Histone Deacetylase (HDAC) Inhibitors in Oncology. *Drug Saf.* **42**, 235–245 (2019).

98.   Safa, A. R. Role of histone deacetylase 6 (HDAC6) in cancers . **1**, (2017).

99.   Maharaj, K. *et al.* Silencing of HDAC6 as a therapeutic target in chronic lymphocytic leukemia. *Blood Adv.* **2**, 3012–3024 (2018).

100.   Hackanson, B. *et al.* HDAC6 as a target for antileukemic drugs in acute myeloid leukemia. *Leuk. Res.* **36**, 1055–1062 (2012).

101.   Santo, L. *et al.* Preclinical activity, pharmacodynamic, and pharmacokinetic properties of a selective HDAC6 inhibitor, ACY-1215, in combination with bortezomib in multiple myeloma. *Blood* **119**, 2579–2589 (2012).

102.   Huang, P. *et al.* Selective HDAC inhibition by ACY-241 enhances the activity of paclitaxel in solid tumor models. *Oncotarget* **8**, 2694–2707 (2017).

103.   Qian, X. *et al.* Activity of PXD101, a histone deacetylase inhibitor, in preclinical ovarian cancer studies. *Mol. Cancer Ther.* **5**, 2086–2095 (2006).

104.   Yoshida, M. [Potent and specific inhibition of mammalian histone deacetylase both in vivo and in vitro by trichostatin A]. *Tanpakushitsu Kakusan Koso.* **52**, 1788–1789 (2007).

105.   Cameron, E. E., Bachman, K. E., Myöhänen, S., Herman, J. G. & Baylin, S. B. Synergy of demethylation and histone deacetylase inhibition in the re-expression of genes silenced in cancer. *Nat. Genet.* **21**, 103–107 (1999).

106.   Ungerstedt, J. S. *et al.* Role of thioredoxin in the response of normal and transformed cells to histone deacetylase inhibitors. *Proc. Natl. Acad. Sci. U. S. A.* **102**, 673–678 (2005).

107.   Derissen, E. J. B., Beijnen, J. H. & Schellens, J. H. M. Concise Drug Review: Azacitidine and Decitabine. *Oncologist* **18**, 619–624 (2013).

108.   Suraweera, A., O'Byrne, K. J. & Richard, D. J. Combination therapy with histone deacetylase inhibitors (HDACi) for the treatment of cancer: Achieving the full therapeutic potential of HDACi. *Front. Oncol.* **8**, 1–15 (2018).

109.   Kalac, M. *et al.* HDAC inhibitors and decitabine are highly synergistic and associated with

unique gene-expression and epigenetic profiles in models of DLBCL. *Blood* **118**, 5506–5516 (2011).

110. Vogl, D. T. *et al.* Ricolinostat, the first selective histone deacetylase 6 inhibitor, in combination with bortezomib and dexamethasone for relapsed or refractory multiple myeloma. *Clin. Cancer Res.* **23**, 3307–3315 (2017).

111. Anighoro, A., Bajorath, J. & Rastelli, G. Polypharmacology : Challenges and Opportunities in Drug Discovery Department of Life Science Informatics , B-IT , LIMES Program Unit Chemical Biology and Medicinal. *J. Med. Chem.* **57**, 7874–7887 (2014).

112. Fu, R. geng, Sun, Y., Sheng, W. bing & Liao, D. fang. *Designing multi-targeted agents: An emerging anticancer drug discovery paradigm. European Journal of Medicinal Chemistry* vol. 136 (Elsevier Masson SAS, 2017).

113. Bhatia, S. *et al.* Discovery of the First-in-Class Dual Histone Deacetylase-Proteasome Inhibitor. *J. Med. Chem.* **61**, 10299–10309 (2018).

114. Wu, Y. W. *et al.* A novel dual HDAC and HSP90 inhibitor, MPT0G449, downregulates oncogenic pathways in human acute leukemia in vitro and in vivo. *Oncogenesis* **10**, (2021).

115. Toure, M. & Crews, C. M. Small-molecule PROTACS: New approaches to protein degradation. *Angew. Chemie - Int. Ed.* **55**, 1966–1973 (2016).

116. Li, X. & Song, Y. Proteolysis-targeting chimera (PROTAC) for targeted protein degradation and cancer therapy. *J. Hematol. Oncol.* **13**, 1–14 (2020).

117. Rodriguez-gonzalez, A. *et al.* Role of the Aggresome Pathway in Cancer : Targeting Histone Deacetylase 6 – Dependent Protein Degradation. 6–11 (2008) doi:10.1158/0008-5472.CAN-07-5989.

118. Afgan, E. *et al.* The Galaxy platform for accessible, reproducible and collaborative biomedical analyses: 2018 update. *Nucleic Acids Res.* **46**, W537–W544 (2018).

119. Widmann, J. *et al.* RNASTAR: An RNA structural alignment repository that provides insight into the evolution of natural and artificial RNAs. *Rna* **18**, 1319–1327 (2012).

120. Robinson, M. D., McCarthy, D. J. & Smyth, G. K. edgeR: A Bioconductor package for differential expression analysis of digital gene expression data. *Bioinformatics* **26**, 139–140 (2009).

121. Yates, A. D. *et al.* Ensembl 2020. *Nucleic Acids Res.* **48**, D682–D688 (2020).

122. Szklarczyk, D. *et al.* STRING v11: Protein-protein association networks with increased coverage, supporting functional discovery in genome-wide experimental datasets. *Nucleic Acids Res.* **47**, D607–D613 (2019).

123. Mcconkey, D. Proteasome and HDAC : who ' s zooming who ? Genomic imbalances in Hodgkin lymphoma. **116**, 308–309 (2012).

124. Hideshima, T., Richardson, P. G. & Anderson, K. C. Mechanism of action of proteasome inhibitors and deacetylase inhibitors and the biological basis of synergy in multiple myeloma. *Mol. Cancer Ther.* **10**, 2034–2042 (2011).

125. Stenzel, K. *et al.* Alkoxyurea-Based Histone Deacetylase Inhibitors Increase Cisplatin Potency in Chemoresistant Cancer Cell Lines. *J. Med. Chem.* **60**, 5334–5348 (2017).

126. Kalac, M. *et al.* HDAC inhibitors and decitabine are highly synergistic and associated with unique gene-expression and epigenetic profiles in models of DLBCL. *Blood* **118**, 5506–5516 (2011).

127. Inaba, H. & Pui, C. H. Immunotherapy in pediatric acute lymphoblastic leukemia. *Cancer Metastasis Rev.* **38**, 595–610 (2019).

128. Yoon, S. & Eom, G. H. HDAC and HDAC Inhibitor: From Cancer to Cardiovascular Diseases. *Chonnam Med. J.* **52**, 1 (2016).

129. Mann, B. S., Johnson, J. R., Cohen, M. H., Justice, R. & Pazdur, R. FDA Approval Summary: Vorinostat for Treatment of Advanced Primary Cutaneous T-Cell Lymphoma. *Oncologist* **12**, 1247–1252 (2007).

130. Bondarev, A. D. *et al. Recent developments of HDAC inhibitors: Emerging indications and novel molecules. British Journal of Clinical Pharmacology* vol. 87 (2021).

131. Osko, J. D. & Christianson, D. W. Structural Basis of Catalysis and Inhibition of HDAC6 CD1, the Enigmatic Catalytic Domain of Histone Deacetylase 6. *Biochemistry* **58**, 4912–4924 (2019).

132. Bali, P. *et al.* Inhibition of histone deacetylase 6 acetylates and disrupts the chaperone function of heat shock protein 90: A novel basis for antileukemia activity of histone deacetylase inhibitors. *J. Biol. Chem.* **280**, 26729–26734 (2005).

133. Depetter, Y. *et al.* Selective pharmacological inhibitors of HDAC6 reveal biochemical activity but functional tolerance in cancer models. *Int. J. Cancer* **145**, 735–747 (2019).

134. Lin, A. *et al.* Off-target toxicity is a common mechanism of action of cancer drugs undergoing clinical trials. *Sci. Transl. Med.* **11**, (2019).

135. Haberland, M. *et al.* in tumor cells Genetic dissection of histone deacetylase requirement. **106**, 7751–7755 (2016).

136. Roche, J. & Bertrand, P. Inside HDACs with more selective HDAC inhibitors. *Eur. J. Med. Chem.* **121**, 451–483 (2016).

137. Park, S. B. *et al.* Chemotherapy-induced peripheral neurotoxicity: A critical analysis. *CA. Cancer J. Clin.* **63**, 419–437 (2013).

138. Chatterjee, K., Zhang, J., Honbo, N. & Karliner, J. S. Doxorubicin cardiomyopathy. *Cardiology* **115**, 155–162 (2010).

139. Zilberman, Y. *et al.* Regulation of microtubule dynamics by inhibition of the tubulin deacetylase HDAC6. *J. Cell Sci.* **122**, 3531–3541 (2009).

140. Tu, H. J. *et al.* The anticancer effects of MPT0G211, a novel HDAC6 inhibitor, combined with chemotherapeutic agents in human acute leukemia cells. *Clin. Epigenetics* **10**, 1–13 (2018).

141. Avula. 基因的改变NIH Public Access. *Bone* **23**, 1–7 (2014).

142. Vergani, B. *et al.* Novel Benzohydroxamate-Based Potent and Selective Histone Deacetylase 6 (HDAC6) Inhibitors Bearing a Pentaheterocyclic Scaffold: Design, Synthesis, and Biological Evaluation. *J. Med. Chem.* **62**, 10711–10739 (2019).

143. Asfaha, Y. *et al.* Novel alkoxyamide-based histone deacetylase inhibitors reverse cisplatin resistance in chemoresistant cancer cells. *Bioorganic Med. Chem.* **28**, 115108 (2020).

144. Pflieger, M. *et al.* Novel α,β-unsaturated hydroxamic acid derivatives overcome cisplatin resistance. *Bioorganic Med. Chem.* **27**, 115036 (2019).

145. Minegishi, Y. *et al.* Mutations in the human λ5/14.1 Gene result in B cell deficiency and agammaglobulinemia. *J. Exp. Med.* **187**, 71–77 (1998).

146. Kumar, R. A. *et al.* A de novo 1p34.2 microdeletion identifies the synaptic vesicle gene RIMS3

as a novel candidate for autism. *J. Med. Genet.* **47**, 81–90 (2010).

147.   Sanjo, H., Kawait, T. & Akira, S. DRAKs, novel serine/threonine kinases related to death-associated protein kinase that trigger apoptosis. *J. Biol. Chem.* **273**, 29066–29071 (1998).

148.   Kang, S. W. *et al.* PKCβ modulates antigen receptor signaling via regulation of Btk membrane localization. *EMBO J.* **20**, 5692–5702 (2001).

149.   Davidson, C. E., Reese, B. E., Billingsley, M. L. & Yun, J. K. Stannin, a protein that localizes to the mitochondria and sensitizes NIH-3T3 cells to trimethyltin and dimethyltin toxicity. *Mol. Pharmacol.* **66**, 855–863 (2004).

150.   Matsuda, S., Matsuda, Y. & D'Adamio, L. BRI3 inhibits amyloid precursor protein processing in a mechanistically distinct manner from its homologue Dementia gene BRI2. *J. Biol. Chem.* **284**, 15816–15825 (2009).

151.   PROVOST, P. *et al.* Coactosin-like protein, a human F-actin-binding protein: critical role of lysine-75. *Biochem. J.* **359**, 255–263 (2001).

152.   Barr, S. D., Smiley, J. R. & Bushman, F. D. The interferon response inhibits HIV particle production by induction of TRIM22. *PLoS Pathog.* **4**, 1–11 (2008).

153.   Pao, C. S., Barker, B. L. & Benovic, J. L. Role of the amino terminus of G protein-coupled receptor kinase 2 in receptor phosphorylation. *Biochemistry* **48**, 7325–7333 (2009).

154.   Eckfeld, K. *et al.* RASSF4/AD037 is a potential Ras effector/tumor suppressor of the RASSF family. *Cancer Res.* **64**, 8688–8693 (2004).

155.   De Smedt, E. *et al.* Loss of RASSF4 Expression in Multiple Myeloma Promotes RAS-Driven Malignant Progression. *Cancer Res.* **78**, 1155–1168 (2018).

156.   Puthalakath, H. *et al.* Bmf: a proapoptotic BH3-only protein regulated by interaction with the myosin V actin motor complex, activated by anoikis. *Science* **293**, 1829–1832 (2001).

157.   Guillaume, B. *et al.* Down-Regulation of c-Fos/c-Jun AP-1 Dimer Activity by Sumoylation. *Mol. Cell. Biol.* **25**, 6964–6979 (2005).

158.   Qing, J., Zhang, Y. & Derynck, R. Structural and functional characterization of the transforming growth factor-beta -induced Smad3/c-Jun transcriptional cooperativity. *J. Biol. Chem.* **275**, 38802–38812 (2000).

159.   Di Bacco, A. & Gill, G. The secreted glycoprotein CREG inhibits cell growth dependent on the mannose-6-phosphate/insulin-like growth factor II receptor. *Oncogene* **22**, 5436—5445 (2003).

160.   B., S. S., S., D. A., A., T. G. & Vojo, D. Human IRGM Induces Autophagy to Eliminate Intracellular Mycobacteria. *Science (80-.).* **313**, 1438–1441 (2006).

161.   Rice, G. I. *et al.* Mutations involved in Aicardi-Goutières syndrome implicate SAMHD1 as regulator of the innate immune response. *Nat. Genet.* **41**, 829–832 (2009).

162.   Roos, J. *et al.* STIM1, an essential and conserved component of store-operated Ca2+ channel function. *J. Cell Biol.* **169**, 435–445 (2005).

163.   Kajander, T. *et al.* Dual interaction of factor H with C3d and glycosaminoglycans in host-nonhost discrimination by complement. *Proc. Natl. Acad. Sci. U. S. A.* **108**, 2897–2902 (2011).

164.   Wang, Y. *et al.* Human 1A6/DRIM, the homolog of yeast Utp20, functions in the 18S rRNA processing. *Biochim. Biophys. Acta - Mol. Cell Res.* **1773**, 863–868 (2007).

165.	Boylan, K. L. M. *et al.* A transgenic mouse model of plasma cell malignancy shows phenotypic, cytogenetic, and gene expression heterogeneity similar to human multiple myeloma. *Cancer Res.* **67**, 4069–4078 (2007).

166.	Simões-Pires, C. *et al.* HDAC6 as a target for neurodegenerative diseases: What makes it different from the other HDACs? *Mol. Neurodegener.* **8**, (2013).

167.	Reßing, N. *et al.* Multicomponent Synthesis, Binding Mode, and Structure-Activity Relationship of Selective Histone Deacetylase 6 (HDAC6) Inhibitors with Bifurcated Capping Groups. *J. Med. Chem.* **63**, 10339–10351 (2020).

168.	Kuendgen, A. & Lübbert, M. Current status of epigenetic treatment in myelodysplastic syndromes. *Ann. Hematol.* **87**, 601–611 (2008).

169.	Böhm, H. J. *et al.* Fluorine in medicinal chemistry. *ChemBioChem* **5**, 637–643 (2004).

170.	Justyna, W. 乳鼠心肌提取 {HHS} {Public} {Access}. *Physiol. Behav.* **176**, 139–148 (2017).

171.	Pflieger, M. *et al.* Oxa Analogues of Nexturastat A Demonstrate Improved HDAC6 Selectivity and Superior Antileukaemia Activity. *ChemMedChem* **16**, 1798–1803 (2021).

172.	Zhang, Y. *et al.* Mice Lacking Histone Deacetylase 6 Have Hyperacetylated Tubulin but Are Viable and Develop Normally. *Mol. Cell. Biol.* **28**, 1688–1701 (2008).

173.	Sellmer, A. *et al.* Marbostat-100 Defines a New Class of Potent and Selective Antiinflammatory and Antirheumatic Histone Deacetylase 6 Inhibitors. *J. Med. Chem.* **61**, 3454–3477 (2018).

174.	Kale, A. J. & Moore, B. S. resistance. **55**, 10317–10327 (2013).

175.	Song, H. *et al.* Discovery of specific HDAC6 inhibitor with anti-metastatic effects in pancreatic cancer cells through virtual screening and biological evaluation. *Bioorg. Chem.* **97**, 103679 (2020).

176.	Harvey, L. *et al. Molecular Cell Biology. 4th edition. Journal of the American Society for Mass Spectrometry* (2000). doi:10.1016/j.jasms.2009.08.001.

177.	Marks, P. A. *et al.* Histone deacetylases and cancer: Causes and therapies. *Nat. Rev. Cancer* **1**, 194–202 (2001).

List of publications and presentations

Publications included in this thesis:

Multicomponent Synthesis, Binding Mode, and Structure−Activity Relationship of Selective Histone Deacetylase 6 (HDAC6) Inhibitors with Bifurcated Capping Groups

Nina Reßing+, **Melf Sönnichsen+**, Jeremy D. Osko, Andrea Schöler, Julian Schliehe-Diecks, Alexander Skerhut, Arndt Borkhardt, Julia Hauer, Matthias U. Kassack, David. W. Christianson, Sanil Bhatia*, and Finn K. Hansen* **(shared first authorship)**

Oxa Analogues of Nexturastat A Demonstrate Improved HDAC6 Selectivity and Superior Antileukaemia Activity

Marc Pflieger+, **Melf Sönnichsen+**, Nadine Horstick-Muche, Jing Yang, Julian Schliehe-Diecks, Andrea Schöler, Arndt Borkhardt, Alexandra Hamacher, Matthias U. Kassack, Finn K. Hansen, Sanil Bhatia*, and Thomas Kurz* **(shared first authorship)**

Synergistic induction of apoptosis in resistant head and neck carcinoma and leukemia by alkoxyamide-based histone deacetylase inhibitors

Leandro A. Alves Avelar+, Christian Schrenk+, **Melf Sönnichsen+**, Alexandra Hamacher, Finn K. Hansen, Julian Schliehe-Diecks, Arndt Borkhardt, Sanil Bhatia*, Matthias U. Kassack*, Thomas Kurz* **(shared first authorship)**

Hydroxamic Acids Immobilized on Resins (HAIRs): Synthesis of Dual-Targeting HDAC Inhibitors and HDAC Degraders (PROTACs)

Laura Sinatra, Jan J Bandolik, Martin Roatsch, **Melf Sönnichsen**, Clara T Schoeder, Alexandra Hamacher, Andrea Schöler, Arndt Borkhardt, Jens Meiler, Sanil Bhatia, Matthias U Kassack, Finn K Hansen

Development of Fluorinated Peptoid-Based Histone Deacetylase (HDAC) Inhibitors for Therapy-Resistant Acute Leukemia

Nina Reßing, Julian Schliehe-Diecks, Paris R. Watson, **Melf Sönnichsen**, Abigail D. Cragin, Andrea Schöler, Jing Yang, Linda Schäker-Hübner, Arndt Borkhardt, David W. Christianson, Sanil Bhatia, and Finn K. Hansen

Poster presentation:

Selective HDAC6 inhibitors as a therapeutic option in resistant pediatric acute lymphoblastic leukemia

Melf Sönnichsen, Alexandra Herrlich, Mark Pflieger, Thomas Kurz, Sanil Bhatia, Arndt Borkhardt, and Julia Hauer

EMBO Workshop, B-cell development and leukemia, 08 - 11 March 2019, Salamanca, Spain